MICROCOPY RESOLUTION TEST CHART

NATIONAL BUREAU OF STANDARDS 1963 A

DIRECT RF A-O PROCESSOR SPECTRUM ANALYZER

FINAL ENGINEERING REPORT

COVERING THE PERIOD

OCTOBER 1979 TO JULY 1981

AUGUST 1981

OBJECT: TO DEVELOP AND DEMONSTRATE A BRAGG-TYPE ACOUSTO-OPTIC DEFLECTOR PROCESSOR CAPABLE OF WIDEBAND RF SIGNAL PROCESSING FOR PERFORMING SIGNAL ACQUISITION AND SPECTRAL ANALYSIS.

PREPARED UNDER CONTRACT NO. N00173-79-C-0239

FOR THE
NAVAL RESEARCH LABORATORY
WASHINGTON, D.C. 20375

⟁ TELEDYNE MEC

DTIC
ELECTE
JUN 7 1983
B

DISTRIBUTION STATEMENT A

Approved for public release;
Distribution Unlimited

83 06 01 092

DIRECT RF A-O PROCESSOR SPECTRUM ANALYZER

FINAL ENGINEERING REPORT

COVERING THE PERIOD

OCTOBER 1979 TO JULY 1981

AUGUST 1981

OBJECT: TO DEVELOP AND DEMONSTRATE A BRAGG-TYPE ACOUSTO-OPTIC
DEFLECTOR PROCESSOR CAPABLE OF WIDEBAND RF SIGNAL
PROCESSING FOR PERFORMING SIGNAL ACQUISITION AND SPECTRAL
ANALYSIS.

PREPARED UNDER CONTRACT NO. N00173-79-C-0239

FOR THE

NAVAL RESEARCH LABORATORY
WASHINGTON, D.C. 20375

DTIC
ELECTE
JUN 7 1983
B

PREPARED BY

C. L. GRASSE
TELEDYNE MEC
3165 Porter Drive
Palo Alto, California

REPORT DOCUMENTATION PAGE	READ INSTRUCTIONS BEFORE COMPLETING FORM

1. REPORT NUMBER	2. GOVT ACCESSION NO. *AI29700*	3. RECIPIENT'S CATALOG NUMBER

4. TITLE (and Subtitle)	5. TYPE OF REPORT & PERIOD COVERED
Direct RF A-O Processor Spectrum Analyzer	Final Engineering Report October 1979 to July 1981
	6. PERFORMING ORG. REPORT NUMBER

7. AUTHOR(s)	8. CONTRACT OR GRANT NUMBER(s)
C. L. Grasse	N00173-79-C-0239

9. PERFORMING ORGANIZATION NAME AND ADDRESS	10. PROGRAM ELEMENT, PROJECT, TASK AREA & WORK UNIT NUMBERS
Solid State Division Teledyne MEC 3165 Porter Drive Palo Alto, CA 94304	NRL Spec No. 57R16-34-002 Rev. A

11. CONTROLLING OFFICE NAME AND ADDRESS	12. REPORT DATE
	August 1981
	13. NUMBER OF PAGES

14. MONITORING AGENCY NAME & ADDRESS(If different from Controlling Office)	15. SECURITY CLASS. (of this report)
	Unclassified
	15a. DECLASSIFICATION/DOWNGRADING SCHEDULE N/A

16. DISTRIBUTION STATEMENT (of this Report)

Approved for public release; distribution unlimited.

17. DISTRIBUTION STATEMENT (of the abstract entered in Block 20, if different from Report)

18. SUPPLEMENTARY NOTES

19. KEY WORDS (Continue on reverse side if necessary and identify by block number)

Acousto-optics, Acoustics, Bulk wave, Spectrum analysis, Bragg cell.

20. ABSTRACT (Continue on reverse side if necessary and identify by block number)

The primary objective of the Direct RF A-O Processor Spectrum Analyzer program described in this report was to develop and demonstrate a design approach, along with the associated processing technologies, for a wide-band acousto-optic Bragg cell spectrum analyzer. The signal processor used to demonstrate feasibility of the technical approach consisted of two bulk-wave acousto-optic deflectors. The Spectrum Analyzer operated from 4 to 8 GHz and was used to demonstrate the performance requirements of

DD FORM 1473 EDITION OF 1 NOV 65 IS OBSOLETE
1 JAN 73

FOREWORD

This report was prepared by the Solid State Division of Teledyne MEC, Palo Alto, California, under Naval Research Laboratory Contract No. N00173-79-C-0239. The Direct RF A-O Processor Spectrum Analyzer program was sponsored by the Naval Electronic Systems Command with technical support provided by the Naval Research Laboratory. The program technical monitor for NRL was Mr. Anthony "Tony" E. Spezio. This program was conducted at Teledyne MEC under the supervision of Dr. Ernst K. Kirchner. The project engineer was Mr. Charles L. Grasse, with technical assistance and support provided by Mr. Eric Reichelderfer. The report covers the period from October 1979 to July 1981.

TABLE OF CONTENTS

TABLE OF CONTENTS
(CONTINUED)

TABLE OF CONTENTS
(CONTINUED)

LIST OF APPENDICES

RE: Proprietary Information, Appendix B,
Figure 11
Delete Appendix B per Mr. Anthony Spezio, Pro-
ject Officer, NRL

Accession For	
NTIS GRA&I	✓
DTIC TAB	☐
Unannounced	☐
Justification	
By	
Distribution/	
Availability Codes	
Dist	Avail and/or Special
A	

LIST OF ILLUSTRATIONS

LIST OF ILLUSTRATIONS
(CONTINUED)

LIST OF ILLUSTRATIONS
(CONTINUED)

LIST OF ILLUSTRATIONS
(CONTINUED)

LIST OF TABLES

EXECUTIVE SUMMARY

The primary objective of the Direct RF A-O Processor Spectrum Analyzer
program described in this report was to develop design and processing
technologies for a wideband acousto-optic Bragg cell signal processor.
The spectrum analyzer used to demonstrate feasibility was made up of
two two-channel, bulk-wave, acousto-optic deflectors. The device
operates from 4 to 8 GHz and was used to demonstrate the performance
requirements of NRL Specification No. 57R16-34-002, Rev. A, for a
"Direct RF A-O Processor and Spectrum Analyzer."

The performance goals of this program included a demonstration of
technical feasibility, in both design and manufacture, of the key
spectrum analyzer element — the wideband acousto-optic Bragg cell.
The Bragg cell component consists of a single-crystal, optically trans-
parent substrate, with deposited wideband piezoelectric transducers
used to convert the received RF signals into acoustic energy. The
acousto-optic crystal material selected for the spectrum analyzer
demonstration was 35° Y-axis rotated, X-axis propagating, lithium
niobate. Although a material with a moderate acousto-optic figure of
merit, lithium niobate's low acoustic propagation loss yielded a Bragg
cell deflector with the best overall efficiency.

The acousto-optic component developed on this program consisted of
four channels, one for each of the frequency bands: 4-5 GHz, 5-6 GHz,
6-7 GHz and 7-8 GHz. Each channel was designed to have a 1 GHz
bandwidth transducer. The location of each transducer was staggered to
provide full coverage of the 4 to 8 GHz frequency band. By depositing
the transducers on a curved surface on the acousto-optic substrate, con-
siderable enhancement of the effective Bragg acousto-optic interaction
bandwidth was achieved. By utilizing the curved surface, the complete
4 to 8 GHz band could be covered by implementation of all four channels
on a single acousto-optic substrate.

Performance of the multi-channel 4 to 8 GHz spectrum analyzer was demonstrated using the test set shown in Figure 1. The peripheral optic and optical processing components, when orchestrated with the acousto-optic device, made up the rest of the demonstration hardware. A helium-neon (6328 Å) laser was used, followed by lenses used to shape the beam in accordance with the acousto-optic interaction region desired within the acoustic substrate. After passing through the Bragg cell, the light is recollimated and focused onto the detector array. The photodetector array detects the deflected light and transforms it into a video signal for further processing or display.

Several technological achievements were realized during the course of this program. Most important were the development of techniques for "shaping" and high quality polishing the curved transducer surface. This was viewed as being the most critical process in realizing a broadband Bragg device. Although still a critical process, the required polishing techniques are now easily accomplished using standard procedures.

The Direct RF A-O Processor and Spectrum Analyzer demonstrated the feasibility of using acousto-optic signal processing to provide wide bandwidth signal identification and spectral analysis. In the applications envisioned for this type of processor, there are any number of key performance requirements. As pointed out in the Statement of Work, however, none are more important than the ability to perform wideband spectrum analysis. The requirement for a wide bandwidth spectrum analyzer was satisfied. Key to achieving this goal were the processing techniques that enabled the fabrication of a Bragg cell capable of covering the full 4 GHz operation bandwidth.

In the demonstration data given on page 4, some of the more important performance results achieved are compared with their specification requirements.

FIGURE 1. ACOUSTO-OPTIC SPECTRUM ANALYZER
DEMONSTRATION TEST SETUP.

PERFORMANCE SUMMARY

REQUIREMENT	SPECIFICATION	PERFORMANCE
FREQUENCY RANGE (GHz)		
• Band 1	4-5	3.9 - 5.0 (4.4 dB BW)
• Band 2	5-6	4.8 - 6.0 (9 dB BW)
• Band 3	6-7	5.8 - 7.1 (3.5 dB BW)
• Band 4	7-8	7.0 - 8.0 (7.8 dB BW)
INPUT SIGNAL LEVEL (dBm)	+10/channel	+20/channel
EFFICIENCY (% PER RF WATT)		
• Band 1	4.0	.0023 - .0063
• Band 2	3.5	.0005 - .0035
• Band 3	3.0	.00075 - .0017
• Band 4	2.0	.00015 - .0009
DYNAMIC RANGE (dB)	50	15 - 16 (*)
RESOLUTION (MHz)	5	2 - 4

(*)
Limited by the photodetector, scattered light dynamic range.

An acousto-optic efficiency that was lower than desired was obtained, which also affected the analyzer's sensitivity and dynamic range. However, through this program we have a much better understanding of the efficiency and how its contributors relate to the overall performance of Bragg cell processors and analyzers. The most important specifications from an overall spectrum analyzer performance point of view are the system's dynamic range and sensitivity. Demonstration tests conducted on this program, as well as similar testing on other Bragg cell devices and systems, has indicated that achieving the ultimate performance in these areas will depend more on peripheral electronics than on the acousto-optic Bragg cell — whose dynamic range, for example, is approximately 50 dB.

All in all, the Direct RF A-O Processor and Spectrum Analyzer program has demonstrated the feasibility of using bulk-wave acousto-optic processing techniques for wideband spectral analysis. There is still work to be done, but the realization of a total performance, wideband, bulk acousto-optic spectrum analyzer processor — capable of operating in tomorrow's systems and environments — is much closer than it was yesterday.

I. INTRODUCTION

A. Program Objective and Purpose

The objective of this program was to provide the technology development necessary for the realization of a wideband acousto-optic signal-processing Bragg cell for use in RF spectrum analyzers. The Bragg cell acousto-optic deflector and its peripheral optical processing will be used to demonstrate the requirements of NRL Specification 57R16-34-002, Rev. A, "Direct RF A-O Processor and Spectrum Analyzer." Sponsorship of the program was through the Naval Electronic Systems Command, with technical support from the Naval Research Laboratory. The technical monitor was Mr. A. E. Spezio of NRL.

The more specific goal of this important effort was to demonstrate the technical feasibility, both in design and manufacture, of a wideband acousto-optic processor/spectrum analyzer. Involved with achieving this objective is the critical validation of the basic design approach and technique. Perhaps the most important items in this validation process are the acousto-optic fabrication techniques necessary for the realization of the analyzer's key element, the Bragg cell. Figure 2 illustrates the acousto-optic Bragg cell used to make up the Direct RF A-O Processor and Spectrum Analyzer.
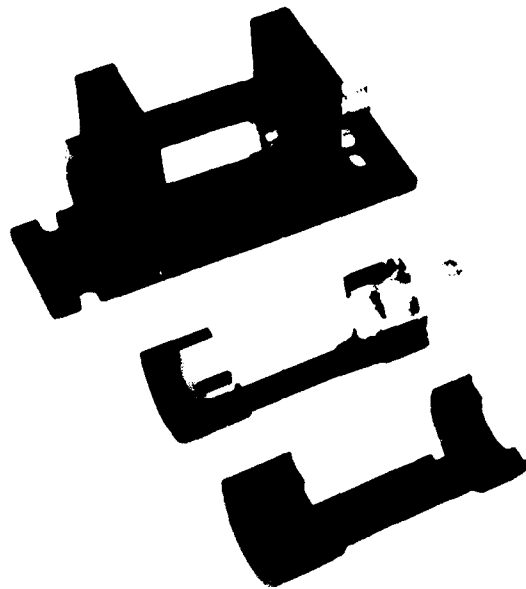
14-1182

FIGURE 2.   THE ACOUSTO-OPTIC BRAGG CELLS USED IN
THE DIRECT RF A-O PROCESSOR SPECTRUM ANALYZER.

B.   An Outline of Material Contained in this Report

Following this introduction, the technical section of the Direct RF A-O
Processor Spectrum Analyzer Final Report is divided into two parts: Section
II, the design portion, and Section III, the test results and conclusions
portion.   The design section describes in detail the technical approach used
to manufacture the Bragg cell spectrum analyzer. A discussion of the basic
concept is presented first, followed by a description of the analysis and
design of the acousto-optic Bragg cell deflector and its optical processor.
Charts and graphs, as well as the mathematical design calculations, are
presented.   In each area, the basic design is related to the desired spec-
trum analyzer performance.

A third section of the report contains the results of the development and
demonstration testing, including all data taken during evaluation of the

spectrum analyzer. This section also offers recommendations and con-
clusions based on the data taken, highlighting in detail how each
performance area could be improved in either its manufacture or its
operation.

Contained at the end of this report is a series of supportive appendices,
which provide backup to key techniques, processes and calculations
used in the development of the Direct RF A-O Processor and Spectrum
Analyzer.

II.   TECHNICAL DISCUSSION

A.   Concept

The Direct RF Acousto-Optic Processor Spectrum Analyzer was achieved
through the use of wideband acousto-optic techniques and specialized
optical processing. The schematic configuration of Figure 3 represents
the basic layout used in the spectrum analyzer. This approach is
designed to achieve a wideband RF signal processor capable of signal
acquisition and spectral analysis over the specified 4 to 8 GHz fre-
quency range.

The spectrum analyzer is made up of two basic optical processors —
the acousto-optic Bragg cell deflector and the optical lens system.

The Bragg cell consists of an appropriately oriented single-crystal
optically transparent substrate. One end of the substrate is manufactured
with an optically polished, cylindrically-curved surface. It is on this
face that the piezoelectric transducers used to convert the microwave
electromagnetic energy into acoustic energy are fabricated. For this
application, the RF coverage has been broken up into four continuous
bands, or channels. The center frequencies of the respective channels
are 4.5 GHz, 5.5 GHz, 6.5 GHz and 7.5 GHz. Each of the channels
has a minimum 1 GHz of bandwidth, thereby ensuring coverage of the full
4 GHz frequency range required by the analyzer.

A piezoelectric transducer array, with one transducer for each channel,
is deposited on the acousto-optic crystal's curved surface. When the
transducer is excited with an RF signal within its band of operation, a
traveling sound wave is set up inside the acoustic substrate. The
alternate compression and rarefaction of the crystalline structure due
to the propagating sound wave causes a change in the substrate's
optical index of refraction. This change in refractive index sets up an
optical diffraction grating. The grating spacing is equivalent to the
acoustic wavelength, and causes the substrate to deflect light energy.
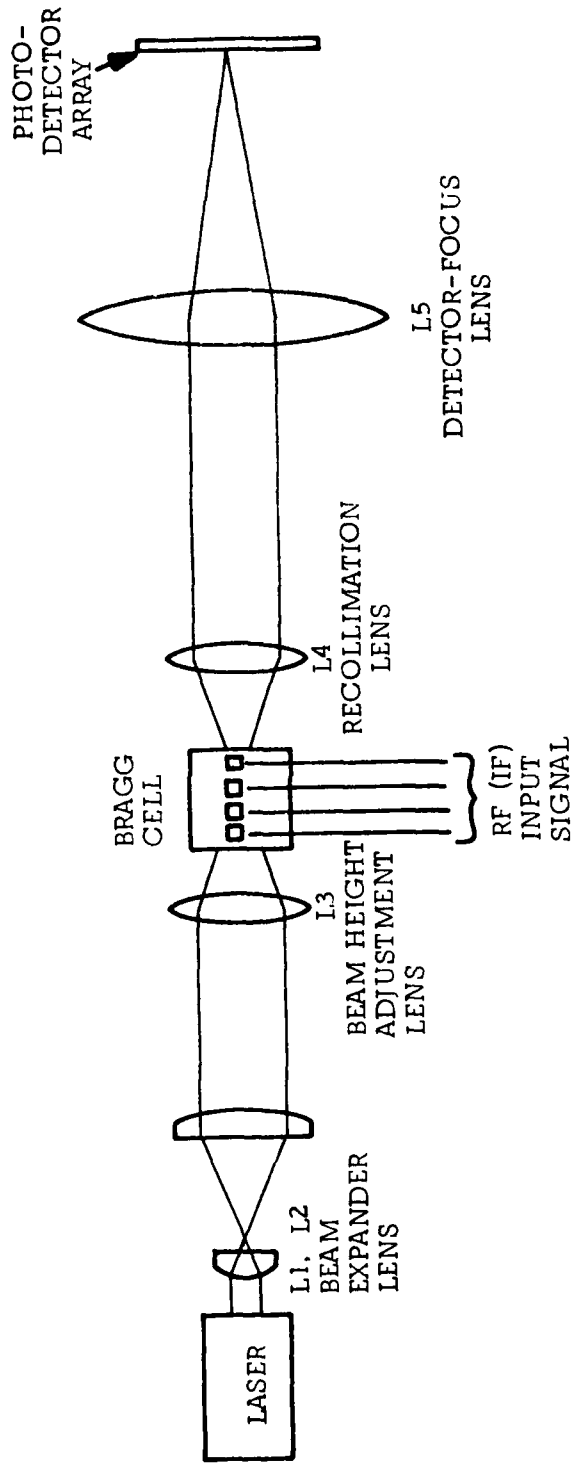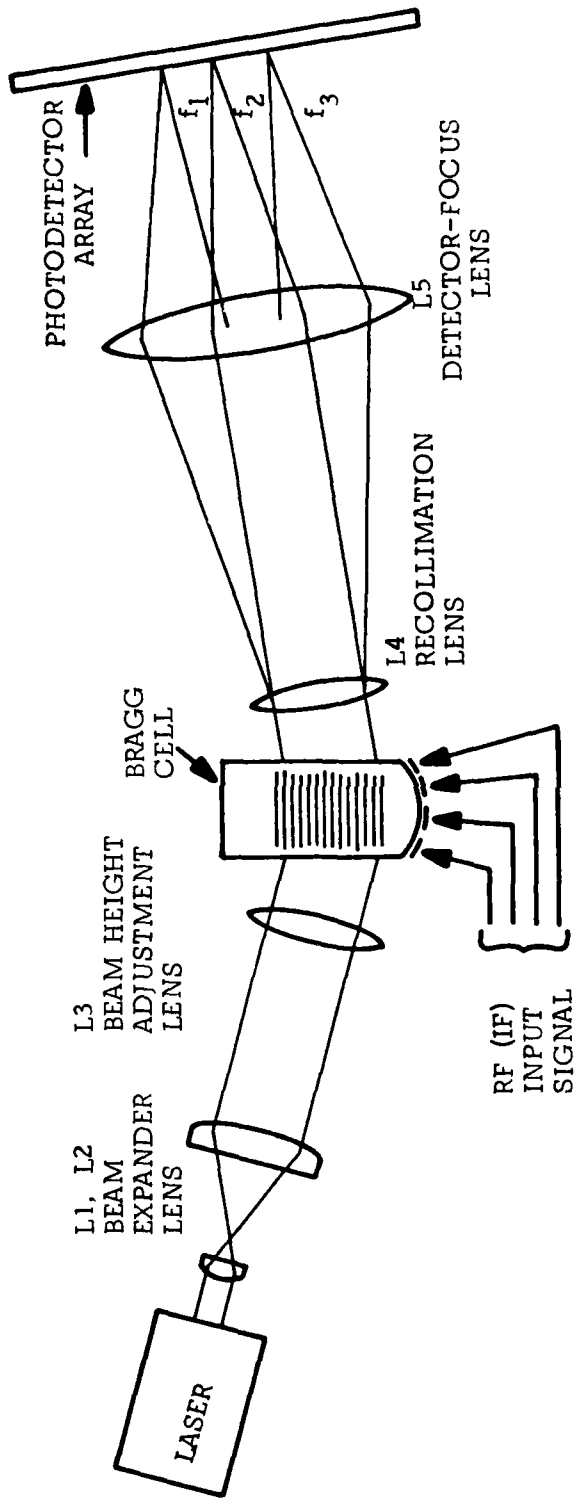
FIGURE 3. BASIC LAYOUT OF SPECTRUM ANALYZER.

The interaction of the light and sound signals is the mechanism by which spectrum analysis takes place.

As stated above, spectral analysis is performed by the acousto-optic interaction and deflection of the incident laser beam by the propagating acoustic wave. As the sound wave frequency is changed, due to a received signal of a different frequency, so is the "grating" spacing generated by the variation in the index of refraction. Since the angle of the deflected light is directly proportional to the grating spacing, it is also proportional to the frequency of the received RF signal. This deflection versus frequency phenomenon is the characteristic on which acousto-optic spectral analysis is based.

Referring again to Figure 3, it is pertinent to discuss the fundamentals of the optical portion of the acousto-optic processor. The helium-neon laser used to produce the light signal must have its beam dimensions modified so the desired frequency resolution and optimum efficiency of interaction with the acoustic signal (within the Bragg cell substrate) will occur. For the best efficiency, a rectangular beam shape is desirable. To achieve this shape, the laser beam is passed through a beam expander (L1-L2), where the exit beam diameter is chosen to equal the beam width desired within the acoustic crystal. The height of the beam within the substrate is controlled by passing the "expanded" beam through a cylindrical lens (L3), with the substrate located near the focal plane of the lens. After passing through the acoustic substrate, the now deflected light is recollimated by another cylindrical lens (L4) located approximately one focal length away from the acoustic crystal. A spherical lens (L5) is then used to focus the deflected light signal onto a photodetector array. The detected output, which uniquely describes the frequency of the received RF signal, is now ready for further processing by the electronic support measures (ESM) equipment and peripheral electronics.

-11-

In summary, the deflection property of the acousto-optic interaction within the Bragg cell crystal causes the incident laser (light) beam to be deflected in angle by an amount proportional to the frequency of the received RF signal. The optical lens system provides for the precise positioning of the deflected, diffraction-limited optical signal "spot" on the photodetector. Thus, the frequency spectrum of the input signal has been transformed to the position of the focused laser spot. The "positional" information is then converted to an electrical signal by the linear array of photodetectors.

In the following section, the rationale and analytical backup for the design are described in detail. Since the major developmental task is directed toward the acousto-optic Bragg cell component, most of the effort described is centered on its design and performance.

B.   Design Approach, Rationale and Analysis

Optical processors demonstrating spectral analysis capability have been fabricated with instantaneous bandwidths of up to 1 GHz, and resolutions of 0.5 MHz. Based on the current state of the art for wide-bandwidth acousto-optic Bragg devices, achieving a 4 GHz operational bandwidth required that the Bragg cell itself be the major developmental area of this program.

1.   Design of the Acousto-Optic Bragg Cell Component

The Bragg type acousto-optic deflector operates by the interaction of an acoustic wave with a laser beam, within an appropriately orientated optically transparent, crystal. The deflection of the laser light beam is associated with the change in the optical index of refraction accompanying the change in the density of the crystalline material; i.e., the change in optical polarizability associated with the strain on the atoms and molecules

of the acousto-optic crystal. The critical design parameter associated
with the acousto-optic deflection process is the determination of the
specific Bragg angle which will provide the highest deflection efficiencies
possible over the entire 4 GHz bandwidth.

a. Bragg Angle Considerations

The acousto-optic deflection process for plane monochromatic optical
and acoustic waves is one in which simple wave-energy-momentum
conservation principles apply. For an incident laser beam of wave
vector $k = \omega/c$, deflected by a low intensity acoustic wave of wave
vector $K = \Omega/v$, the applicable energy-momentum relations are:

$$\omega_s = \omega \pm \Omega$$
$$k_s = k \pm K$$

For Bragg deflection, as shown in Figure 4, the total deflection angle
is $2\theta_B$, with the Bragg angle given by:

$$\theta_B = \sin^{-1} \frac{1}{2} \left(\frac{K}{k}\right) = \sin^{-1} \frac{1}{2} \left(\frac{\lambda_o}{\lambda_a}\right) \qquad (1)$$

λ_o = wavelength of the light (optical) signal.
λ_a = wavelength of the acoustic signal.

In theory, if the angle of the incident laser beam differs from θ_B, then the
intensity of the deflected light (the Bragg cell output) would be zero for
the case of two plane waves. In essence (for a given laser beam angle)
deflection would occur only at one frequency.

Bandwidth Considerations

In practice, however, the preceding condition does not exist since the
laser and acoustic beams are really of finite width. In addition, diffrac-
tion effects will cause the wave vectors to contain angular distribution

COMPONENT OF
ACOUSTIC WAVE AT
BRAGG ANGLE

PATH OF LASER BEAM

θ_1

AIR

θ_B θ_2

ACOUSTO-OPTIC CRYSTAL
WITH REFRACTIVE INDEX = n

θ_3

θ_B

$2\theta_B$

AIR

θ_4
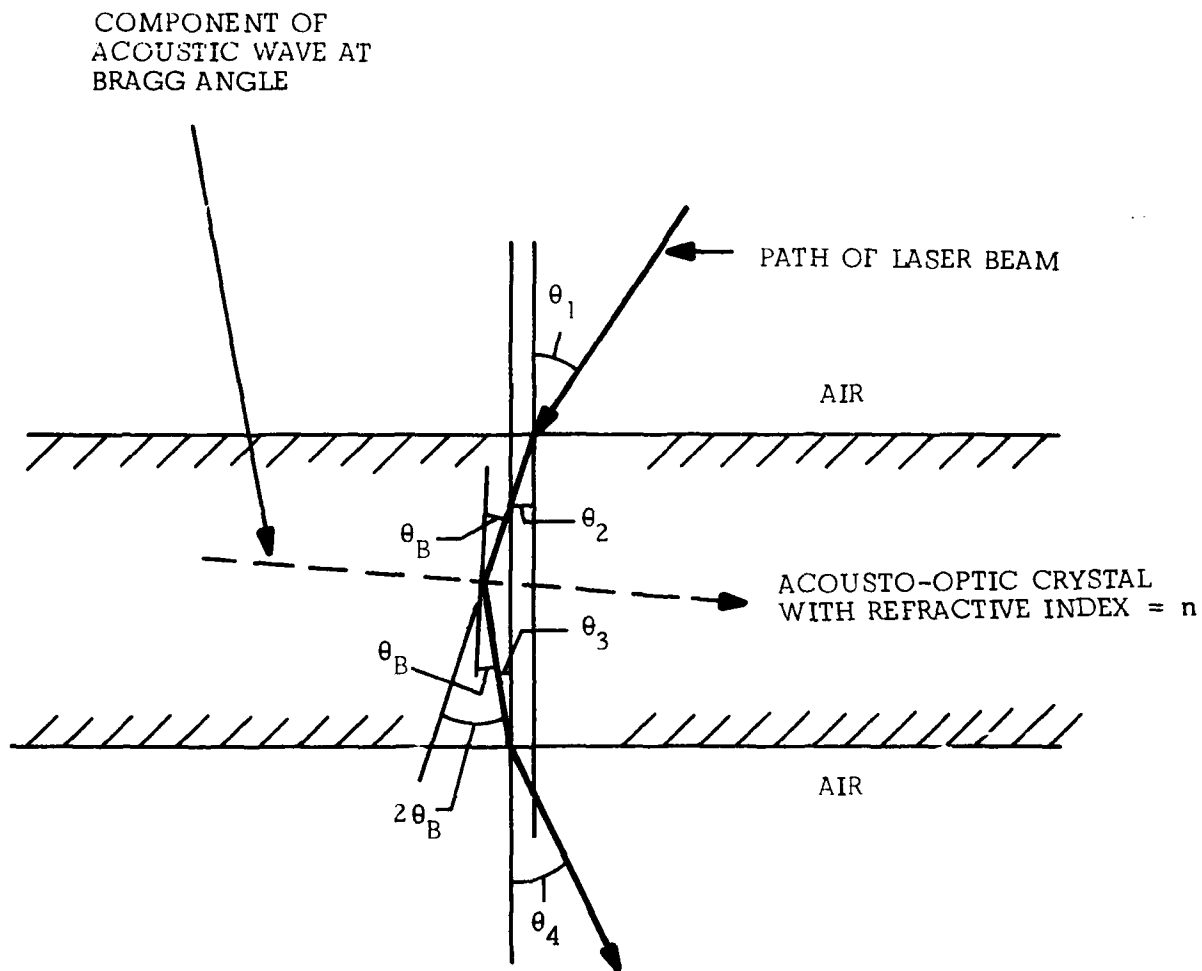
FIGURE 4.   DIAGRAM SHOWING THE PATH OF THE
DEFLECTED LASER BEAM PASSING THROUGH
AN ACOUSTO-OPTIC CRYSTAL.

-14-

components which also satisfy the Bragg condition. These components will also contribute to the deflection of the laser beam, and deflection will occur over a finite band of acoustic frequencies. The intensity of the deflected light is proportional to the plane wave component of the acoustic beam, decreasing as the angular distribution (bandwidth) of the wave vectors increases. This is the expected bandwidth of operation versus deflection efficiency trade-off.

An alternative approach to using diffraction phenomena to increase the angular distribution of the acoustic wave and gain bandwidth is to focus the acoustic energy within the crystal. By using a cylindrical transducer surface to launch the acoustic energy, considerable enhancement of the effective Bragg acousto-optic interaction bandwidth can be achieved.

This ability to focus the acoustic signal is particularly important when operating at higher frequencies, such as the 4 to 8 GHz band developed here, since it substantially reduces the need for extremely small transducers. In short, focusing is merely a way of producing the narrow acoustic beam waist (or large diffraction angle) which would normally have to be diffraction-produced by narrowing the standard, flat transducer. The detailed design of the curved-surface transducer is presented in II-1-c of this section.

b. Acousto-Optic Material Selection

The first choice to be made in the design of the acousto-optic component is the selection of the acousto-optic material. There are a number of factors to be considered in the choice of a material for this application, but the most critical are its acousto-optic interaction efficiency, its acoustic propagation loss, and the quality of its optical transmission characteristic.

There are essentially three materials which can be considered candidates for this application: tellurium dioxide (TeO_2), gallium phosphide (GaP) and lithium niobate ($LiNbO_3$). All three are transparent to the helium-

neon laser signal (wavelength: 6328 Å) to be used in the evaluations.

In Table I below, the two most critical performance-effective characteristics
for each candidate acousto-optic material are presented.

TABLE I

ACOUSTO-OPTIC MATERIAL CHARACTERISTICS

MATERIAL	FIGURE OF MERIT (M_2) [1]	ACOUSTIC ATTENUATION
GaP	29.5	$3.8 \frac{dB}{\mu sec} GHz^2$
TeO_2	22.9	$6.3 \frac{dB}{\mu sec} GHz^2$
$LiNbO_3$	4.6	$0.1 \frac{dB}{\mu sec} GHz^2$

(1) I. C. Chang, IEEE Transactions Sonics and Ultrasonics, Vol. SU-23,
No. 1, January 1976, pp. 2-22.

Based on the figures of merit, it would appear that GaP would be the material
of choice, as it is some 8 dB [10 log (29.5/4.6)] superior to $LiNbO_3$ and
about 1 dB better than TeO_2. However, for high resolution processing,
acoustic propagation distance and loss are also important. To satisfy the
5 MHz resolution requirement of this research and development effort,
the Bragg device will need a minimum of .200 microseconds of propagation
time through the interaction region. Based on this acousto-optic aperture
and the attenuation equations of Table I, Table II illustrates the relative
propagation characteristics over the bandwidth of interest for the candidate
materials.

TABLE II

ACOUSTIC PROPAGATION LOSS

MATERIAL	PROPAGATION LOSS [1]		
	4 GHz	6 GHz	8 GHz
LiNbO$_3$	0.64 dB	1.44 dB	2.56 dB
GaP	24.32 dB	54.72 dB	97.28 dB
TeO$_2$	40.32 dB	90.72 dB	161.28 dB

(1) For a .200 μsec acousto-optic interaction aperture, located
.050 inch from the transducer face of the substrate.

Reviewing this data, it is seen that the acoustic attenuation of GaP is
substantially greater than that of lithium niobate, particularly at the
higher frequencies. This means that the overall efficiency in dB per watt
of RF drive power will be substantially higher for LiNbO$_3$. Therefore,
LiNbO$_3$ was the material selected for our acousto-optic Bragg cell
component.

c. Transducer Design

The electrical requirements of the Bragg cell acousto-optic processor are
broken down into four frequency bands, per Paragraph 6.1 of 57R16-34-002,
Rev. A. TMEC therefore elected to manufacture the acousto-optic com-
ponent with four channels, one for each of the referenced frequency bands.
The four-channel acousto-optic Bragg device is illustrated in Figure 5.
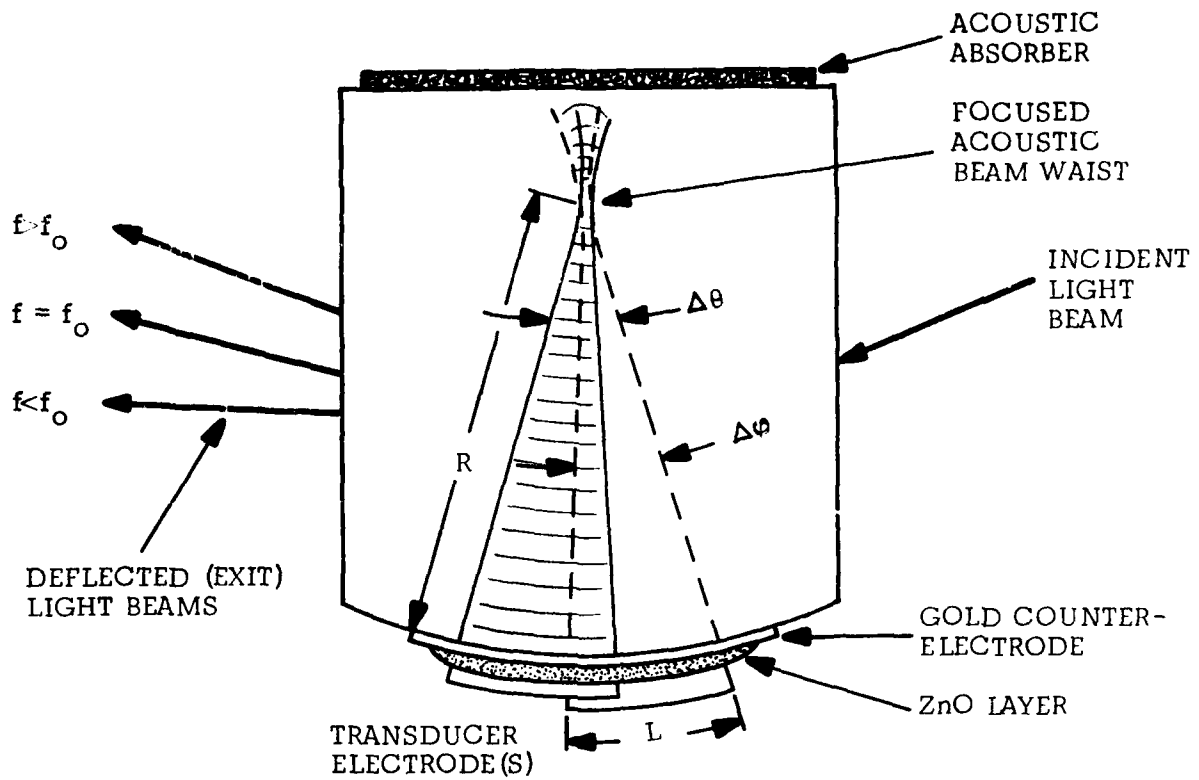
FIGURE 5A. TOP VIEW SHOWING THE FOCUSED ACOUSTIC BEAM PATHS (TRANSDUCER "OVERLAP" IS INDICATED TO DEMONSTRATE CONTIGUOUS CHANNEL OPERATION).
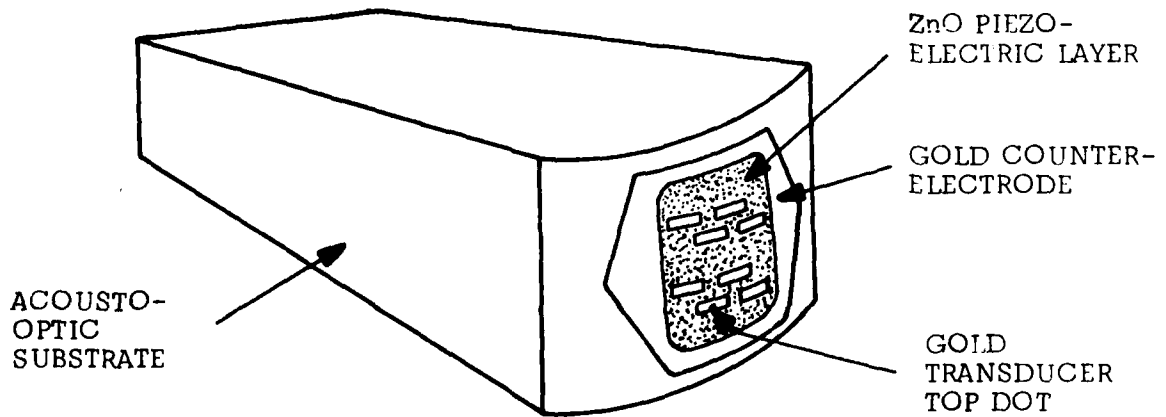
FIGURE 5B. ISOMETRIC VIEW SHOWING ACOUSTIC TRANSDUCER ARRAY DEPOSITED ON THE CYLINDRICAL SURFACE OF THE ACOUSTO-OPTIC CRYSTAL.

FIGURE 5. CONCEPTUAL VIEW OF THE ACOUSTO-OPTIC CRYSTAL AND ITS TRANSDUCER ARRAY.

Transducer Location

The basic Bragg cell deflector device consists of a lithium niobate acousto-optic crystal with four zinc oxide (ZnO) piezoelectric transducers deposited on its cylindrical surface. The acoustic waves propagate down what is essentially the X-axis of the crystal, while the laser beam propagates in the crystal along an axis 35° off the Y-axis toward the Z-axis (Figure 6). (The laser beam actually enters the crystal at an angle displaced by the Bragg angle from this axis.) The polarization of the laser beam is perpendicular to the acoustic wave propagation direction.

Coverage of the 4 GHz bandwidth is achieved by making each of the four independent ZnO transducers capable of operation over a 1 GHz frequency range. The respective center frequencies are 4.5 GHz, 5.5 GHz, 6.5 GHz and 7.5 GHz. The necessary acousto-optic interaction bandwidth from each channel was achieved by use of the cylindrical transducer surface. This "cylindrically focused" bandwidth can be determined analytically by using the following expression.

$$\Delta f = (1.8 \, n v \, \Delta \varphi \cos \theta_B) / \lambda_o \qquad (2)$$

where

Δf = the bandwidth, per acoustic channel

n = the index of refraction of the $LiNbO_3$ acousto-optic crystal = 2.2

v = the acoustic velocity = 6.57×10^5 cm/sec

θ_B = the Bragg angle from Equation (1)

$\Delta \varphi$ = focused angle per transducer (Figure 3)

λ_o = the laser wavelength = 6328Å

---

* E. I. Gordon, Applied Optics. Vol. 5, No. 10, October 1966, pp. 1629-1639.

PROPAGATING
ACOUSTIC WAVE (X-AXIS)

90°

BRAGG ANGLE
(EXTERNAL)

PATH OF
INCIDENT
OPTICAL
SIGNAL

PATH OF
EXITING
OPTICAL
SIGNAL

TRANSDUCER SURFACE

TOP VIEW

Z-AXIS

PATH OF INCIDENT
OPTICAL
SIGNAL

(TRANSDUCER
SURFACE)

PATH OF EXITING
OPTICAL
SIGNAL

Y-AXIS

END VIEW
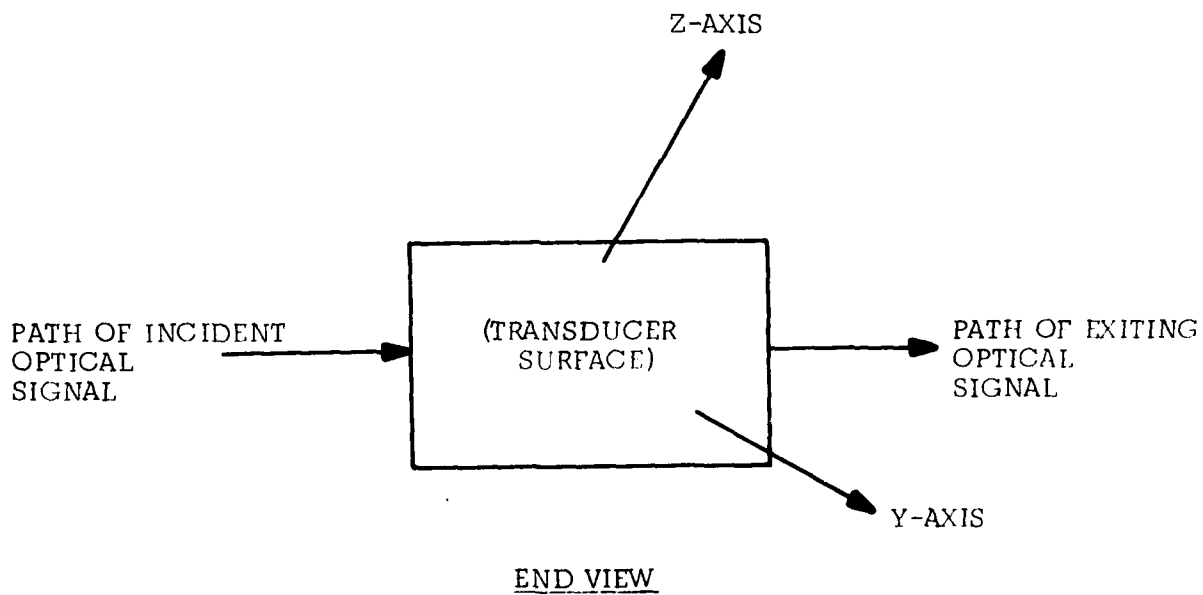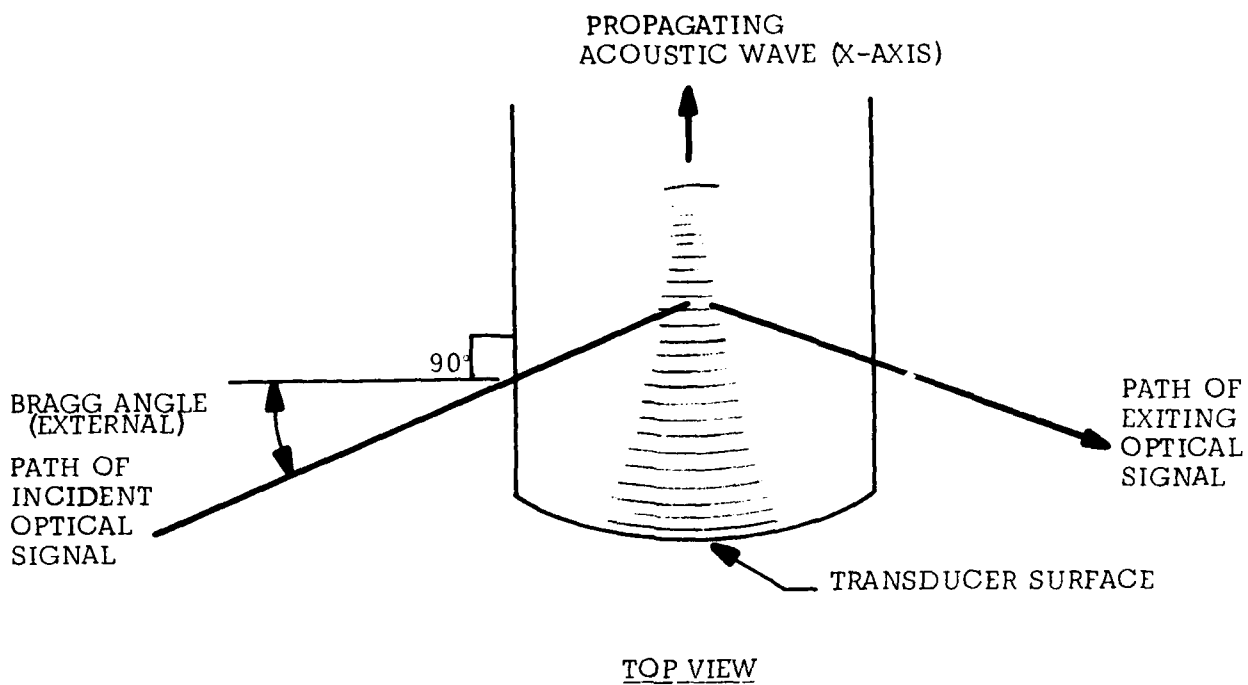
FIGURE 6. RELATIONSHIP OF THE OPTICAL SIGNAL
TO THE ACOUSTIC SUBSTRATE AXIS.

Before preceding with the determination of the exact transducer location, a preliminary calculation was made in order to get some insight into the transducer configuration that would be required for the four-channel acousto-optic component. Using the upper frequency band center frequency of 7.5 GHz, and Equation (1), the Bragg angle for that channel was determined to be $21.2°$. The cosine of this angle is 0.932. Since the Bragg angle will be smaller for the other bands, and hence the $\cos \theta_B$ closer to unity, we will set $\cos \theta_B$ to be equal to one in Equation (2). Solving Equation (2) for this condition, we obtain:

$$\Delta f_{channel} = 4.11 \times 10^{10} \Delta \phi \tag{3}$$

Using Figure 3a, the length (L) of the acoustic transducer in the direction of laser propagation can be related to the radius of curvature (R) for the cylindrical surface

$$L = R \Delta \phi \tag{4}$$

We then determined the maximum angular increment required per channel to ensure optimum Bragg angle acousto-optic efficiency for the full GHz bandwidth. (Appendix B gives the Bragg angle versus frequency results for lithium niobate.) From Table B-1, this angle is found to be

$$\Delta \theta = (10.086 - 5.023) = 5.064 \text{ degrees} = 0.0884 \text{ radians} \tag{5}$$

If we assume that all transducers are in line, the maximum value of $\Delta \phi$ is given by

$$\Delta \phi \leq \Delta \theta / \text{ number of channels} \tag{6}$$

Substituting $\Delta \phi$, from Equation (4) into Equation (3), and then using the results of Equations (5) and (6), we find that

$$\Delta f_{channel} \leq 3.63 \times 10^9 \text{ Hz/four (4) channels} \qquad (7)$$

The results of Equation (7) clearly indicate that each individual in-line channel will have less than the required 1 GHz bandwidth. The reason for this is that, in the in-line configuration, the transducer dimension L cannot be made large enough to produce all the acoustic wave vectors necessary to deflect light over the full channel bandwidth. In other words, each channel transducer must have a physical separation from its neighboring channel. Due to this separation, some of the acoustic wave vector components are missing, and it is these missing frequency components which leave regions within the passband where deflection will not occur.

The problem of channel bandwidth was reasonably easy to overcome by using two acousto-optic crystals. Each crystal would have two transducers, each covering alternate bands. That is, one crystal would accommodate channels 1 and 3, while the other would have channels 2 and 4. Figure 7(a) conceptually details how this multi-channel, dual crystal arrangement was configured. This configuration allows each channel's transducer to be sufficiently long (in the L direction) to produce the necessary Bragg-matched acoustic wave vectors for operation over the full bandwidth of each channel. A second arrangement was also investigated — one in which all four of the transducers would be deposited on a single substrate [Figure 7(b)]. The key element in this arrangement is the staggered location of every other transducer. This, as in the dual-crystal configuration, will allow the transducer length to be appropriately designed for full bandwidth Bragg operation.

Having determined the basic configuration required to achieve the full operational bandwidth, we proceeded with the detailed calculation of transducer channel location. This was done by using Equations (1) and (2), setting the $\Delta f_{channel}$ equal to 1 GHz, and solving for the center frequency Bragg angle and $\Delta \varphi$ of each channel. The results are tabulated in Table III.

CHANNEL NO. 1
TRANSDUCER
4-5 GHz

CHANNEL NO. 3
TRANSDUCER
6-7 GHz
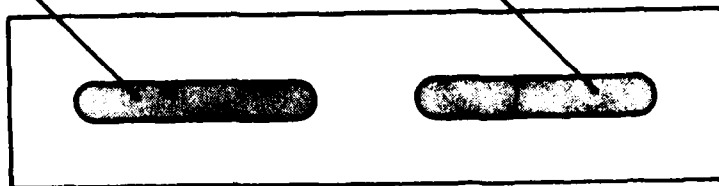
FIRST ACOUSTO-OPTIC SUBSTRATE

SECOND ACOUSTO-OPTIC SUBSTRATE
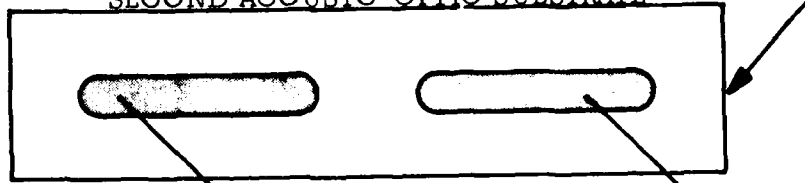
CHANNEL NO. 2
TRANSDUCER
5-6 GHz

CHANNEL NO. 4
TRANSDUCER
7-8 GHz

FIGURE 7A.   MULTI-CHANNEL, DUAL-CRYSTAL
TRANSDUCER ARRANGEMENT.

ACOUSTO-OPTIC SUBSTRATE
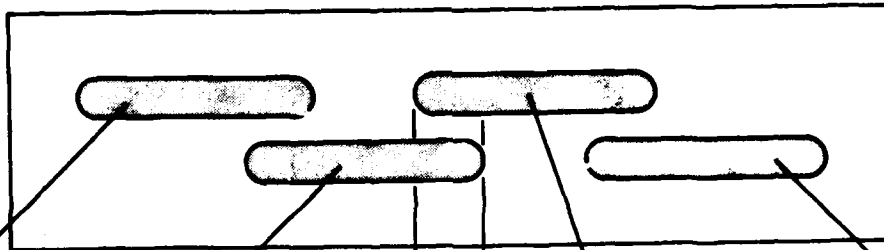
CHANNEL NO. 1
TRANSDUCER
4-5 GHz

CHANNEL NO. 2
TRANSDUCER
5-6 GHz

CHANNEL NO. 3
TRANSDUCER
6-7 GHz

CHANNEL NO. 4
TRANSDUCER
7-8 GHz

"OVERLAP"
REGION

FIGURE 7B.   MULTI-CHANNEL, SINGLE-CRYSTAL
TRANSDUCER ARRANGEMENT.

FIGURE 7.   MULTI-CHANNEL TRANSDUCER CONFIGURATIONS.

TABLE III

BRAGG ANGLE AND CHANNEL-FOCUS ANGLE ($\Delta\varphi$) DATA

FREQUENCY BAND	CENTER FREQUENCY	BRAGG ANGLE (1) (θ_B)	$\cos \theta_B$	$\Delta\varphi$
1	4.5 GHz	12.5°	.976	.0249 radian
2	5.5 GHz	15.4°	.964	.0252 radian
3	6.5 GHz	18.2°	.950	.0256 radian
4	7.5 GHz	21.2°	.932	.0261 radian

(1) The externally referenced Bragg angle; see Appendix B.

Transducer Length

We then set the radius of curvature (R) of the cylindrical surface to be 0.5 inch. (There was nothing "magic" about the selection of this number. It was merely a convenient value.) Next, using equation (4), we determined the length (L) of each transducer.

$$L = R\Delta\varphi = 0.5" \; \Delta\varphi \tag{8}$$

by substituting in the values just obtained for $\Delta\varphi$. The calculated dimensions are contained in Table IV.

TABLE IV

TRANSDUCER LENGTH DIMENSION

FREQUENCY BAND	CHANNEL-FOCUS ANGLE ($\Delta \gamma$)	TRANSDUCER LENGTH (L)
1	.0249 radian	.01245 inch
2	.0252 radian	.01260 inch
3	.0256 radian	.01280 inch
4	.0261 radian	.01305 inch

Adjacent Channel Spacing

Using the length L tabulation of Table IV, we then calculated the spacing between the transducers for each band-pair, i.e., between channels 1 and 3 and between channels 2 and 4. Selecting the laser incident angle to be at the Bragg angle of the overall center frequency (6.0 GHz), then the angle between the center of each channel's acoustic wave, with respect to the center of the next channel, can be obtained from Table A-1, Appendix A. Using the channel center frequencies of 4.5 GHz, 5.5 GHz, 6.5 GHz and 7.5 GHz, the angular difference between each channel and the long (acoustic propagation direction) axis of the crystal was determined. These values are shown in Table V.

TABLE V

ACOUSTIC CHANNEL SEPARATION

FREQUENCY BAND	$\Delta\theta = \theta - \theta_2$ (Appendix A)	$\Delta\theta$ (radians)	$\Delta\theta$ (inches)	ADJACENT CHANNEL SEPARATION
1	-1.894°	-.033	-.0165	Between 1 and 3: 0.022 inches
2	-0.632°	-.011	-.0055	
3	+0.632°	+.011	-.0055	Between 2 and 4: 0.022 inches
4	+1.902°	+.033	-.0165	

The adjacent channel separation is approximately 1.26° (the difference in the respective $\Delta\theta$'s), which equals 0.022 radian. Since we have alternate channels, the spacing on each crystal is twice this value, or 0.044 radian. Using equation (4) and the 0.5" radius of curvature, we found that the channel separation on each crystal was 0.044 radian x 0.5 inch, or 0.022 inch.

Transducer Height Calculation

The next task was to determine the height of each acoustic transducer required to provide the desired efficiency in each band. The acousto-optic interaction efficiency at band center is given by:

$$Eff = \sin^2 \eta^{1/2}$$

$$\text{where } \eta = \frac{\pi^2}{2\lambda_o^2} \frac{n^6 p^6}{\rho v^3} \frac{P_a L}{H \cos^2\theta_B} \tag{9}$$

and where

ρ = density

p = elasto-optic coefficient

n = index of refraction

v = acoustic velocity

λ_0 = laser wavelength

P_a = acoustic power in the interaction area

H = height of the acoustic beam (transducer)

L = acousto-optic interaction length (along laser propagation direction)

θ_B = Bragg angle

For our selected substrate, lithium niobate, we find that

$$\frac{n^6 p^2}{\rho v^3} = 6.95 \times 10^{-18} \text{ sec}^3 \text{ gm}^{-1}$$

$$n = 2.2$$

$$v = 6.57 \times 10^5 \text{ cm/sec}$$

Using equation (9), and the constants for the LiNbO$_3$ substrate and the HeNe laser, we find that

$$\text{Eff} \approx 0.0856 \frac{P_a L}{H \cos^2 \theta_B} \tag{10}$$

To complete the solution, we needed to know the amount of acoustic power in the interaction region, relative to that power applied to the transducer (P_{inc}). To do this, it was necessary to take into account both the conversion loss of the piezoelectric transducer and the acoustic propagation loss. From the design data given in Table VI, we determined the conversion loss versus frequency for each acoustic channel.

TABLE VI

TRANSDUCER DESIGN - CONVERSION LOSS

INPUT PARAMETERS		
T (0, 1)	THICK ZINC-OXIDE FILM (ANGS.)	2300
T (1, 1)	THICK GOLD COUNTER ELECT. (ANGS.)	2000
T (6, 1)	THICK TOP DOT GOLD (ANGS.)	1300
D (1, 1)	D (2, 1) (MILS) DOT DIAM. 7.14	(EQUIVALENT TRANSDUCER AREA)

BOND DIAM. 3 (MILS)

L (8, 1)   SERIES WIRE - INDUCTANCE (NH)   .4

LONGITUDINAL WAVE ALONG X(A) AXIS LINBO$_3$...CRYSTAL VEL. = 65.49E+04

CM/SEC DELAY = .500 MICROSEC   CRYSTAL LENGTH = .1289 INCHES

BAND 1: 4-5 GHz

FREQUENCY (GHz)	CONV LOSS (dB)	MATCHED (1) CONV LOSS (dB)	ROD LOSS (dB)	DIFFR. LOSS-1 (dB)	DIFFR. LOSS-3 (dB)	INSER LOSS (dB)	TRIPLE TRAVEL (dB)
4.00	20.6	14.5	2.8	.7	2.2	44.7	10.5
4.20	21.5	15.1	3.1	.7	2.0	46.8	10.2
4.40	22.4	15.2	3.4	.7	2.0	48.7	10.2
4.60	23.0	15.0	3.7	.6	1.9	50.4	10.5
4.80	23.6	14.8	4.0	.6	1.8	51.9	10.9
5.00	24.1	14.5	4.4	.6	1.7	53.1	11.4

BAND 2: 5-6 GHz

FREQ (GHz)	CONV LOSS (dB)	MATCHED (1) CONV LOSS (dB)	ROD LOSS (dB)	DIFFR. LOSS-1 (dB)	DIFFR. LOSS-3 (db)	INSER LOSS (dB)	TRIPLE TRAVEL (dB)
5.00	24.1	16.8	4.4	.6	1.7	53.1	11.4
5.20	24.4	16.9	4.7	.6	1.7	54.1	12.0
5.40	24.6	17.1	5.1	.5	1.6	54.9	12.7
5.60	24.8	16.9	5.5	.5	1.5	55.5	13.4
5.80	24.8	16.8	5.9	.5	1.5	56.0	14.3
6.00	24.8	16.8	6.3	.5	1.4	56.3	15.3

BAND 3: 6-7 GHz

FREQ (GHz)	CONV LOSS (dB)	MATCHED (1) CONV LOSS (dB)	ROD LOSS (dB)	DIFFR. LOSS-1 (dB)	DIFFR. LOSS-3 (dB)	INSER LOSS (dB)	TRIPLE TRAVEL (dB)
6.00	24.8	17.4	6.3	.5	1.4	56.3	15.3
6.20	24.6	17.3	6.7	.5	1.4	56.4	16.3
6.40	24.4	17.2	7.2	.4	1.3	56.5	17.5
6.60	24.2	17.1	7.6	.4	1.3	56.6	18.9
6.80	24.1	17.2	8.1	.4	1.3	56.7	20.4
7.00	24.1	17.2	8.6	.4	1.2	57.2	21.9

BAND 4: 7-8 GHz

FREQ (GHz)	CONV LOSS (dB)	MATCHED (1) CONV LOSS (dB)	ROD LOSS (dB)	DIFFR. LOSS-1 (dB)	DIFFR. LOSS-3 (dB)	INSER LOSS (dB)	TRIPLE TRAVEL (dB)
7.00	24.1	17.3	8.6	.4	1.2	57.2	21.9
7.20	24.4	16.9	9.1	.4	1.2	58.3	23.4
7.40	25.1	16.6	9.6	.4	1.2	60.1	24.6
7.60	26.1	16.5	10.1	.4	1.1	62.7	25.4
7.80	27.5	16.7	10.6	.4	1.1	65.9	26.0
8.00	29.0	17.2	11.2	.4	1.1	69.6	26.6

NOTE:

(1) The matched conversion loss was calculated using a simple 3-stage microstrip impedance transformer for each channel. The initial criterion was to provide as flat a conversion loss as possible across each channel. The design particulars of the matching approach are discussed elsewhere in this report.

-29-

Next, we determined the acoustic propagation loss (0.1 dB/μsec - GHz^2 for LiNbO$_3$) for the .200 microsecond acousto-optic "window" needed to provide 5 MHz of resolution. This calculation was similar to the one performed in Paragraph II-I-b, but this time we used several frequencies in each channel. The propagation loss data is summarized in Table VII, along with the tuned and untuned conversion loss for each channel and the calculated acoustic power in the interaction region.

TABLE VII

INTERACTION ACOUSTIC POWER VERSUS INCIDENT RF POWER

FREQUENCY (GHz)	CONVERSION LOSS (dB)		PROPAGATION LOSS (dB) (1)	TOTAL LOSS (dB)	ACOUSTIC INTERACTION POWER (mW) (2)
	Unmatched	Matched		Matched	
4.0	20.6	14.5	.64	15.14	31
4.2	21.5	15.1	.71	15.81	26
4.4	22.4	15.2	.77	15.97	25
4.6	23.0	15.0	.85	15.85	26
4.8	23.6	14.8	.92	15.72	27
5.0	24.1	14.5	1.00	15.5	28
5.0	24.1	16.8	1.00	17.8	16.5
5.2	24.4	16.9	1.08	17.98	16
5.4	24.6	17.1	1.17	18.27	15
5.6	24.8	16.9	1.25	18.15	15.3
5.8	24.8	16.8	1.35	18.15	15.3
6.0	24.8	16.8	1.44	18.24	15.1
6.0	24.8	17.4	1.44	18.84	13
6.2	24.6	17.3	1.54	18.84	13
6.4	24.4	17.2	1.64	18.84	13
6.6	24.2	17.1	1.74	18.84	13
6.8	24.1	17.2	1.84	19.04	12.5
7.0	24.1	17.2	1.96	19.16	12
7.0	24.1	17.3	1.96	19.26	11.8
7.2	25.1	16.9	2.07	18.97	12.7
7.4	27.5	16.6	2.19	18.79	13.2
7.6	26.1	16.5	2.31	18.81	13.1
7.8	27.5	16.7	2.43	18.5	14
8.0	29.0	17.2	2.56	19.76	10.5

(1) For a .200 μsec (.050") interaction aperture, located approximately .050" from the transducer surface.

(2) Available (approximate), matched, acoustic power within the substrate; estimated for 1 watt of incident RF power.

If we substitute the respective values of acoustic power for each channel into equation (10), and use the values calculated for L (Table IV), we can determine the height of each transducer. The NRL specified efficiencies could be theoretically satisfied using the values of H given in Table VIII.

TABLE VIII

TRANSDUCER HEIGHT DIMENSION

FREQUENCY BAND	CENTER FREQUENCY (GHz)	EFFICIENCY SPECIFICATION (¢ PER RF WATT)	TRANSDUCER HEIGHT, H (mils)
1	4.5	4.0	0.75
2	5.5	3.5	0.50
3	6.5	3.0	0.50
4	7.5	3.0	0.60

However, experience dictates that fabricating a transducer which satisfies the dimensions needed for H is probably not possible. Dimensions on the order of 1 mil are more likely, both in the mask and in the transducer itself. This increase in transducer height will result in a lower acousto-optic efficiency. The band center efficiency performance that can be expected from each channel for the minimum transducer height of .001" is summarized below.

FREQUENCY BAND	CENTER FREQUENCY (GHz)	TRANSDUCER HEIGHT, H (mils)	EFFICIENCY (¢ PER RF WATT)
1	4.5	1.0	2.9
2	5.5	1.0	1.7
3	6.5	1.0	1.6
4	7.5	1.0	1.7

These values of H, and the values previously shown for L, precisely define
the transducer patterns for each channel to be deposited on each crystal.
Figure 8 illustrates the configuration and location of each transducer, as
taken directly from the "deposition" artwork used to fabricate the trans-
ducer mask, which is in turn used to deposit the transducers on the
acousto-optic substrate. (Please note that the single-crystal, multiple-
transducer approach was used. This more complex arrangement was
selected in order to gain valuable experience with this type of configuration —
particularly since production, cost-effective hardware will most certainly
be manufactured on a single crystal.)
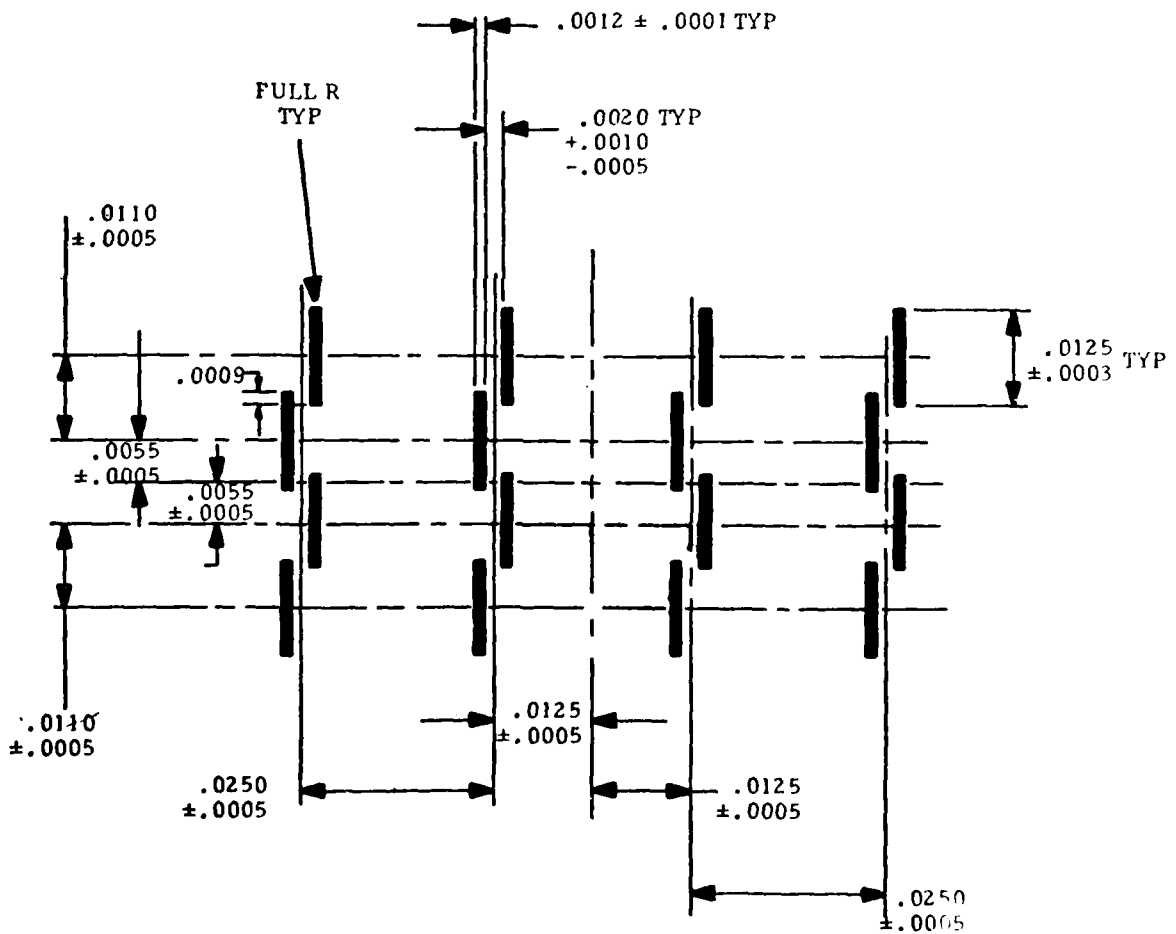
FIGURE 8. MULTI-CHANNEL, SINGLE-CRYSTAL
TRANSDUCER ARRANGEMENT.

-32-

Bragg Cell Substrate Orientation and Configuration

The orientation of the lithium niobate acousto-optic substrate is specified by the parameters shown in Figure 9. The crystal must be long enough to provide the .2 μsec acoustic aperture, which for $LiNbO_3$ is about .052 inch. The additional crystal length shown is required so that the incident laser beam can enter and exit the crystal at the appropriate Bragg angle.

The Bragg cell portion of the processor analyzer has now been completely defined. The next section covers the design considerations and analysis behind the optics used in the spectrum analyzer.

2. Design of the Optics for the Spectrum Analyzer

The optical components which, along with the acousto-optic Bragg cell, make up the remainder of the spectrum analyzer are fairly standard. Referring again to the schematic representation of the demonstration spectrum analyzer, Figure 10, we comment in some detail on each of the constituent components.
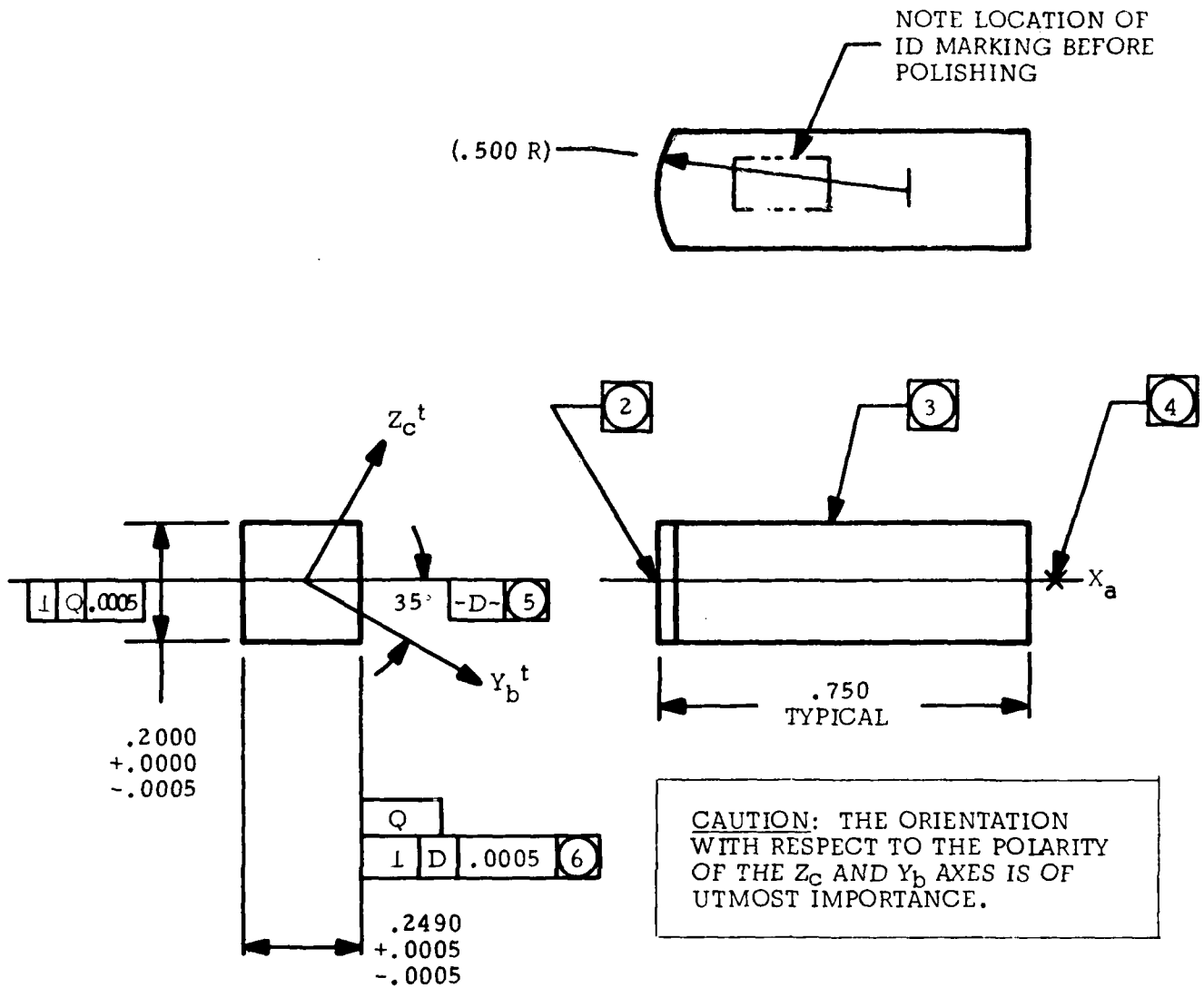
NOTE LOCATION OF ID MARKING BEFORE POLISHING

(.500 R)

NOTES:
1. "BACK" FACE AND "FRONT" FACE POLISHED: $\lambda/4$ OR BETTER (SODIUM LIGHT).

2. END RADIUS OF CURVATURE = .500 + .001 FACE POLISHED: $\lambda/4$ OR BETTER TYPE POLISH/BEST EFFORT.

3. TOP AND BOTTOM FACES FINISH: LAPPED FINISH.

4. LONG AXIS OF ROD ORIENTED ALONG X_a AXIS TO WITHIN: 30 MINUTES.

5. POLISHED SIDE FACES TO BE PARALLEL TO DATUM Q.

6. POLISHED SIDES TO BE PARALLEL 20 ARC SECONDS OR BETTER.

7. END ORIENTATION IS DETERMINED VIA (5) WITH RADIUS OF CURVATURE CENTERED BETWEEN THE POLISHED FACES WITHIN .005 OR BETTER.

8. SURFACE QUALITY (SCRATCH AND DIG): 10-5.

9. .005 TO .010 CHAMFER AT 45°; LONG EDGES.

FIGURE 9. POLISHED LITHIUM NIOBATE ACOUSTO-OPTIC SUBSTRATE DRAWING.

-34-
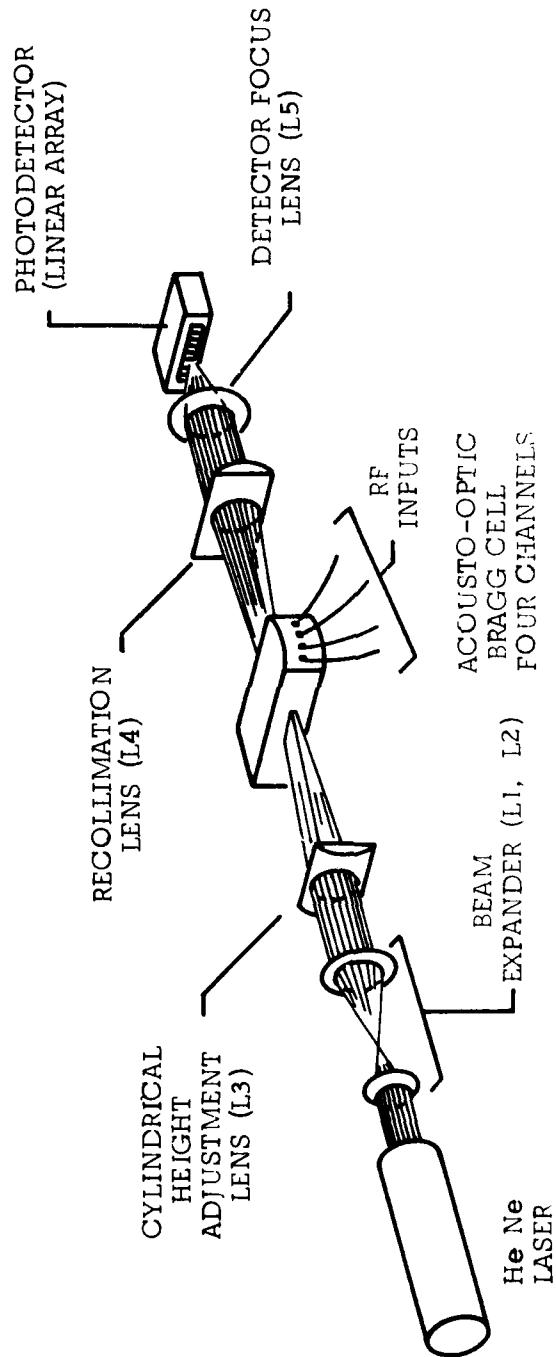
FIGURE 10. SCHEMATIC REPRESENTATION OF THE DIRECT A/O PROCESSOR SPECTRUM ANALYZER.

a. Laser and Beam-Shaping Optics

The light source used in the demonstration of the Direct RF A-O Processor Spectrum Analyzer was a HeNe laser. The operating data and characteristics of this device are shown in Table IX.

TABLE IX

15 mW HELIUM-NEON LASER

Model 124B Specifications

Output

Wavelength:	632.8 nm	1152 nm (opt.)	3391 nm (opt.)
Power TEM$_{oo}$:	15 mW	2 mW	4 mW

Beam Characteristics

Beam Diameter (@ 1/e^2):	1.1 mm	1.4 mm	2.5 mm
Beam Divergence:	.75 mrad	1.0 mrad	1.8 mrad

Optics

Output Mirror:	G3817-005	G3817-002	G3817-003
High Reflector:	G3862-011	G3801-005	G3801-003
Installation & Test:		c/n 124-3	c/n 124-4

Resonator Characteristics

Transverse Mode:	TEM$_{oo}$
Degree of Polarization:	1 x 10^{-3}
Angle of Polarization:	Vertical ±5°
Resonator Configuration:	Long radius
Resonator Length:	70.1 cm
Axial Mode Spacing:	214 MHz
Plasma Excitation:	Direct current, self-starting

Amplitude Stability

Beam amplitude noise (1-100 kHz):	<0.3% rms
Beam amplitude ripple (1-120 Hz):	<0.2% rms
Long term power drift:	<5% over 10°C
Warm-up time:	1 hour

Environmental Capability

Operating temperature:	10°C to 40°C (50°F to 105°F)
Altitude:	Sea level to 3000 m (10,000 ft.)
Humidity:	Below dew point

Power Requirements

Voltage:	115/230 V ±10%
Power:	125 watts

Physical Characteristics

Weight: Laser Head:	11.4 kg (25 lbs.)
Power Supply:	3.5 kg (7.5 lbs.)
Shipping Weight:	17.5 kg (38 lbs.) 2 pieces
Cable Length (Power Supply to Laser):	1.8 meters (6 ft.)

Dimensions in $\frac{mm}{in}$

$\frac{816}{32.13}$

$\frac{47}{1.85}$

$\frac{83}{3.32}$

Beam Expander Lens System

From the above data, we know that the laser beam has a typical beam diameter
of 1 mm. This diameter is not sufficient to cover the 0.2 microsecond aper-
ture (in the beam "width" direction) of the acousto-optic interaction region,
a distance of more than 1.3 mm, and a beam expander is therefore required.
The 2x beam expander, described in Table X, was found to be sufficient to
cover the required resolution aperture, plus any additional aperture required
to support the side lobe-reducing truncation of the optical beam.

TABLE X

BEAM EXPANDER SPECIFICATIONS

The following biconvex lens-pair configuration will provide the beam expansion
necessary to widen the optical beam for this application.
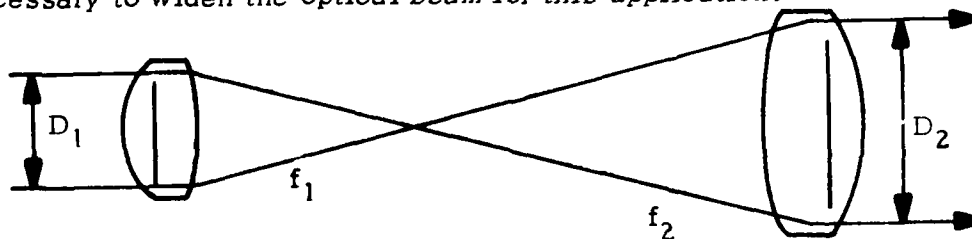
Expansion Ratio: $A = \dfrac{D_2}{D_1} = \dfrac{f_2}{f_1}$

Possibilities for A

A	f_2	f_1
2:1	20	10
	200	100
1.5:1	30	20
	150	100
3:1	30	10
	100	30
5:1	100	20
	150	30
6.5:1	200	30
7.5:1	150	20
10:1	100	10
	200	20
15:1	150	10
20:1	200	10

Expander Optics

f (mm)	Md (mm)	Rd (mm)	Cat. No.	Holder	Aperture Ø (mm)	Cat. No.
			Unmounted			**Mounted**
10	2.2	1.2	31 1301	C	5	06 3092
20	2.6	1.4	31 1302	C	9	06 3093
30	4.5	1.8	31 1303	C	17	06 3094
100	4.5	2	31 1304	31.5	30	03 1754
100	4.5	2	31 1304	in adapter plate		06 3089
150	4	2.4	31 1305	31.5	30	03 1755
150	4	2.4	31 1305	in adapter plate		06 3090
200	4	2.8	31 1306	31.5	30	03 1756
200	4	2.8	31 1306	in adapter plate		06 3091

In order to achieve a 2x expansion of the optical signal,
the 10 and 20 mm focal length lenses are used.

Truncation of the Optical Beam Width

The spectrum analyzer weighting function that ensures a minimum sidelobe and spurious signal contribution is composed of a number of factors including aperture size, acoustic attenuation and the optical amplitude profile. One of the more controllable aspects of these weighting functions is the optical beam profile. Many lasers, such as the HeNe used during this investigation, have a Gaussian beam cross section. However, when illuminated by the received RF pulse, the resultant optical spectrum will have inherent sidelobes. The sidelobe level is determined by how much the beam is truncated by the optical "window" formed with the RF signal. The window, of course, must be at least wide enough to allow interaction with the entire acoustic pulse. For this program, the pulse, or "window," must be at least .200 microseconds long. The effective superposition of the crystal aperture on the optical beam, while lowering unwanted sidelobes, will also cause a degradation in resolution. The loss of resolution comes from a widening of the beam's main lobe (-3 dB point), which is transformed into a larger spot size at the detector. Using the curves of Figure 11, it is possible to determine what truncation should be used to obtain the lowest sidelobe level possible, with the minimum increase in spot size.

The "instantaneous" dynamic range requirement for the spectrum analyzer is 50 dB. From Figure 11, we determined that the truncation ratio needed to achieve more than 50 dB of sidelobe suppression is 2.0 or greater. Figure 11(b) illustrates that, for this particular ratio, there will be an increase in the relative half bandwidth of about 59 percent (from 1.0 to 1.7). To accommodate the needed 50 dB sidelobe truncation window size, the optical aperture will have to be 1.7 times larger than the 0.052 inch aperture needed to satisfy the 5 MHz resolution requirement, or about 0.088 inch.

Figures 11(a) and 11(b) clearly evidence that there will be some effect on both the sidelobe suppression and the resolution due to the insertion loss effects experienced as the acoustic signal moves through the optical aperture.

RELATIVE
OPTICAL
POWER (dB)

HIGHEST
SIDELOBE
LEVEL

(RELATIVE
TO PEAK)
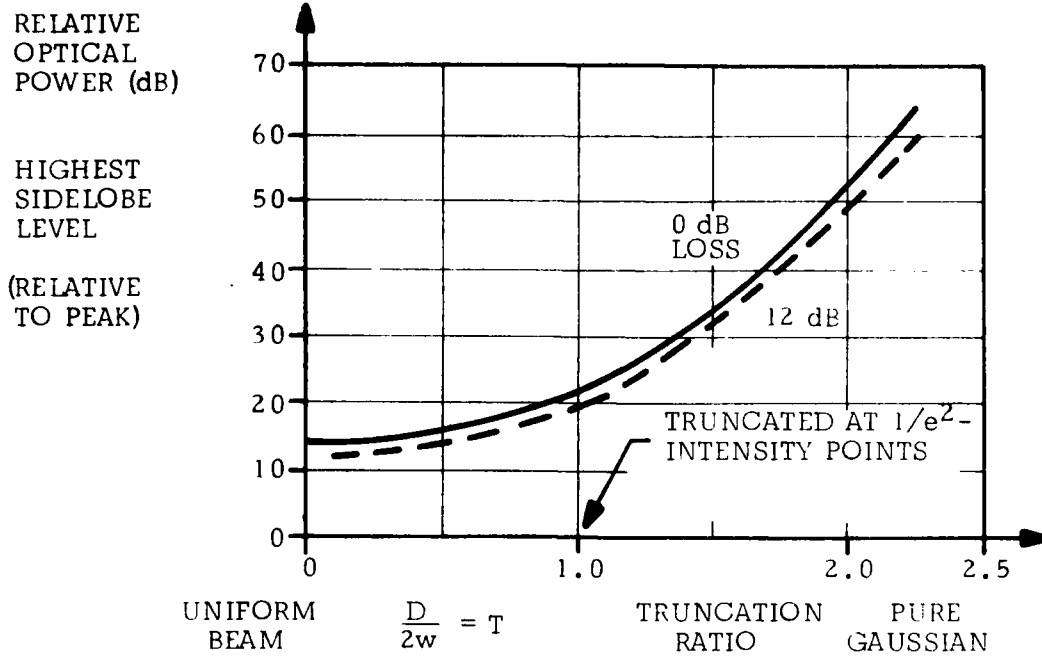
FIGURE 11A. HIGHEST SIDELOBE LEVEL FOR TRUNCATED GAUSSIAN.
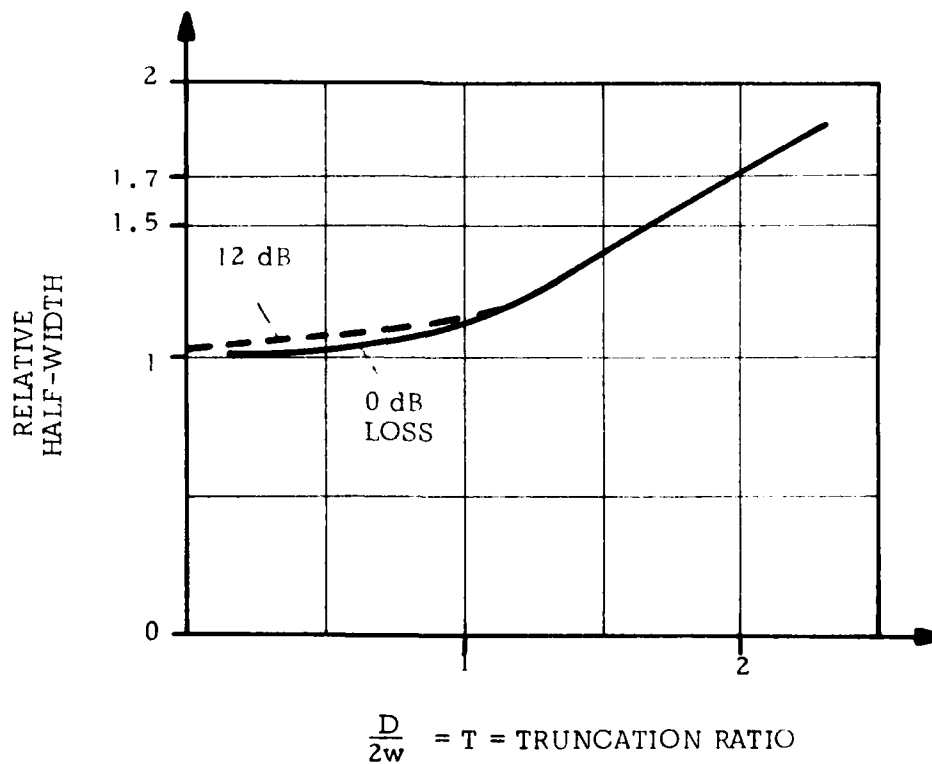
FIGURE 11B. RESOLUTION LOSS DUE TO APODIZATION.

It was determined that the insertion loss across the acousto-optic inter-
action region increased the expected sidelobe level by approximately 2 dB.
To accommodate the higher sidelobe level, our design was modified to use
a truncation ratio of slightly more than 2:1, consistent with about a -52 to
-53 dB sidelobe level. The resulting optical aperture on the Bragg cell
required only a small modification, to about 0.090 inch. (The optical beam
width, including truncation, must accommodate this aperture — approxi-
mately 2.3 mm).

Laser Beam Height Adjustment

The next optical element is the cylindrical lens (L3), which is used to
adjust the height of the optical beam in the acousto-optic interaction region
for optimum efficiency. A predetermined height of about 0.001 inch within
the crystal (essentially equal to the acoustic beam height calculated in the
previous section) was selected. The adjustment of the height can be made
by selecting the appropriate focal length for L3, using the following ex-
pression

$$\frac{\lambda F}{D} \cong H \tag{11}$$

where

λ = the optical wavelength

F = the lens focal length

D = the diameter of the laser beam incident on the lens

The exact optical beam height, with respect to the acoustic wave height (H),
can be adjusted by moving the crystal (the interaction region) either closer
to or farther from the L3 lens. (It was determined that a cylindrical lens
with a focal length of approximately two inches would be appropriate for
this application.) The characteristics of this lens are given in Table XI.

TABLE XI

CYLINDRICAL LENS SPECIFICATIONS
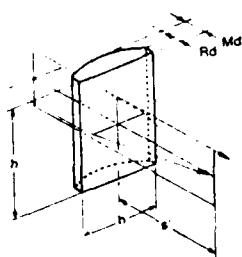
f (mm) ± 5% λ = 588 nm	Cylinder Height (mm) h11	Cylinder Width (mm)	Intersection Distance s' (mm)	Md (mm)	Rd (mm)	Unmounted Cat No	Holder	Aperture (mm)	Mounted Cat No
5	Ø12.5 d10	5	3.2	2.4		31 8801	C	⌀11 5×5	06 3420
10	Ø18 d10	9.5	6.5	4.0		31 8802	C	⌀17×9 5	06 3421
40	Ø18 d10	15 h11	37.7	2.7		31 8814	C	⌀17×15	06 3422
40	60	15 h11	37.7	2.7	1.3	31 8811	TS	58×13	03 1830
40	130	15 h11	37.7	2.7	1.3	31 8812			
60	60	20 h11	57.8	3.0	1.4	31 8821	TS	58×18	03 1831
60	130	20 h11	57.8	3.0	1.4	31 8822			
80	Ø31.5 d10	30 h11	77.2	4.0		31 8834	31.5	⌀30	03 1850
80	60	30 h11	77.2	4.0	1.2	31 8831	TS	58×28	03 1832
80	130	30 h11	77.2	4.0	1.2	31 8832			
100	60	50-0.5	94.5	8.0	1.6	31 8851	TS	58×48	03 1833
150	60	50-0.5	145.6	6.0	1.9	31 8852	TS	58×48	03 1834
200	Ø31.5 d10		196.2	5.0		31 8835	31.5	⌀30	03 1849
200	60	50-0.5	196.2	5.0	2.0	31 8853	TS	58×48	03 1835
250	60	50-0.5	244.6	4.5	2.0	31 8854	TS	58×48	03 1836
300	60	50-0.5	296.0	4.0	2.0	31 8855	TS	58×48	03 1837
− 90	60	50-0.5	− 92.8	4.5	11.5	31 6601	TS	58×48	03 1828
−145	60	50-0.5	−148.2	4.0	8.0	31 6602	TS	58×48	03 1829

The component type selected for this application was a 40 mm focal length lens, with a 15 mm cylinder width and 60 mm cylinder height.

b. Post Bragg Cell Processing Optics

After the laser beam has passed through the Bragg cell acousto-optic crystal and has been deflected, it is in need of additional optical processing in order for it to be adequately detected. First, the diverging beam that exits the acousto-optic crystal must be recollimated. The then parallel beam can be focused on the output photodetector array.

Recollimation Lens

The output or recollimation lens (L4) is identical to that cylindrical lens used to adjust the height of the laser beam. The characteristics of this lens were given in Table XI.

Focusing Lens

The final optical component to be considered is the output spherical lens (L5). Using equation (11), and knowing that a diffraction-limited optic spot (at the detector) is needed, we determined the characteristics required of this lens. Specifically, a focal length of approximately 3.6 inches (91.7 mm) was used to provide the 0.001 inch diffraction-limited spot needed by the detector. Table XII illustrates the performance specification for this lens.

TABLE XII

FOCUSING-SPHERICAL (BICONVEX) LENS SPECIFICATIONS
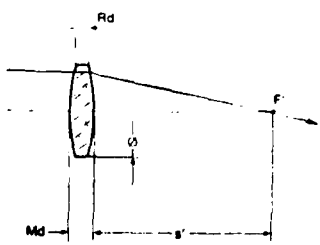
f (mm) ±5% λ = 588 nm	Ø (mm) h11	Intersection Distance s' (mm)	Md (mm)	Rd (mm)	Unmounted Cat No	Holder	Aperture (mm)	Mounted Cat No
10	10	9.9	3.5	1.4	31 1100	C	9	06 3019
12.5	12.5	11.4	4.2	1.0	31 1177	C	11.5	06 3032
16	18	14.5	6.5	1.3	31 1178	C	17	06 3033
20	22.4	17.0	7.8	1.4	31 1138	C	21.4	06 3020
25	22.4	23.0	6.5	1.7	31 1108	C	21.4	06 3021
30	22.4	28.0	6.0	2.0	31 1110	C	21.4	06 3022
40	22.4	38.0	5.0	2.0	31 1114	C	21.4	06 3023
50	22.4	48.5	4.5	2.1	31 1115	C	21.4	06 3024
60	22.4	58.8	4.0	2.0	31 1116	C	21.4	06 3025
80	22.4	79.0	3.5	2.0	31 1117	C	21.4	06 3026
100	22.4	99.0	3.5	2.3	31 1118	C	21.4	06 3027
150	22.4	148.7	3.0	2.2	31 1119	C	21.4	06 3028
200	22.4	200.0	3.0	2.4	31 1120	C	21.4	06 3029

The 100 mm (focal length) lens, with a 22.4 mm height and a 99 mm intersection distance was selected for use in demonstrating the spectrum analyzer.

The design will more than accommodate a sweep (deflection) of approximately 1 inch at the focal plane (surface) of the detector array. This was determined by the total required deflection angle (from 15 to 36.3°) as presented in Appendix A of this report.

c. Photodetector Array

The design of the output optical system was predicated on the use of the Reticon photodetector array, Model No. RL-1024C. This unit has 1024 detectors, each spaced at 0.001 inch, making it more than adequate to provide the 800 (4 GHz ÷ 5 MHz per pixel) individually resolvable photo-detector cells (pixels) necessary to provide the 5 MHz of resolution required over the full 4 GHz bandwidth.

A detailed description of the photodetector array is presented in Appendix B.

3. Technology Assessments

Many critical techniques and technologies are required to realize hardware capable of demonstrating the spectral analysis performance required by this program. Optical design and the utilization of optical components and signal processing techniques were, of course, very important, but even more important was the ability to realize the critical acousto-optic component itself. This ability encompasses the expertise necessary to design the best component possible, as well as the skills necessary to make its manufacture a reality.

a. Design Considerations and Trade-Offs

Several design approaches were considered during the evolution of the chosen design. Techniques involving both the transducer design and the number of channels used to cover the full bandwidth were evaluated before determining the optimum approach described earlier in this section.

Faceted Surface Technique

The acousto-optic component design which employs a "faceted" transducer surface, as opposed to a cylindrical one, is illustrated in Figure 12. Basically, the crystal has facets, or flat surfaces polished on the transducer face — one for each transducer. In this approach, the bandwidth of each channel is achieved by the diffraction of the acoustic wave, as opposed to the focused wave provided by the curved surface transducers. This approach requires that the transducer dimension (L), in the direction of the laser beam, be approximately 0.001 inch in length to provide the full 1 GHz bandwidth required by each channel. In addition, the efficiency calculation requirement dictates that the height (H) of each transducer be an order of magnitude smaller than this size. As pointed out earlier (Section II-B-1c, "Transducer Height Calculation") dimensions of this
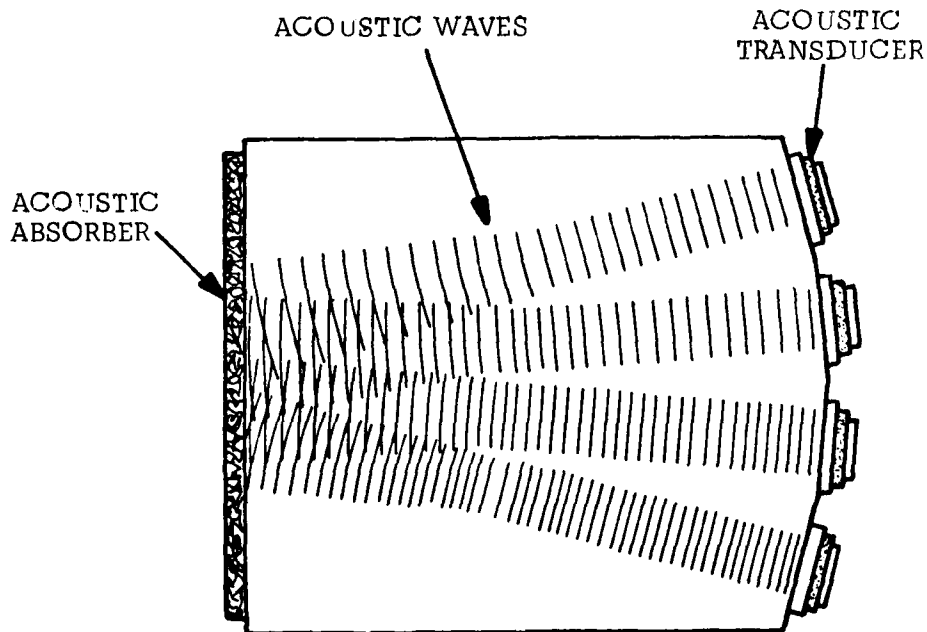
FIGURE 12. ALTERNATE ACOUSTO-OPTIC COMPONENT DESIGN.

magnitude are extremely difficult to fabricate in a transducer deposition mask, not to mention the problems involved with realizing the actual transducer itself. The key problem involved with trying to obtain the 0.001 inch dimension in the width (L) direction is that it makes obtaining the required gigahertz channel bandwidths almost impossible. In the curved surface approach, a change of 0.001 inch in the larger L-dimension will have only a small effect on bandwidth; however, a 0.001 inch error in the faceted-L dimension (up to 0.002 inch, for example) could reduce the bandwidth by as much as 50 percent.

Another drawback to the faceted-surface approach is the polishing of each individual facet. Many experts in the field of crystal polishing were questioned during the design process, with the nearly unanimous opinion that the faceted design would be significantly more difficult to polish than would the curved surface.

Channel-Bandwidth Design

In the chosen design, a trade-off between overall performance and the number of channels used to cover the 4 GHz bandwidth was carefully considered. The ultimate trade-off was between performance and circuit complexity; i.e., the complexity of efficiently getting RF signals into the Bragg cell. Four channels were chosen to cover the required bandwidth because four was the minimum number of channels that would, with a reasonably small amount of complexity, meet all specifications of the spectrum analyzer.

It should be noted, however, that a contingency design plan was formulated using a larger number of RF channels should the design performance so dictate. Increasing the number of channels does have certain advantages. Most significantly, a larger number of channels reduces the band of frequencies that needs to be covered by a given channel — a fact which should result in a lower transducer conversion loss, and hence provide a larger margin of safety in meeting the efficiency specification.

b.   Critical Technology Requirements

The key to producing a Bragg cell capable of performing in accordance with the specification is being able to fabricate a piezoelectric transducer array that will, collectively, operate over the full 4 to 8 GHz frequency range. The following paragraphs discuss briefly those techniques required to produce such transducers.

Transducer Surface Finish

During previous discussions we have stressed the importance of having a high quality surface finish, or polish, on each A-O crystal. Polishing was, in fact, the most important process to be used in the manufacture of the Bragg cell. In short, the transducer surface must be essentially free of "pits and scratches" in the active transducer area. The importance of this is shown schematically by Figure 13, which illustrates the effect of a typical one micron defect beneath the active transducer area. The problem areas (as indicated by the two arrows) occur primarily at the edges of the defect, where the counter-electrode, zinc oxide and transducer layers become very thin. This "thinning" is due primarily to the size of the pit, particularly its depth, which is substantially larger than the thickness of the various layers being deposited. In the worst-case condition, the zinc oxide layer is not continuous around the edge of the crater, allowing the transducer top electrode metalization to come into contact with the counter-electrode, shorting out the transducer. Even if the transducer is not shorted during the deposition process, the zinc oxide layer will not only be substantially thinner in these areas, but could also be poorly oriented crystallographically. The thin zinc oxide causes higher electromagnetic field concentrations to occur in that area of the transducer for a given level of RF input power. The result is a higher incidence of transducer failure, as the increased RF field intensity breaks down the thinner zinc oxide, again shorting the transducer. If the transducer doesn't fail, which isn't often the case, poor crystal growth orientation will substantially affect its electrical performance. The determination of a polished surface finish specification was a major output of this program.

GOLD TRANSDUCER
TOP ELECTRODE
(1100 Å)

ZINC OXIDE
PIEZOELECTRIC
LAYER
(2300 Å THICK)

>0.5 μ

A SURFACE
PIT

~1μ
(10,000 Å)

GOLD
COUNTER ELECTRODE
(2000 Å THICK)

ACOUSTO-OPTIC
SUBSTRATE
(POLISHED SURFACE)
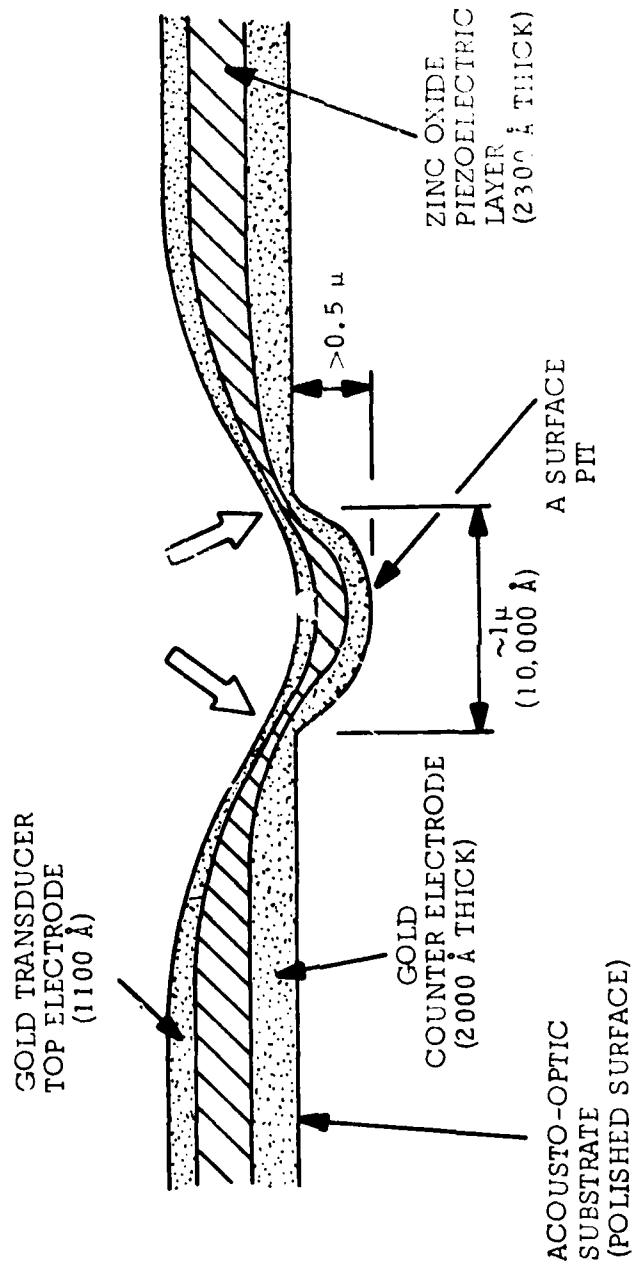
FIGURE 13.   EFFECT OF SURFACE DEFECTS ON TRANSDUCER
FABRICATION AND PERFORMANCE.

Transducer Fabrication Processes

Another important area critical to the manufacture of the acousto-optic
Bragg cell is the transducer deposition process. In this process (or
more correctly, processes) the counterelectrode, the zinc oxide layer,
and the transducer (top) electrode are deposited on the acousto-optic
substrate. Although all layers are important, the zinc oxide and top
electrodes most acutely affect the performance of the Bragg cell.
In the following table, these two important deposition parameters are
listed, along with their design thicknesses, and allowable tolerances.
The zinc oxide deposition is critical as it determines the frequency
response of the transducer, while the top electrode can become highly
resistive (lossy) and bond poorly if too thin, or affect the transducer's
higher frequency conversion loss if deposited too thick.

DEPOSITION PROCESS	DESIGN THICKNESS (Angstrom Units)	TOLERANCE (Angstrom Units)
Zinc Oxide Deposition	2300	±100
Transducer Electrode	1100	± 50

It is clear that the performance success of the Direct RF A-O Processor
Spectrum Analyzer was heavily dependent upon our ability to obtain quality
polished transducer surfaces, as well as being able to achieve the desired
deposition parameters. Beyond question, however, is that the most critical
technology barrier to the successful completion of this program was the sur-
face polish of the curved transducer surface. In the following section, the
extent to which we were able to deal with these and other technical consid-
erations in the manufacture of the spectrum analyzer is presented, as are
the results and conclusions of the demonstration tests.

III. TEST RESULTS AND CONCLUSIONS

A. Fabrication of the Acousto-Optic Bragg Cell

The previous section presented the design approach to realizing the Direct RF Acousto-Optic Processor Spectrum Analyzer, along with some preliminary estimates as to what its performance might be. This section is the logical extension of that design — the manufacture and test of the demonstration hardware.

The acousto-optic Bragg cell component, as stated, consists of an appropriately oriented, single-crystal, optically transparent substrate. On this substrate are deposited the special piezoelectric transducers used to convert the received RF signal into acoustic energy. The subject matter of this section traces the manufacture of the acousto-optic component from the specification of the crystal, to its polishing and preparation, through to the deposition of its transducers.

1. Acousto-Optic Substrate

The acousto-optic substrate material selected for the spectrum analyzer demonstration is lithium niobate. Although this material has a relatively low figure of merit, its low acoustic propagation loss will yield a device with the best overall acousto-optic efficiency.

a. Substrate Specification

Of great importance in achieving high yields for acoustic device processing is the specification and inspection of the acousto-optic substrate material. In the procuring of materials for Bragg cell components, we use the identical procedures that have made Teledyne a leader in acoustic delay lines as well as acousto-optic products. Briefly, the following information is used:

- Designation of the type of crystal...including whether it is single or polycrystalline material.

- Designation of the grade of material desired (acousto-optic grade for this application).

- Designation of the crystalline orientation, with respect to the substrate axis (35° rotated Y-cut, X-propagating).

- Designation of the substrate's cross section dimensions and tolerances...with special instructions concerning the curved surface.

- Designation of the substrate length.

- Specification of the surface finish required...for transducers and optical faces.

- *Designation of parallelism for end and side faces.*

- Designation of the condition of crystal edges.

- Designation of acceptance conditions.

The internal quality of the acousto-optic substrate must also be carefully specified. A standard acoustic substrate specification is one whose requisites include being free of strains and striations when viewed under high intensity light at 20X magnification. Also key in obtaining predictable and repeatable results from acoustic material is the crystallographic orientation specification.

Substrate Specification - Rough Cut and Polished

Typical examples of the specifications used to procure material for this program are shown in Figures 14 and 15. Figure 14 illustrates the basic substrate material specification, which includes the crystallographic orientation and the crystal's prepolished dimensions. Figure 15 is

-50-

the final substrate configuration drawing, which contains the designations for the curved-transducer surface, the substrate's final dimensions and, again, its proper acousto-optic orientation.
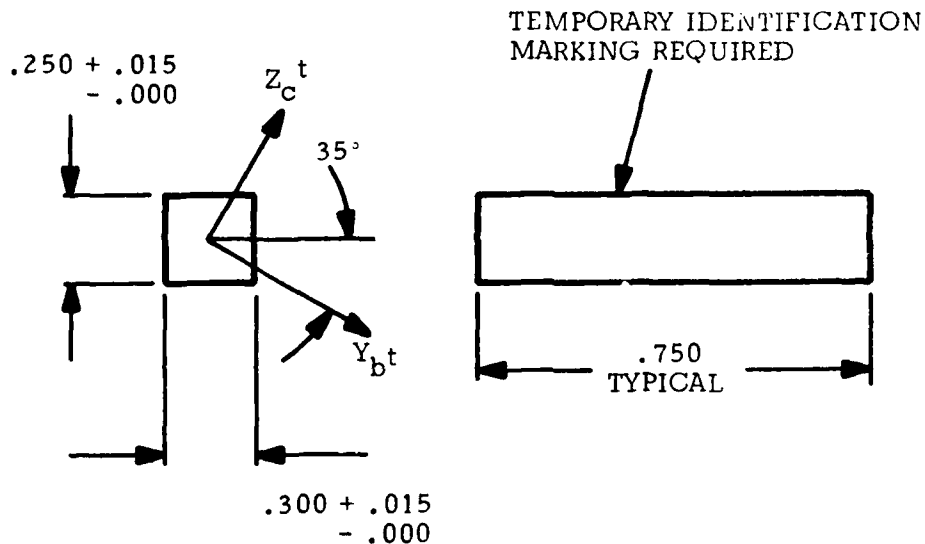
NOTES:

1. Material: X-propagation, 35° rotated Y-cut.

2. Refer to Dwg. No. 104792 (Figure 13) for orientation and additional specifications.

3. Crystals are to be unpolished.

4. Method of testing polarity of axis to be furnished with data.

5. All dimensions are in inches.

FIGURE 14. ROUGH CUT LITHIUM NIOBATE ACOUSTO-OPTIC SUBSTRATE SPECIFICATION.

FIGURE 15. POLISHED LITHIUM NIOBATE ACOUSTO-OPTIC
SUBSTRATE DRAWING.

NOTES:

1. "BACK" FACE AND "FRONT" FACE POLISHED: $\lambda/4$ OR BETTER (SODIUM LIGHT).

2. END RADIUS OF CURVATURE = .500 + .001 FACE POLISHED: $\lambda/4$ OR BETTER TYPE POLISH/BEST EFFORT.

3. TOP AND BOTTOM FACES FINISH: LAPPED FINISH.

4. LONG AXIS OF ROD ORIENTED ALONG X_a AXIS TO WITHIN: 30 MINUTES.

5. POLISHED SIDE FACES TO BE PARALLEL TO DATUM Q.

6. POLISHED SIDES TO BE PARALLEL 20 ARC SECONDS. OR BETTER.

7. END ORIENTATION IS DETERMINED VIA ⑤ WITH RADIUS OF CURVATURE CENTERED BETWEEN THE POLISHED FACES WITHIN .005 OR BETTER.

8. SURFACE QUALITY (SCRATCH AND DIG): 10-5.

9. .005 TO .010 CHAMFER AT 45°; LONG EDGES.

b. Surface Finish - Polished

The Technology Assessment section of this report discussed the importance
of having a high quality polish for the acousto-optic substrate; the need
for a defect-free surface is nowhere more acute than it is on the curved
transducer surface.

Curved Transducer Surface

It was stated on several occasions during the design discussion that the
success of this program would hinge more on the quality of the transducer
surface polish than any other facet of our processes. As the program pro-
gressed, the truth of this was clearly borne out.

The program began in earnest during the late months of 1979, with the
first polished, curved-surface acousto-optic substrates due during the
first quarter of 1980. Early on, however, our two prime vendors, after
submitting quotations, decided to no-bid the job. An immediate search
was made to secure alternative sources for polishing the crystals. (The
material supplier would provide rough cut blanks to our specification,
with the rough blanks then polished to size by another vendor.) Two new
"polish" vendors were placed under contract in January (1980), and
polished crystals were received in April. The polished transducer surfaces
were examined and found to be less than satisfactory. However, for the
sake of expediting the program, it was decided to go ahead and try to
deposit transducers. The next several months were spent attempting to
deposit usable transducers on the received material. We were unsuccessful,
as the surfaces were just too rough and yielded shorted and poorly deposited
transducers. Refer to Figure 13 and its accompanying discussion for a
description of how the various surface pits and scratches, induced by a
poor polish, can affect the transducer deposition and, hence, the device's
performance. Figure 16 illustrates a typical transducer surface from the
acousto-optic substrates received during much of the contractual period
of this program. This type of defect was responsible for transducer
failure via the mechanisms described in Figure 13.
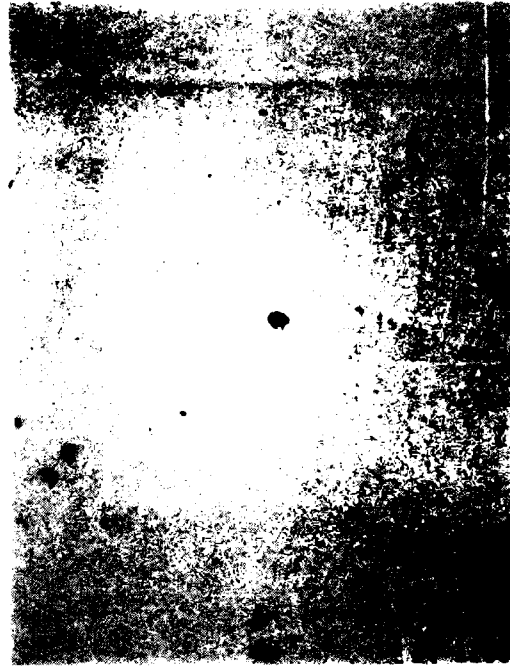
MAGNIFICATION: 15X   MAGNIFICATION: 65X

FIGURE 16. CURVED-TRANSDUCER SURFACE WITH A DEFECTIVE POLISH—
SHOWING PITS, SCRATCHES AND OTHER FLAWS.

During the period of mid-1980 to the end of the year, two meetings were held
with Tony Spezio, the program's technical representative from the Naval
Research Laboratory. The latter of these two visits was to witness testing
on a "partial" Bragg cell — one whose operation was restricted to 500 MHz
in the 5.5 to 7.0 GHz frequency range, due to surface-finish induced de-
fective transducers. During the meeting, the transducer surface finish
problem was discussed in detail, and the prospects of finding a qualified
vendor were assessed. It was decided that the remainder of the program,
in both time and dollars, would be devoted to perfecting the curved sur-
face polish technique and developing a qualified vendor. In addition, a
request for additional funds and a time extension were discussed, and
later officially requested.

The work continued in earnest over the remainder of the year and into 1981 in an attempt to define a reliable source of polished, curved transducer surfaces. The search ranged from the acoustic crystal polishing laboratory at Stanford University to a variety of "commercial" houses, including one firm that had been working closely with us over the past six or seven months. In June of this year (1981), after several marginal to poor samples, we received the first batch of substrates that had an acceptable surface finish. These crystals clearly would support the fabrication of transducers. Figure 17 illustrates the quality of a typical surface finish...one which exhibits virtually no surface defects whatsoever, even at magnification of greater than 200X.

14-1170

MAGNIFICATION: 63X   MAGNIFICATION: 320X

FIGURE 17. CURVED-TRANSDUCER SURFACE SHOWING AN
            EXTREMELY SMOOTH POLISH.

Polish Specification

Based on our recently successful results in obtaining quality transducer surfaces, we have produced a "preliminary" surface finish specification. The specification is predicated on emphasizing that area which is to be dedicated to the transducers...while offering relaxed criteria for the peripheral areas. Figure 18 illustrates, schematically, the specification format we are currently evaluating. The advantage of this approach is that it eliminates "counting," or density type determinations, of defects in a given area. It is based simply on achieving a maximum of one-tenth micron type defects in the active transducer area, without unduly specifying those areas unlikely to be used, or play a part in the deposition process.

COUNTER ELECTRODE AREA

This area shall be defect free when examined under 30x magnification.

EDGE AREA

This area may have some edge "clipping" and other defects — as long as they do not extend into the COUNTER ELECTRODE AREA.

25 mils

25 mils

50 mils

50 mils

TRANSDUCER AREA (150 mils x 150 mils)
This area shall be defect free when examined under 60x magnification.
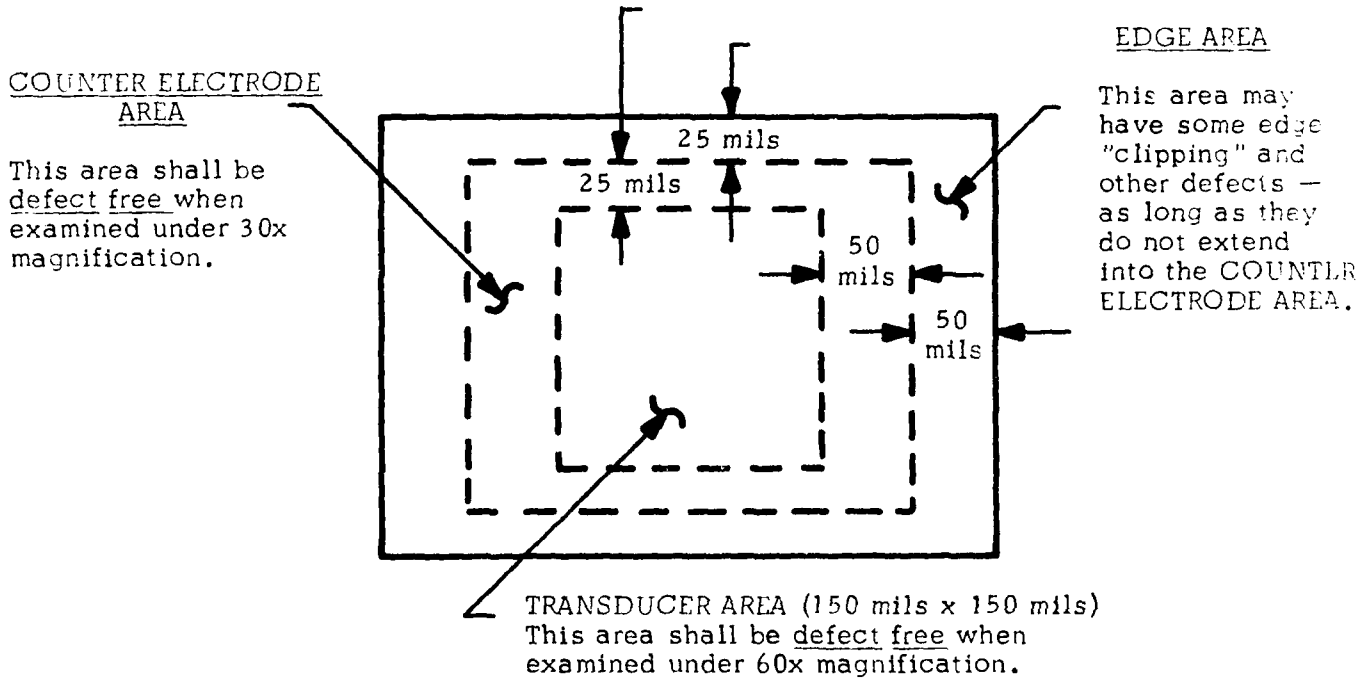
FIGURE 18. PRELIMINARY SURFACE SPECIFICATION, AS A FUNCTION OF CRITICAL AREAS, FOR THE BRAGG CELL TRANSDUCER SURFACE.

Optical Faces

The optical surfaces must also have a high quality finish in order to minimize the level of scattered light that can result from surface defects. Figure 19 illustrates a typical optical face, showing what is an acceptable number of surface defects.
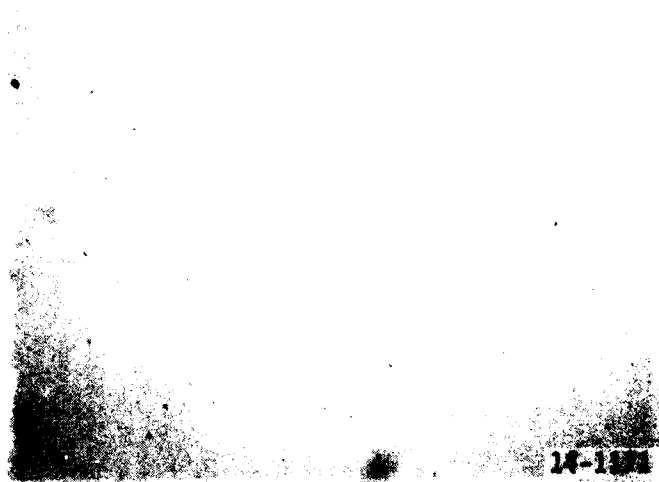
MAGNIFICATION: 320X

FIGURE 19. EXAMPLE OF AN ADEQUATELY POLISHED
OPTICAL SURFACE.

c. Anti-Reflective Techniques

When operating a Bragg cell receiver or spectrum analyzer, it is necessary to reduce the amount of light reflected from the surface of the acousto-optic crystal. During the course of developing our technology, we

investigated and utilized two basic techniques — the Brewster angle and the more standard anti-reflective coating.

Brewster Angle

The Brewster angle approach is illustrated in Figure 20. The technique is predicated on matching the angle of the incident light signal and the index of refraction of the acousto-optic substrate via Snell's relationships. The incident Brewster angle for lithium niobate is 65.6 degrees.
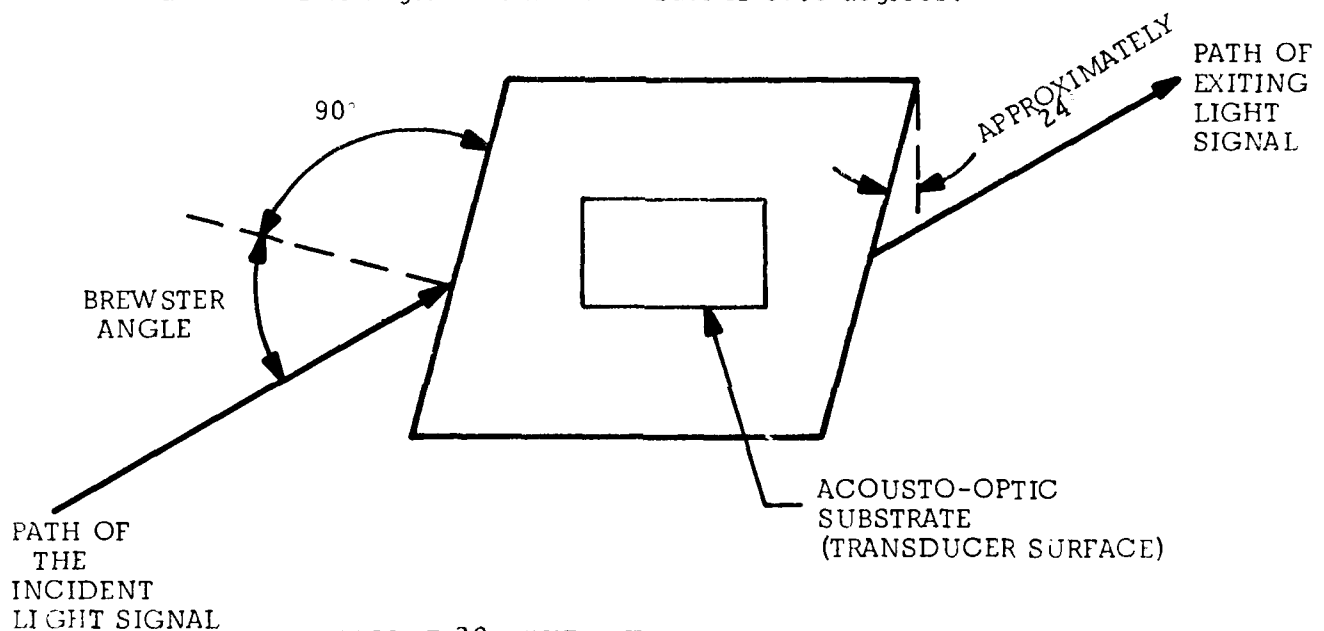
FIGURE 20. THE BREWSTER ANGLE APPROACH
TO AN ANTI-REFLECTING SURFACE.

As shown by Figure 20, the Brewster approach involves an additional precision polishing step (the 24 -to-normal side faces) to ensure that the proper Brewster relationships are achieved.

Over a period of time, TMEC has manufactured Bragg-type acousto-optic devices which have employed the Brewster approach. On average, the percentage of incident light reflected has been between 1 and 2 percent.

which is less than satisfactory. These values are almost an order of magnitude in excess of what would be expected.

Anti-Reflective Coatings

The other technique used to reduce the level of reflected incident light utilizes a special coating applied to the optical faces. In this approach, a special film is applied to a precisely-controlled thickness, a thickness which is directly related, in wavelengths, to the frequency of light it is desired to efficiently transmit. The effect of this coating is to "match" (optically speaking) the incident light and the acousto-optic substrate. TMEC results in this area have been excellent, as demonstrated by Figure 21, which is a spectrophotometry plot of the reflected light and indicates only about 0.5 percent of the incident light is being reflected. We have verified the data, both before and after predeposition cleaning processes and the actual deposition of the piezoelectric transducers. Based on the data, the anti-reflective coating approach was used on the demonstration test crystals for this program.

2. Acoustic Transducer Mask

The deposition mask for the transducer's top electrode was described in the design section, with a detail of the mask drawing given in Figure 8. As was described, these masks are quite thin and extremely difficult to manufacture when very small openings are involved. The transducer height dimension (0.001 inch) designed for this application certainly qualifies as small.

The transducer mask is produced from a special bi-layered material — nickel-clad beryllium copper. This material is carefully etched to produce the desired pattern dimensions, a process which has been very effective over the years. However, obtaining the 0.001 inch wide slit required by this design was more difficult than any trans-ducers successfully manufactured with this process in the past.

REFLECTED LIGHT (%)

4.17

0.421
0.387

REFERENCE (0%)
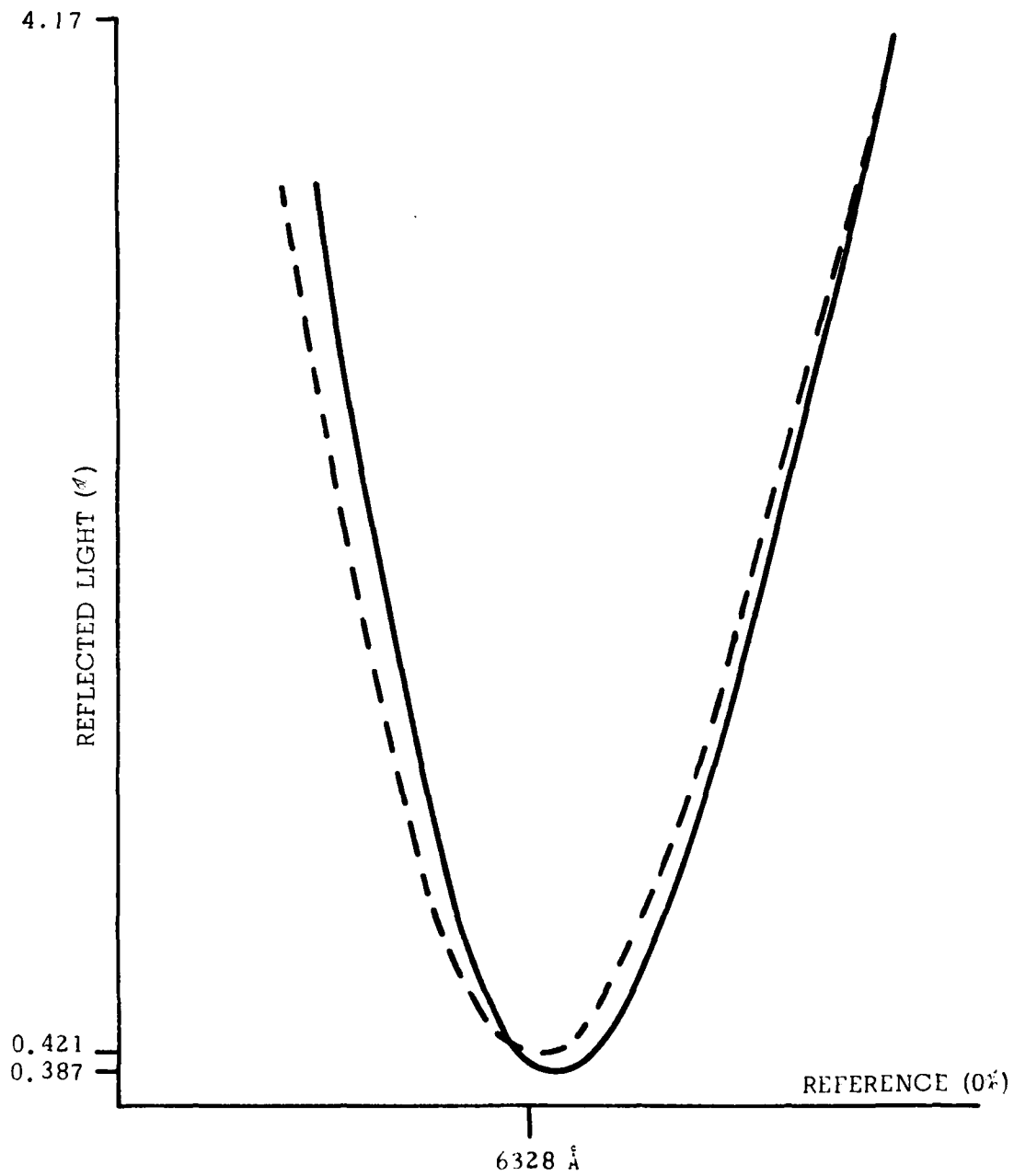
6328 Å

FIGURE 21. SPECTROPHOTOMETRY PLOT OF THE A/R
COATING AT 6328Å WAVELENGTH.

a. Mask Evaluation

The transducer mask was received on schedule and its dimensions checked with an optical comparator. The results of this dimension check, compared with the desired design parameters of Figure 8, are summarized in the table below. It is obvious that the transducer height dimension is larger than desired by a factor of two, a fact that definitely affected Bragg cell performance.

PARAMETER	DESIGN DIMENSION (inches)	MEASURED DIMENSION (inches)
TRANSDUCER HEIGHT	0.001 ± .0001	0.002
TRANSDUCER LENGTH	0.0125 ± .0003	0.015
TRANSDUCER OVERLAP	0.001 ± .0005	0.002

Effect on Bragg Cell Performance

We have learned from our previous analysis that increasing the height of the transducer will have an adverse effect on the Bragg cell's efficiency. Therefore, with the transducer height now expected to be approximately 0.002 inch, the band center efficiency estimates must be revised. The estimates are summarized on the following page.

FREQUENCY BAND	CENTER FREQUENCY (GHz)	TRANSDUCER HEIGHT, H (inches)	EFFICIENCY (% PER RF WATT)
1	4.5	0.002	0.9
2	5.5	0.002	0.8
3	6.5	0.002	0.75
4	7.5	0.002	0.8

One of the highest priorities of the Evaluation Section to follow is a complete review of the Bragg cell efficiency model, adding to it considerations for both Bragg bandwidth and acoustic diffraction. TMEC now has sufficient experience with similar acousto-optic devices to approximate more accurately the level of performance expected from a given Bragg cell.

3. Piezoelectric Transducer Deposition

The deposition of zinc oxide (ZnO) transducers, using what is known as "sputtering" techniques, have been demonstrated to produce excellent results. Other techniques are available for the fabrication of this type of thin-film transducer, but in general they yield inconsistent results.

a. Sputtering Techniques - General

Sputtering in one form or another is the most logical method for depositing thin films of piezoelectric and dielectric material. The basic compound material (in TMEC's case, zinc) is deposited without adjusting its composition. In this way, sputtering lays down films in a stoichemetric fashion difficult to realize with evaporation techniques.

Triode Sputtering

Triode sputtering permits lower pressure in the sputtering system,

providing an atmosphere where the mean-free electron path is long, collisions are few, and the directivity of the sputtered mat~~tal is high. The basic operation of a triode system is as follows. A t sten fila-ment is heated to its emission temperature and an electron beam is established between the filament and anode, with two magnetic field coils used to focus the beam. Argon gas is admitted into the system through a leak valve and is ionized by the electron beam. A high negative voltage is applied to the target, causing it to be bombarded by positive argon ions. The high energy ions dislodge molecular sized particles of zinc oxide which deposit themselves on the nearby sub-strate. The substrate-to-target distance is maintained smaller than the mean-free-path of an electron to minimize the number of collisions in transmit and, thereby, reduce the spreading of the beam. With a well directed beam, it is possible to deposit a film oriented parallel to the substrate and obtain shear-wave transducers, or to rotate the substrate holder so that film orientation is perpendicular to the substrate and, hence, obtain longitudinal-wave transducers, such as are used on this program.

B. Bragg Cell Efficiency Model

The design section of this report presented a simple set of equations for use in defining and predicting some of the more important performance characteristics of the Bragg cell. Of all these characteristics and parameters, none are more important than those which define the acousto-optic efficiency. The key efficiency-related equations, however, as presented again below, provide only an approximation of the performance which may be expected from a given set of design parameters.

- Acousto-Optic Interaction Efficiency (Band center):

$$Eff = 0.0856 \quad \frac{P_a L}{H \cos^2 \theta_B} \tag{12}$$

where

P_a = Acoustic power in the interaction area

L = Acoustic transducer length (along laser propagation direction)

H = Height of acoustic transducer

θ_B = Bragg angle

- Acoustic Transducer Length:

$$L = R\Delta\varphi$$

  where

  R = the transducer surface radius of curvature

  $\Delta\varphi$ = the transducers angle of focus (Figure 3)

- Bragg Angle:

$$\theta_B = \sin^{-1} 1/2 \left(\frac{\lambda_o}{\lambda_a}\right)$$

  where

  λ_o = the wavelength of the optical signal

  λ_a = the wavelength of the acoustic signal

The principal areas of concern in defining a proper model are those physical parameters that deal with the acoustic power (P_a) in the interaction region, the length of the interaction region as defined by a curved-surface transducer, and the bandwidth limitations inherent in the Bragg angle — acoustic beam momentum relationship. The following paragraphs cover each of these in detail, eventually ending up with an efficiency model for the acousto-optic Bragg cell.

1. Loss-Efficiency Considerations

The acousto-optic efficiency (in terms of the percent of incident light

L = Acoustic transducer length (along laser propagation direction)

H = Height of acoustic transducer

θ_B = Bragg angle

- Acoustic Transducer Length:

  $$L = R\Delta\varphi$$

  where

  R = the transducer surface radius of curvature

  $\Delta\varphi$ = the transducers angle of focus (Figure 3)

- Bragg Angle:

  $$\theta_B = \sin^{-1} 1/2 \left(\frac{\lambda_o}{\lambda_a}\right)$$

  where

  λ_o = the wavelength of the optical signal

  λ_a = the wavelength of the acoustic signal

The principal areas of concern in defining a proper model are those physical parameters that deal with the acoustic power (P_a) in the interaction region, the length of the interaction region as defined by a curved-surface transducer, and the bandwidth limitations inherent in the Bragg angle — acoustic beam momentum relationship. The following paragraphs cover each of these in detail, eventually ending up with an efficiency model for the acousto-optic Bragg cell.

1.   Loss-Efficiency Considerations

The acousto-optic efficiency (in terms of the percent of incident light

deflected per watt of RF incident power) depends upon how much acoustic power can be placed into the interaction region of the acoustic substrate. The losses which limit this transfer of power are dependent upon both the acoustic substrate material and the bulk acoustic wave transducer design.

a. Transducer Conversion Loss

Basic to the operation of an acousto-optic device is the efficient generation of the acoustic wave which will eventually interact with the incoming optical beam. The generation of the acoustic wave is accomplished by a piezoelectric transducer which converts the received electromagnetic energy into acoustic energy. In short, the mechanical displacement which takes place in the transducer film couples to the atoms within the acoustic substrate on which it is deposited, causing a similar mechanical displacement. The displacement within the crystal propagates down its length, forming the acoustic wave or beam.

The "conversion" loss encountered in the transformation of electromagnetic energy into acoustic energy is a major contributor to the overall loss of broad-bandwidth Bragg cells. In the bulk acoustic wave technology, the zinc oxide piezoelectric transducer material is chosen for its maximum conversion efficiency and ease of fabrication over a wide range of microwave frequencies. The transducer itself is designed to provide the lowest possible conversion loss over the required operational bandwidth. Using the established characteristics for acoustic thin-film transducers and substrates* in the generation of longitudinal bulk-wave energy, and the equivalent circuit conceived by Mason** we have developed a computer design program which accurately models conversion loss as a function of the given design parameters. The results closely approximate the design theory.

---

* Microwave Acoustics Handbook, Vol. 3, Bulk Wave Velocities, RADC, 1980.

** W. P. Mason, Electromechanical Transducers and Wave Filters, 1948, pp. 201-209, 399-404.

Table VI in the design section, "Transducer Design-Conversion Loss, " illustrates the conversion loss calculations performed during the design phase.

b. Acoustic Propagation Loss

Another loss contributor is the propagation loss of the acoustic substrate. For lithium niobate, it is the low propagation loss of 0.1 dB/μsec $-$ GHz^2 that makes it the most appealing material for high-frequency, broadband Bragg cells. Like conversion loss, the propagation loss characteristics of bulk acoustic substrates are well known and can generally be accurately predicted.

c. Acoustic Diffraction Loss

The diffraction loss of the acoustic transducer must also be considered in the model for determining efficiency. The specific condition of concern is the rapid divergence of acoustic energy due to the small height dimension (about 0.002 inch) of the transducer.

The characteristics of a propagating acoustic wave radiated from a rectangular transducer are relatively well known. Analysis of the diffraction characteristics in both the near-field and far-field of the transducer are straightforward, although the analysis becomes somewhat more complex due to the anisotropy of the lithium niobate crystal. The region between the near and far field is particularly difficult to analyze and approximations are necessary to obtain good agreement between theoretically predicted results and measured diffraction losses. If the distance between the transducer and the acousto-optic interaction region is more than $D^2/_\lambda$, the far-field approximation should be used. The table on the following page shows that for the 4 to 8 GHz Bragg cell, the interaction region is between near and far field regions.

FREQUENCY (GHz)	NEAR FIELD BOUNDARY $\sim D^2/\lambda$ (inch)	MEASURED DISTANCE TRANSDUCER TO A-O INTERACTION REGION (inch)
4.0	.062	.075
5.0	.078	.100
6.0	.092	.125
7.0	.108	.175
8.0	.122	

Our computational approach was to analyze the diffraction in an isotropic acoustic material. The calculated diffraction loss was then corrected for the acousto-optic substrate anisotropy, using an anisotropy factor obtained by curve-fitting the slowness curves presented in the Microwave Acoustic Handbook, Vol. 3, Bulk Wave Velocities. For acoustic propagation along the X-axis of lithium niobate, the presence of anisotropy causes an increase in the angle of diffraction, and hence, an increase in the amount of acoustic energy lost.

A preliminary computer model has been generated and the initial results analyzed. Figure 22 illustrates the initial test results. For example, when the acousto-optic interaction takes place between 0.050 and 0.100 inch from the transducer, a 5 to 7 dB loss of efficiency would be expected due to the contribution of diffraction loss. If the interaction took place between 0.100 and 0.150 from the transducer, a loss of as much as 10 dB in efficiency would be expected.
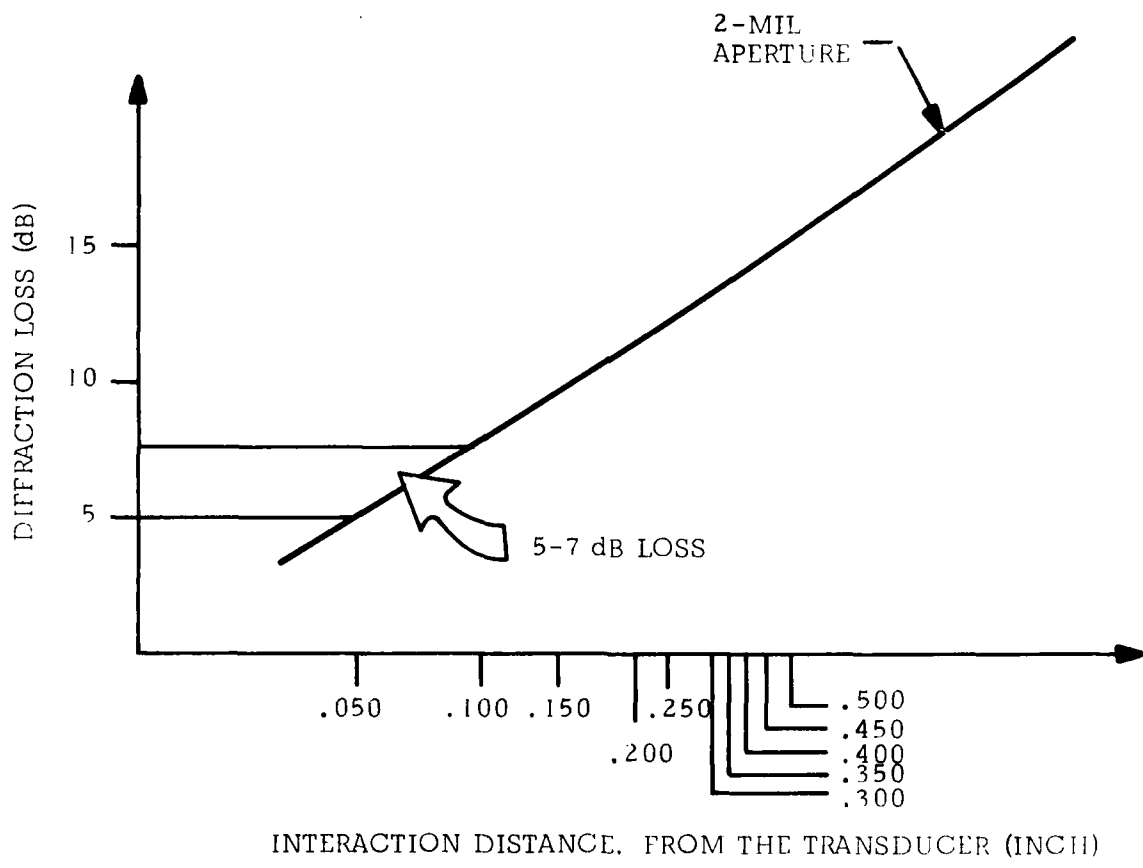
FIGURE 22. CALCULATED DIFFRACTION LOSS EFFECTS IN ANISOTROPIC LITHIUM NIOBATE MATERIAL.

The calculated values for diffraction loss were then compared to diffraction loss values determined from tests conducted which measured the actual acoustic beam spreading encountered.
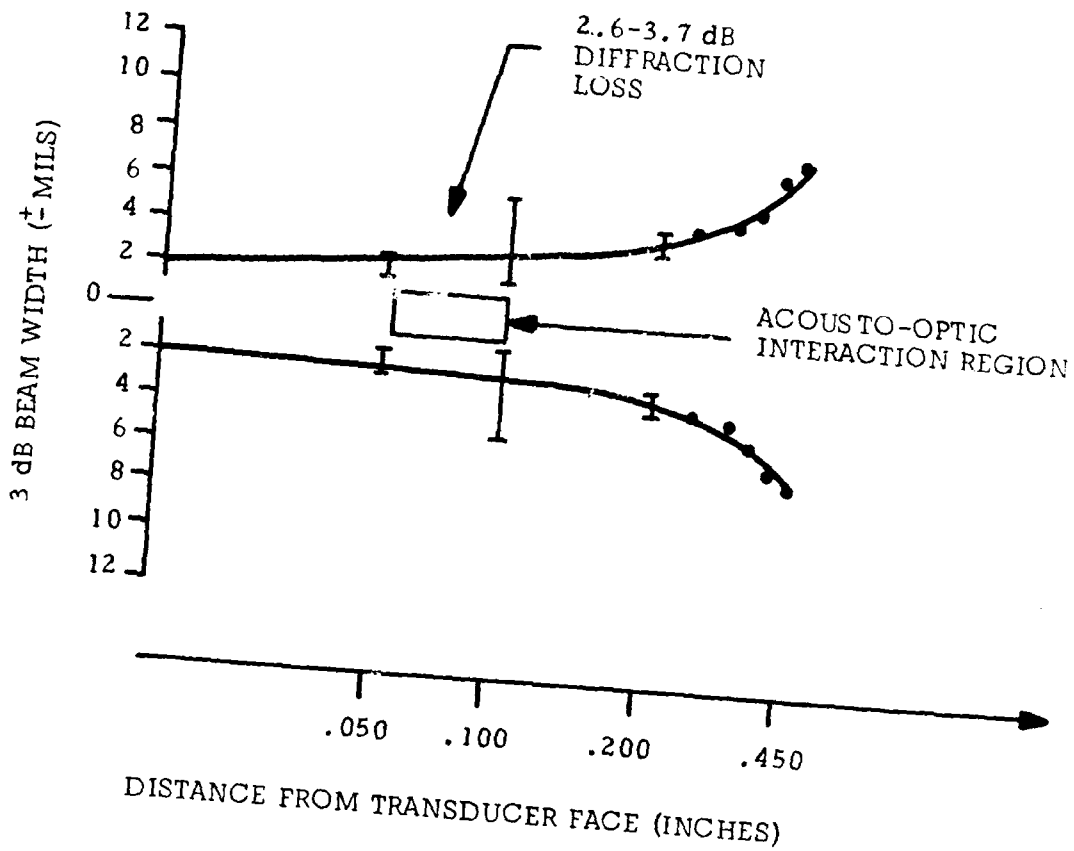
FIGURE 23. MEASURED DIFFRACTION LOSS EFFECTS IN ANISOTROPIC LITHIUM NIOBATE MATERIAL.

Figure 23 presents some typical beam spreading data taken at 4.0 GHz. When superimposed with the interaction region, the effect on efficiency can be readily estimated. Our empirical beam spreading results predicted diffraction losses of the order of 2.6 to 3.7 dB for the lower bands (4-6 GHz)

and approximately twice that much (5 to 7.5 dB) over the 6 GHz to 8 GHz frequency range.

Acousto-optic efficiency calculations indicate a better level of agreement with the measured efficiencies when the beam spreading diffraction data is used rather than the computer analysis. Efforts are continuing with respect to converging the empirical data and the theoretically predicted information into a well-behaved model.

2.   Bandwidth-Efficiency Considerations

The "efficiency" equation used to describe the performance of acousto-optic Bragg cells presented previously in this section is a band-center calculation. Because of this, it does not treat the full acousto-optic efficiency response and bandshape of a Bragg cell.

a.   Bragg Angle and Mismatch Bandwidth

In the presentation of TMEC's design approach (Section II of this report), we discussed the virtues of a focused acoustic beam in achieving a wide range of Bragg diffraction angles, as opposed to an acoustic beam which depends upon diffraction to achieve its bandwidth. Even with the superior attributes of the "focused" approach, some diffraction will occur and it will dilute the level of acoustic energy available to deflect the incident light signal. We must remember that there are frequency components across the full transducer bandwidth that will satisfy the Bragg condition. The transducer design guarantees this. However, the effects of diffraction will reduce the amount of acoustic energy available in any given Bragg-matched frequency component as the frequencies approach the band edges. The result is that less of the light beam is efficiently diffracted.

The efficiency must be determined for each frequency according to the curved transducer's acoustic intensity at the angle required for a Bragg-

matched condition. It has also been shown* that the intensity and the angle (and, hence, frequency) of the scattered light are completely independent of the position of the incident light beam along the acoustic beam.

The scattering or Bragg mismatch bandwidth for the simple, uniform transducer has been expressed** as:

$$\Delta f = 1.8 \ (\frac{n\nu^2 \cos \theta}{\lambda_o f_c L}) \tag{13}$$

where

n = the index of refraction

ν = the acoustic velocity

λ_o = the optical wavelength

f_c = the (RF) center frequency

θ = optic-acoustic angle for "non-exact" Bragg conditions

L = the interaction length, beam waist, along the optic signal path (equal to the trans- ducer length for the single, uniform transducer)

However, in our case, the transducer has a more complex, curve-focused geometry, where L is not the beam waist. Referring to the diagram in Figure 3(a) which illustrates the profile of the acoustic beam, the following relationship for beam waist (W_o) emerges

---

* A Review of Acousto-Optical Deflection and Modulation Devices,
   E. I. Gordon, Appendix A; Applied Optics, October 1966.

** I. C. Chang, IEEE Sonic and Ultrasonics, January 1976.

$$W_O = \frac{\nu}{f_C \, \Delta\varphi} \qquad (14)$$

where

ν = the acoustic velocity

f_C = the (RF) center frequency

$\Delta\varphi$ = the focus-angle of a single transducer

If this expression for W_O is substituted for L in equation (13), an expression for the non-exact or Bragg mismatched bandwidth will result:

$$\Delta f = 1.8 \; \left(\frac{n\nu \, \Delta\varphi \cos \theta}{\lambda_O} \right) \qquad (15)$$

This equation defines the 3 dB bandwidth which will result from a particular transducer design, and a given acoustic substrate and light source. The calculation of bandwidth is illustrated for the multi-channel spectrum analyzer Bragg cell in the following table. The calculation is based upon the measured transducer mask dimensions for L (page 61).

CHANNEL NO.	CENTER FREQUENCY (GHz)	CALCULATED BANDWIDTH (Δf) (GHz)
1	4.5	1.20
2	5.5	1.18
3	6.5	1.17
4	7.5	1.15

Effect of Acoustic Diffraction Due to Transducer Width

The previous discussion modeled the bandwidth limitations for the Bragg
cell — detemining in theory what bandwidth should be realized for each
channel of the spectrum analyzer Bragg cell. To complete this segment
of the model, we need to determine the effect that acoustic diffraction in
the transducer width dimension will have on the efficiency-versus-frequency
response. We will call this effect "Bragg angle mismatch." We know from
the literature* that for the simple, uniform transducer, the efficiency spec-
trum (bandwidth) is sin x/x in nature. It would seem logical, therefore,
that the focused transducer would produce a similar but somewhat broader
response, while still being constrained by the 3 dB Δf relationship. This
fact has been borne out by empirical data collected using a variety of
Bragg devices operated over a range of frequencies. Figure 24 illustrates
the range of "shape-functions" we have found to be most representative
of the performances we are achieving in the laboratory. The outer (dotted
line) curve represents the Δf as calculated directly from equation (15);
while the inner curve (solid line) represents the impact of empirical data
on the bandshape. The narrow, more "empirical" response has been found
to be the most representative "efficiency" bandshape model and will be
used in all subsequent efficiency calculations.

b. Effect of Transducer Design on Bandwidth-Efficiency

One final comment should be made concerning bandwidth and efficiency and
how each has been affected by the transducer design. Equation (12) defined
the efficiency for a transducer of length L, in the direction of the light
propagation. The length (L) is also known as the beam waist of the acoustic
signal's profile. For the simple, planar surface transducer, the beam waist
occurs very near the transducer and is indeed "L" in length (Figure 25). On the
other hand, the curved surface transducer beam waist (W_o) is defined at
the point of focus for the acoustic beam profile — at the point where the
beam profile begins to diverge. In the next section, this curved-transducer
value of the beam waist is used to determine the efficiency of our demon-
stration Bragg cell devices.

---

* Spectrum Analysis Using Acousto-Optic Devices, D. L. Hecht, Optical
　　Engineering, September-October 1977 (Vol. 16).

-73-
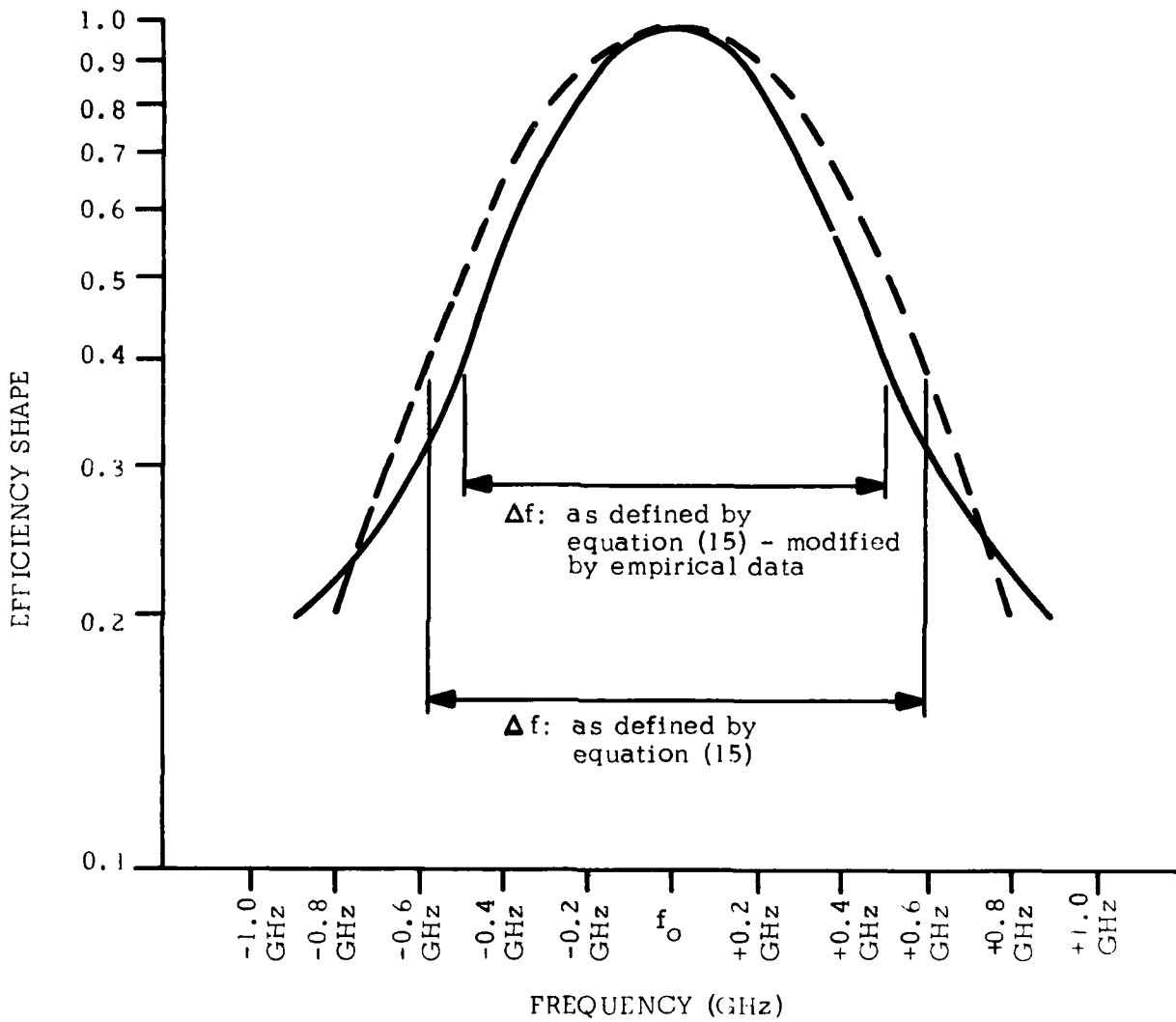
FIGURE 24. BRAGG MISMATCH BEAMWIDTH SHAPE FACTOR..
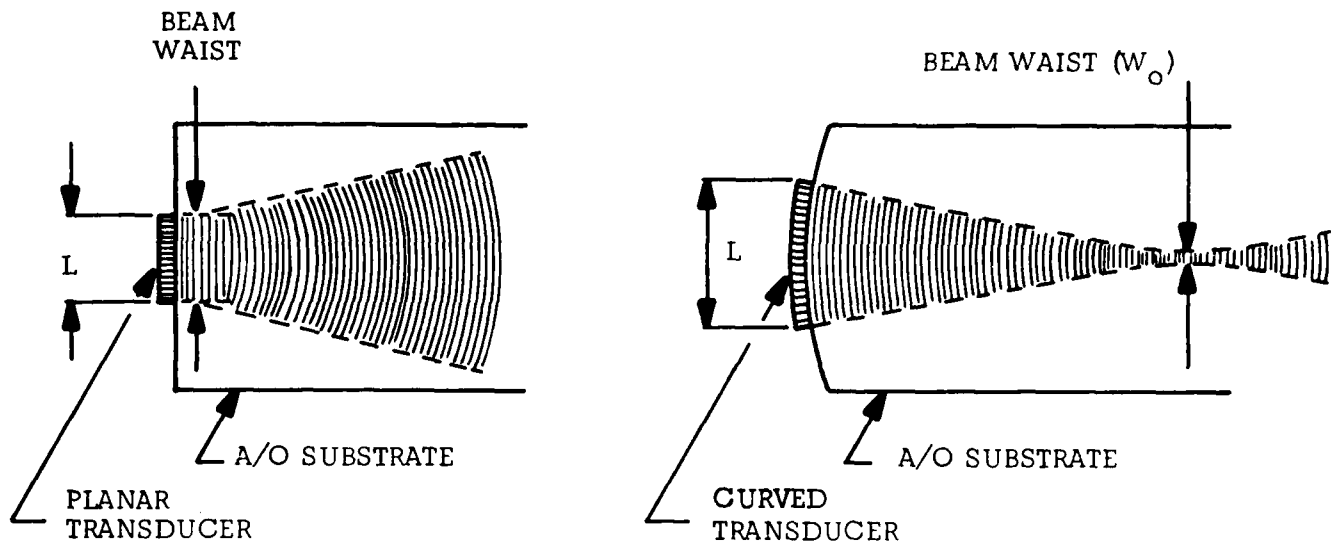
FIGURE 25. THE EFFECT OF THE CURVED-SURFACE TRANSDUCER BEAM WAIST ON EFFICIENCY.

Beam Waist Versus Frequency...and Efficiency

It should be noted that the expression for beam waist (in equation 14) is inversely proportional to the RF frequency of operation. That is, as the frequency increases, the beam waist decreases (becomes narrower in the propagation direction of light beam). As can be seen a little later in the analysis, this "shrinking" beam waist will also have an effect on the efficiency response of the Bragg cell. In short, as the beam waist gets smaller, so does efficiency.

3. Efficiency Calculation Model

The ingredients of an improved Bragg cell "efficiency model" were assembled in previous paragraphs; i.e., the acoustic conversion and propagation losses, the transducer height diffraction losses, and the transducer width diffraction loss contribution. Recalling equation (12),

$$\text{Eff} = 0.0856 \ \frac{P_a L}{H \cos^2 \theta_B}$$

and equation (14);

$$W_o = \frac{\nu}{f_c \, \Delta\varphi}$$

we can construct an improved equation, where W_o is substituted for L:

$$Eff = 0.0856 \, \frac{P_a \, W_o}{H \cos^2 \theta_B} \qquad (16)$$

Using this new equation and adding to it the descriptors and data for acoustic conversion and propagation loss, the transducer height diffraction loss, and band-narrowing shape factor due to the transducer width diffraction loss, we can begin to more accurately approximate the acousto-optic efficiency performance for a Bragg device. Figure 26 illustrates the "flow diagram" for the computational model. In the following paragraphs of this section, two acousto-optic Bragg cells are examined in theory and performance. Each device is evaluated with regard to its operation and to the computer model being constructed to predict and understand its performance.

a. Bragg Cell: AOX-030

The first Bragg cell devices successfully manufactured and tested were fabricated using thicker transducers than would normally be used in designs over this frequency range. However, it was felt that the thicker ZnO layer would be more tolerant of the marginally polished transducer surface conditions we were experiencing.

Deposition Parameters

The following deposition parameters were used in the manufacture of the AOX-030 Bragg cell.
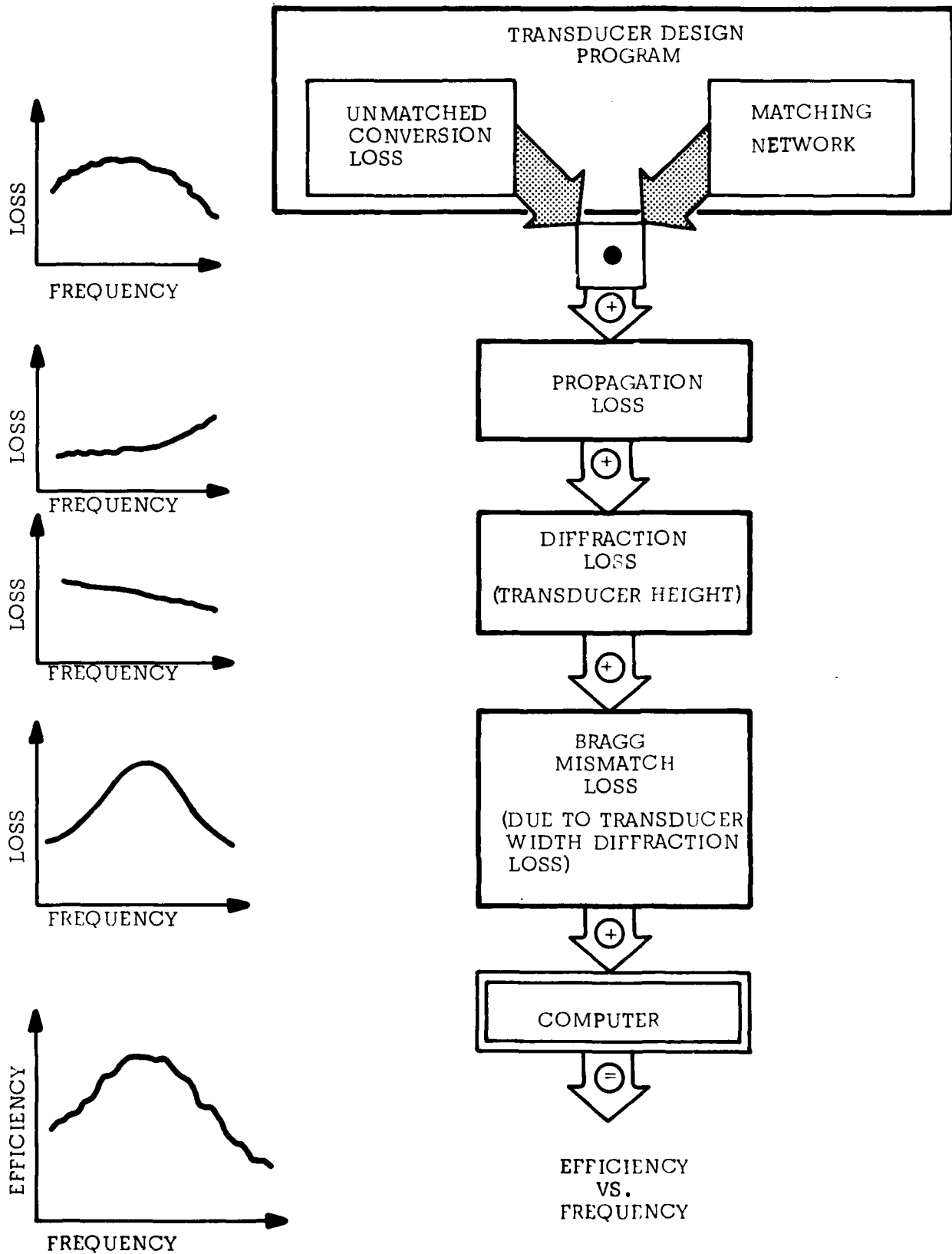
FIGURE 26. THE ACOUSTO-OPTIC BRAGG CELL
EFFICIENCY VERSUS FREQUENCY
COMPUTATIONAL MODEL.

CRYSTAL ID: AOX-030

DEPOSITION PARAMETERS	DESIGN THICKNESS (Å)	ACHIEVED THICKNESS (Å)	MATERIAL
• COUNTER-ELECTRODE	100	100	Cr
	2000	~2000	Au
• ZINC OXIDE LAYER	3500 ± 100	3300 – 3500	ZnO
• TRANSDUCER	100	100	Cr
ELECTRODE	1600 ± 100	~1700	Au

BONDING REQUIREMENTS	QUANTITY	TYPE
• COUNTER-ELECTRODE	~20	Ball, or Two-Lead Pressure Type
• TRANSDUCER ELECTRODE	2 per	Two-Lead Pressure Type

Theoretical Efficiency Calculation for AOX-030

Using equation (16) the efficiency response expected from Bragg cell
AOX-030 was computed. There are basically two types of efficiency
responses calculated here.

- First is the Bragg-matched response. In this response the
  Bragg angle is "matched" at every RF frequency. That is,

the angle between the Bragg cell and the incident light is
changed with each RF frequency so as to provide the optimum
diffraction efficiency. Although unrealistic from an opera-
tional point of view, this type of data defines the efficiency-
performance limits of a given design and set of deposition
parameters.

- The second computation to be made is for the Bragg channel-
matched response: In this calculation the efficiency response
of each channel is computed with the Bragg angle fix-tuned
at each center frequency. This calculation is designed to
provide a reasonably accurate estimate of the Bragg device's
bandwidth and shape, and level of efficiency.

Figure 27 illustrates and compares the computed Bragg-matched data with
that measured in the laboratory. The initial computation shows, in general,
a good agreement with basic response shape. However, it predicts a
higher than realized efficiency. A closer examination revealed that the
added loss (approximately 4 dB) was due to an understated level of diffrac-
tion loss in the model. The reason for the understatement was twofold:
first, the interaction region was positioned further down the substrate
than predicted prior to actual testing. Secondly, our more recent data
tends to support the analytical representation of the diffraction loss, in
some areas, as opposed to the preliminary empirical data presented
earlier in this section. The table on page 81 summarizes:
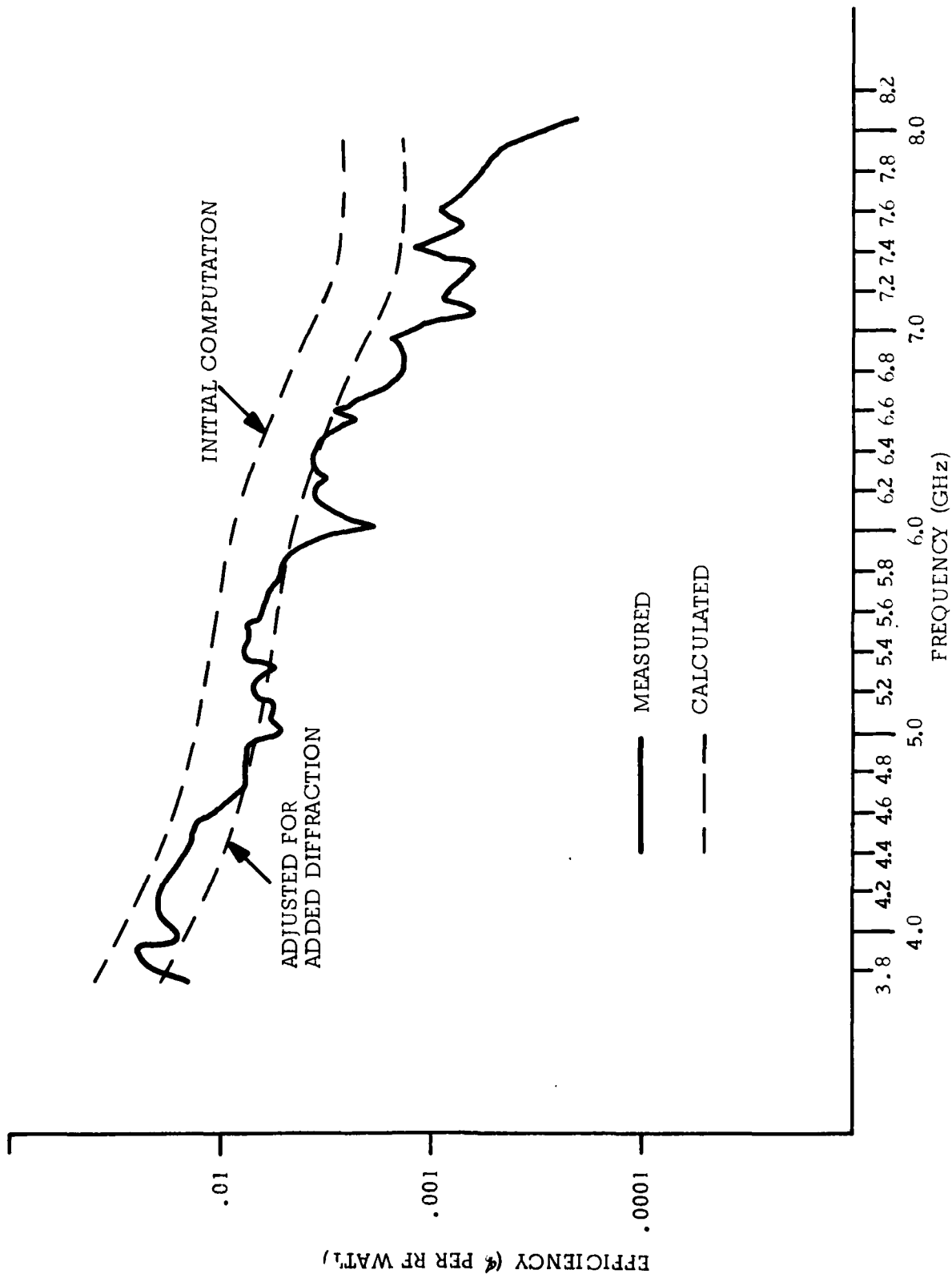
FIGURE 27. THE BRAGG-MATCHED EFFICIENCY CHARACTERISTIC FOR AOX-030.

FREQUENCY BAND (GHz)	DISTANCE FROM THE TRANSDUCER (inches)		PREDICTED DIFFRACTION LOSS (dB) (1)		PREDICTED DIFFRACTION LOSS (dB) (2)	
	(3)	(4)	(3)	(4)	(3)	(4)
4-5	.050	.100	2.7	3.9	5.0	7.5
5-6	.075	.125	3.2	4.1	6.7	8.1
6-7	.100	.150	3.7	4.8	7.5	9.6
7-8	.150	.200	4.6	5.7	9.6	11.8

NOTES:

(1) Based upon preliminary measured data.

(2) Revised estimate based upon computer model for diffraction.

(3) Initial estimate (used in the preliminary efficiency computation).

(4) Revised estimate.

In the 4 to 5 GHz band, the measured diffraction data appears to be understated by about 1.5 dB. As for the other bands: 5 to 6 is understated by about 2.5 to 3.0 dB as is the 6 to 7 band, with band 7 to 8 being off by between 3 and 5 dB. In the following computation, the model is adjusted to take the added loss into consideration.

Figure 28 illustrates the channel-matched data. The computation was modified as follows, based upon the data of Figure 27: The diffraction losses in Channels 1 and 2 were left unchanged because the measured data previously used was felt to be the most accurate and the most substantiatable within the region of 0.150 inch from the transducer. The diffraction loss in Channel 3 was increased by 3 dB, as was the data for the 7 to 8 GHz band. The calculated response of Figure 28 is seen to be substantially improved with respect to the measured data.
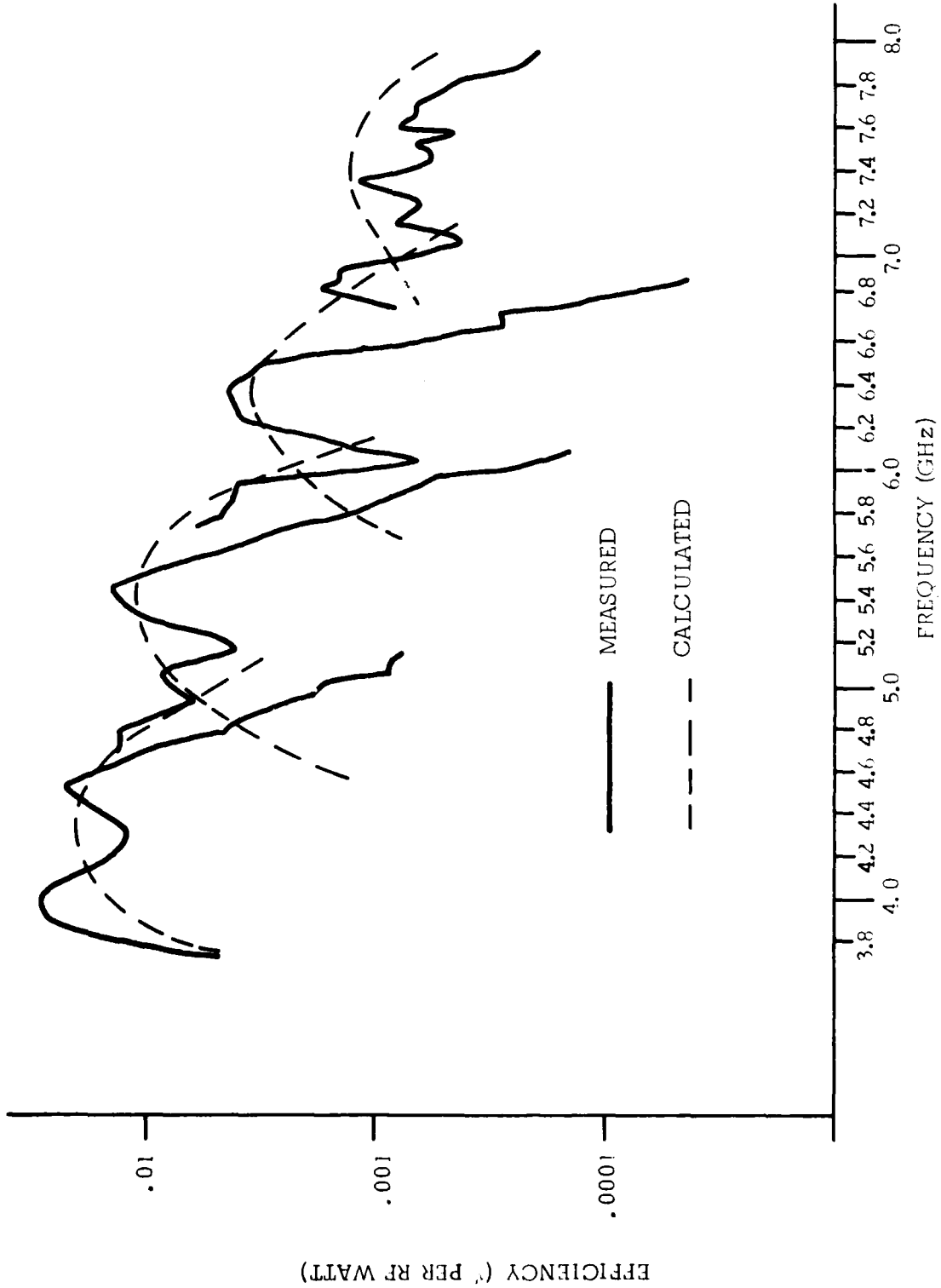
FIGURE 28. THE BRAGG CHANNEL-MATCHED RESPONSE TO AOX-030 (CHANNELS ARE BRAGG-OPTIMIZED AT 4.5 GHz, 5.5 GHz, 6.5 GHz and 7.5 GHz, RESPECTIVELY).

-82-

END
DATE
FILMED
7-83
DTIC
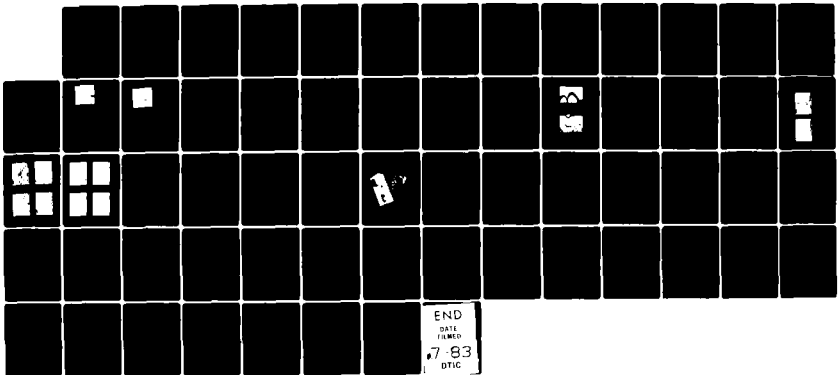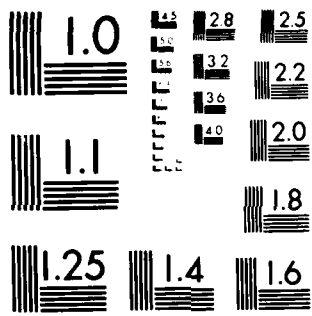
MICROCOPY RESOLUTION TEST CHART
NATIONAL BUREAU OF STANDARDS 1963 A

b. Bragg Cell: AOX-040

Bragg cell AOX-040 represents the first device to contain the full complement of design and deposition parameters.

Deposition Parameters

The following table shows which deposition parameters were used in the manufacture of the AOX-040 Bragg cell.

CRYSTAL ID: AOX-040

DEPOSITION PARAMETERS	DESIGN THICKNESS (Å)	ACHIEVED THICKNESS (Å)	MATERIAL
• COUNTER ELECTRODE	100	100	Cr
	1800	~1800	Au
• ZINC OXIDE LAYER	2300	2200 – 2300	ZnO
• TRANSDUCER ELECTRODE	100	100	Cr
	1100 ± 100	1100 – 1200	Au

BONDING REQUIREMENTS	QUANTITY	TYPE
• COUNTER-ELECTRODE	~20	Ball, or Two-Lead Pressure Type
• TRANSDUCER ELECTRODE	2 per	Two-Lead Pressure Type

Theoretical Efficiency Calculation for AOX-040

Again, using equation (16) and the updated estimates for diffraction, efficiency versus frequency is calculated — this time for Bragg cell AOX-040. As for AOX-030, both the Bragg matched and Bragg channel-matched characteristics were computed for AOX-040.

Figure 29 illustrates the computed Bragg matched efficiency data compared to the actual data. The upper computed curve takes into consideration the "adjusted" diffraction presented in the discussion of the AOX-030 data. The lower computed curve represents an adjustment of another 1.5 dB across the band due to a high level of reflected incident light experienced during testing of this particular cell.* The table below summarizes the data taken.

FREQUENCY RANGE (GHz)	INCIDENT LIGHT (mW)	REFLECTED LIGHT (mW)	PERCENT LIGHT REFLECTED (%)
4-5	16.8	1.06	6.3
5-6	16.8	0.98	5.8
6-7	16.8	0.93	5.5
7-8	16.8	0.85	5.1

---

* The AOX-040 Bragg cell was manufactured with rectangular optical faces which necessitated the use of anti-reflective coatings. The coatings were not optimized at 6328Å, resulting in an increased level of reflected optical light.
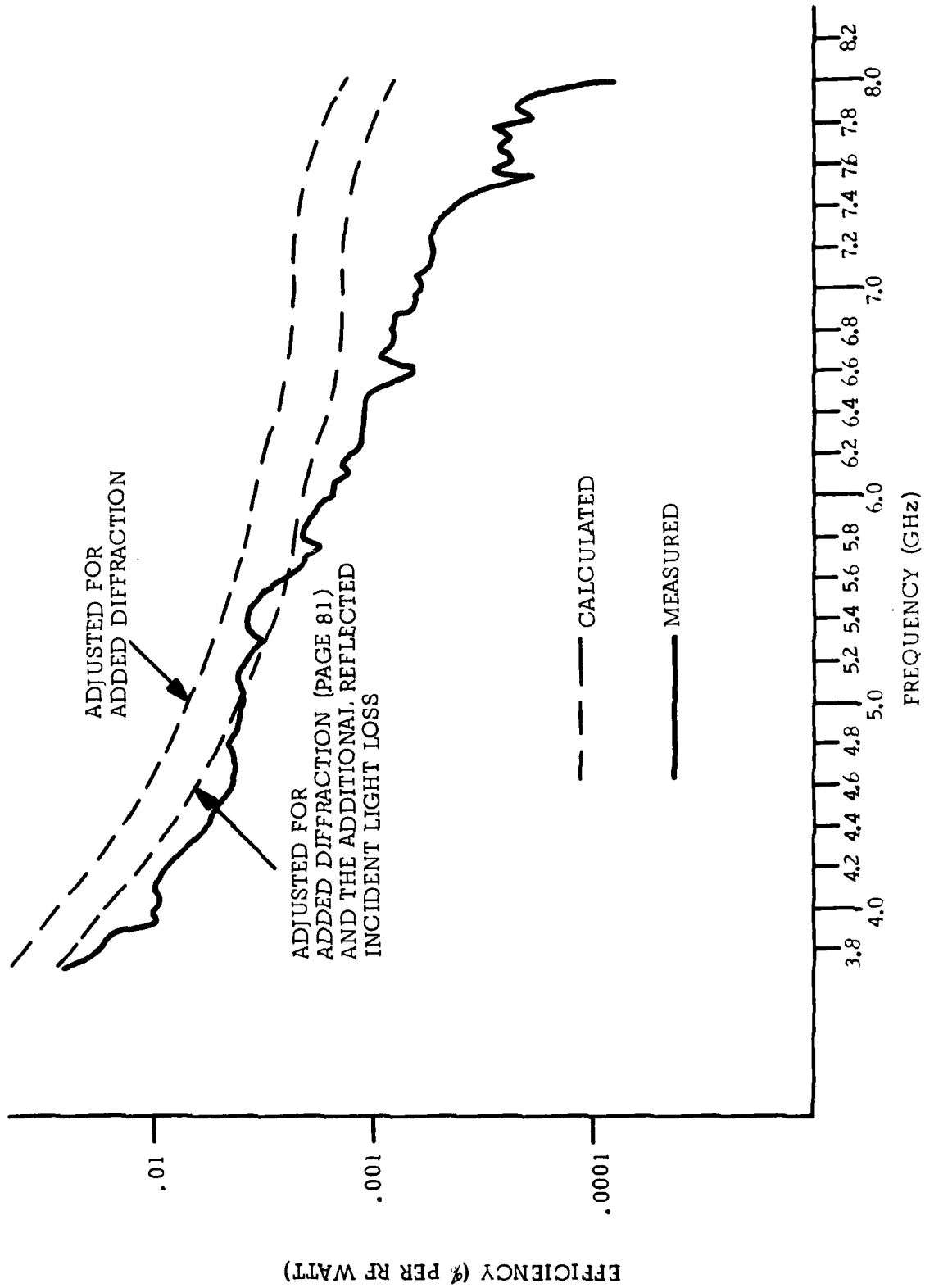
FIGURE 29. THE BRAGG-MATCHED EFFICIENCY CHARACTERISTIC FOR AOX-040.

It would appear that our model is getting closer, at least over half of the bandwidth of interest. Even though both our computation accuracy and our data repeatability (and hence believability) have a yet-to-be-determined level of error, it is still possible to draw some conclusions. Based upon the data taken on this program to date, Channels 1 and 2 (4-5 GHz and 5-6 GHz) appear to agree quite favorably with the computationally adjusted diffraction data. On the other hand, the two upper channels (6-7 GHz and 7-8 GHz) on both the AOX-030 and AOX-040 devices appear to be experiencing added loss — not far from that predicted previously by the adjusted calculations shown in the table on page 81. The conclusions to date can be summarized as follows:

FREQUENCY RANGE (GHz)	INITIAL DIFFRACTION ESTIMATE (dB)	ADJUSTED DIFFRACTION ESTIMATE (dB)	CHANGE IN DIFFRACTION ESTIMATE (dB)
4-5	2.7	7.5	+4.8
5-6	3.2	8.1	+4.9
6-7	3.7	9.6	+5.9
7-8	4.6	11.8	+7.2

Computational results of the "adjusted" efficiency model are shown in Figures 30 and 31. The data represents two separate test conditions; in the first (Figure 30) each A/O channel is tuned at band center, while in the second (Figure 31) each channel is tuned for symmetry of response. In general, the agreement between theory and measured data is fair — despite the fact that the two different tuning conditions tested can cause substantial differences in the respective efficiency response shapes. However, the agreement between theory and actual data continues to be worse over the
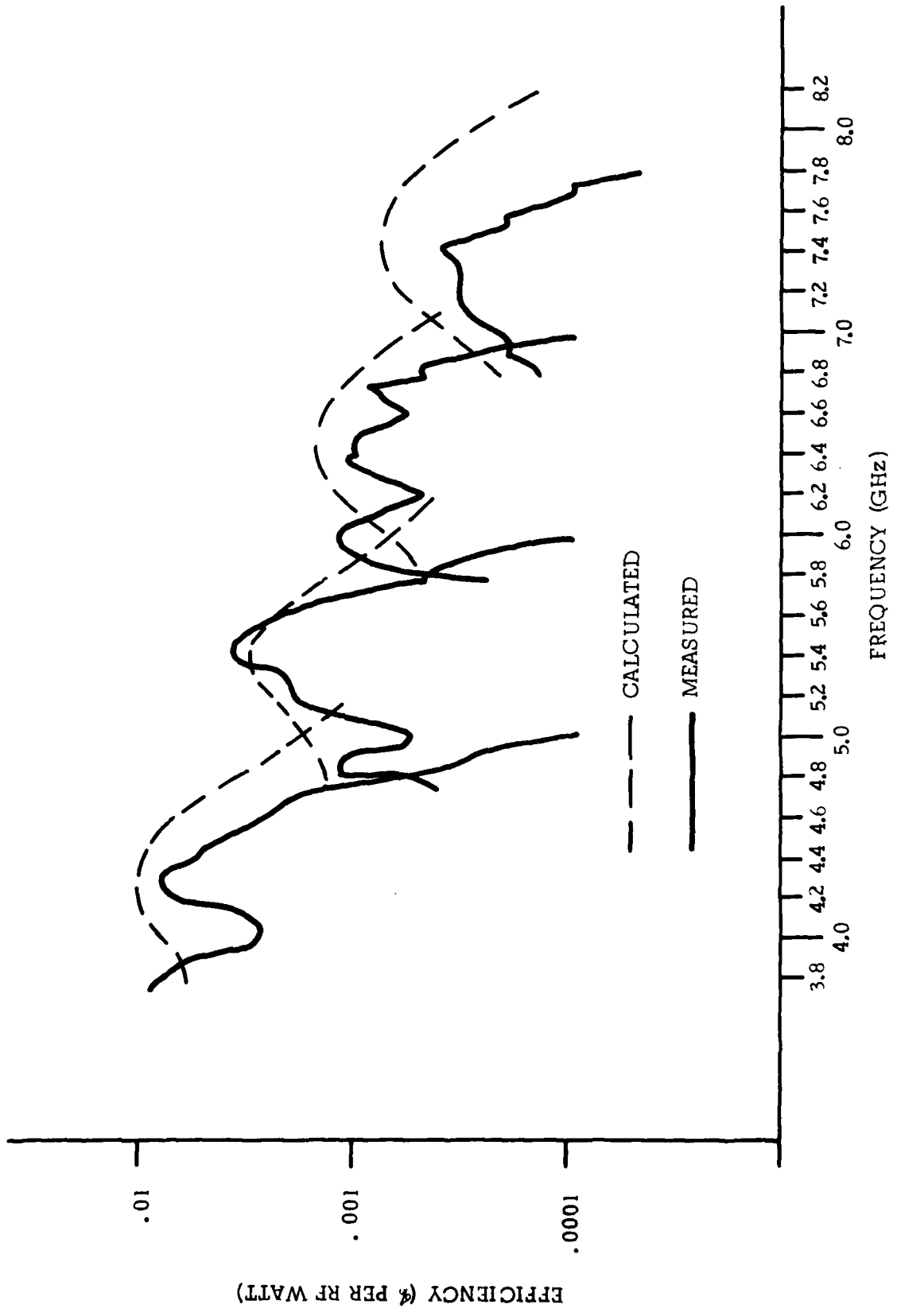
FIGURE 30. THE BRAGG CHANNEL-MATCHED RESPONSE FOR AOX-040. (CHANNELS ARE BRAGG-OPTIMIZED AT 4.5 GHz, 5.5 GHz, 6.5 GHz AND 7.5 GHz. RESPECTIVELY.)

-87-
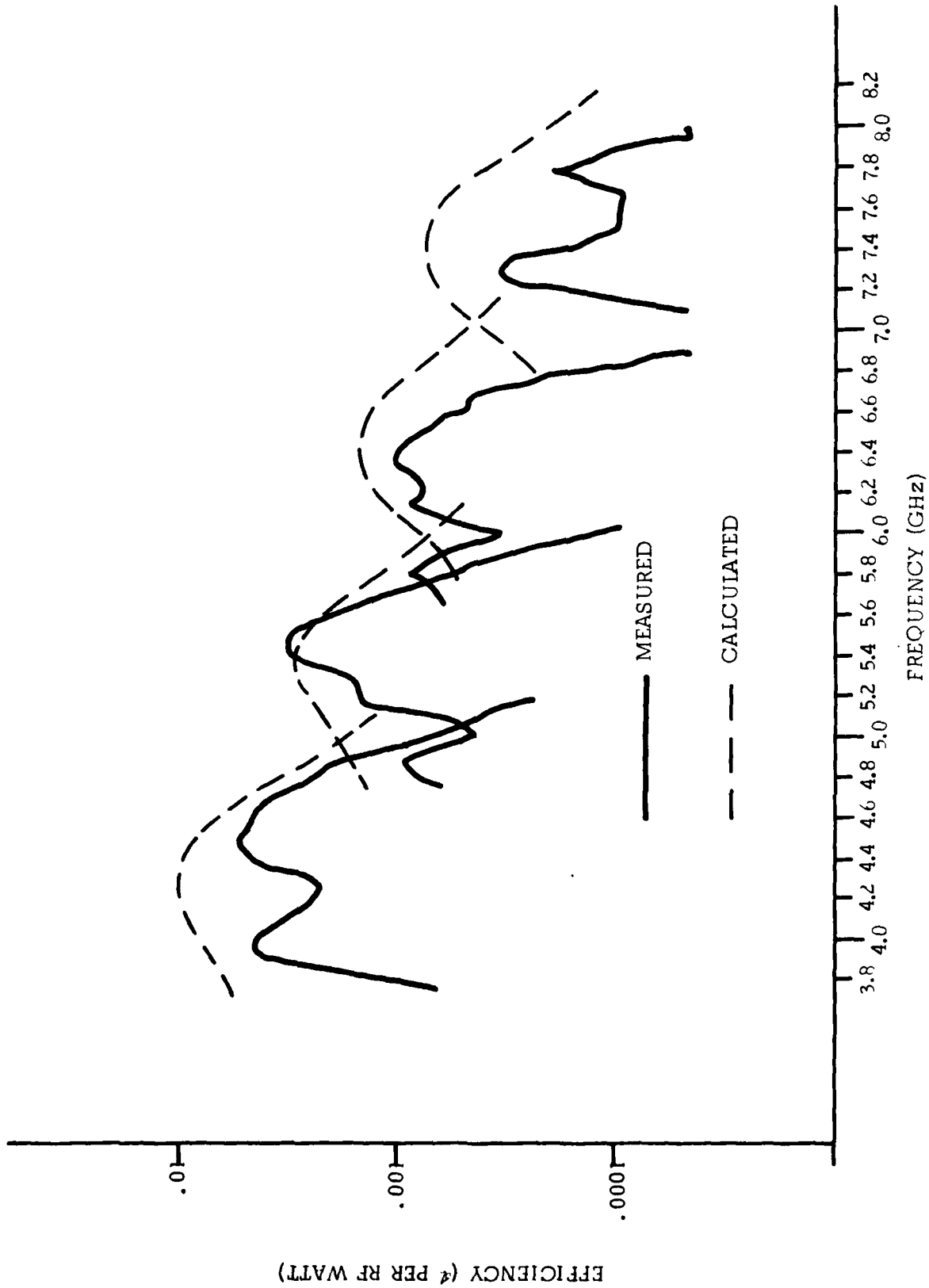
FIGURE 31. THE BRAGG CHANNEL-MATCHED RESPONSE FOR AOX-040. (CHANNELS ARE BRAGG-OPTIMIZED AT 4.7 GHz, 5.6 GHz, 6.6 GHz AND 7.8 GHz. RESPECTIVELY.)

EFFICIENCY (% PER RF WATT)

FREQUENCY (GHz)

MEASURED

CALCULATED

two upper channels. Additional testing revealed that these variations between data and theory are attributable to propagation losses that were larger than expected, which accounts for the low-to-high frequency "slope" of the loss discrepancy. Improperly modeled parasitic and interconnection losses probably also contribute, but to a much lesser degree. These latter losses are involved with the interfacing with the peripheral components (microstrips and indium bonds) via the series bond wire which connects the input circuitry to the transducer.

In summary, we have computed and tested two Bragg cells for operation in a spectrum analyzer. During the course of taking data, we have substantially improved our understanding of the Bragg cell by identifying and beginning to model the loss mechanisms which affect its performance. In the following, these Bragg cells are used to assemble and test the demonstration acoustic-optic spectrum analyzer.

c.   Pre-Evaluation Test Considerations

In the previous section we evaluated two acousto-optic Bragg cell devices for use in the Direct A/O Processor Spectrum Analyzer demonstration. This section describes how these two acousto-optic devices were configured into the desired spectrum analyzer, and how preliminary "tuning" improvements were made to each device to increase its bandwidth coverage and efficiency. Also provided is a brief block-diagram description of the test equipments used to perform the evaluation and demonstration.

1.   Spectrum Analyzer Configuration

The first consideration in creating the spectrum analyzer was to assemble the two acousto-optic Bragg cells into an operable, multi-channel configuration. Reviewing the data presented in Figures 28, 30 and 31, it is seen that the AOX-040 device, although somewhat lower in overall efficiency,

exhibits an adequate capability for covering the bandwidth of Channels
1 and 2. On the other hand, its performance from 6 GHz to 8 GHz is
most certainly inadequate for our demonstration, whereas AOX-030 shows
excellent results in both bandwidth and efficiency. To form the spectrum
analyzer, therefore, AOX-040 will be used over the 4-6 GHz range and
AOX-030 over the 6-8 GHz range. Figure 32 illustrates schematically
how the two-crystal spectrum analyzer could be configured in an opera-
tional system. However, for the experiments and demonstrations required
by this program, each 2 GHz spectrum analyzer band is considered
separately.
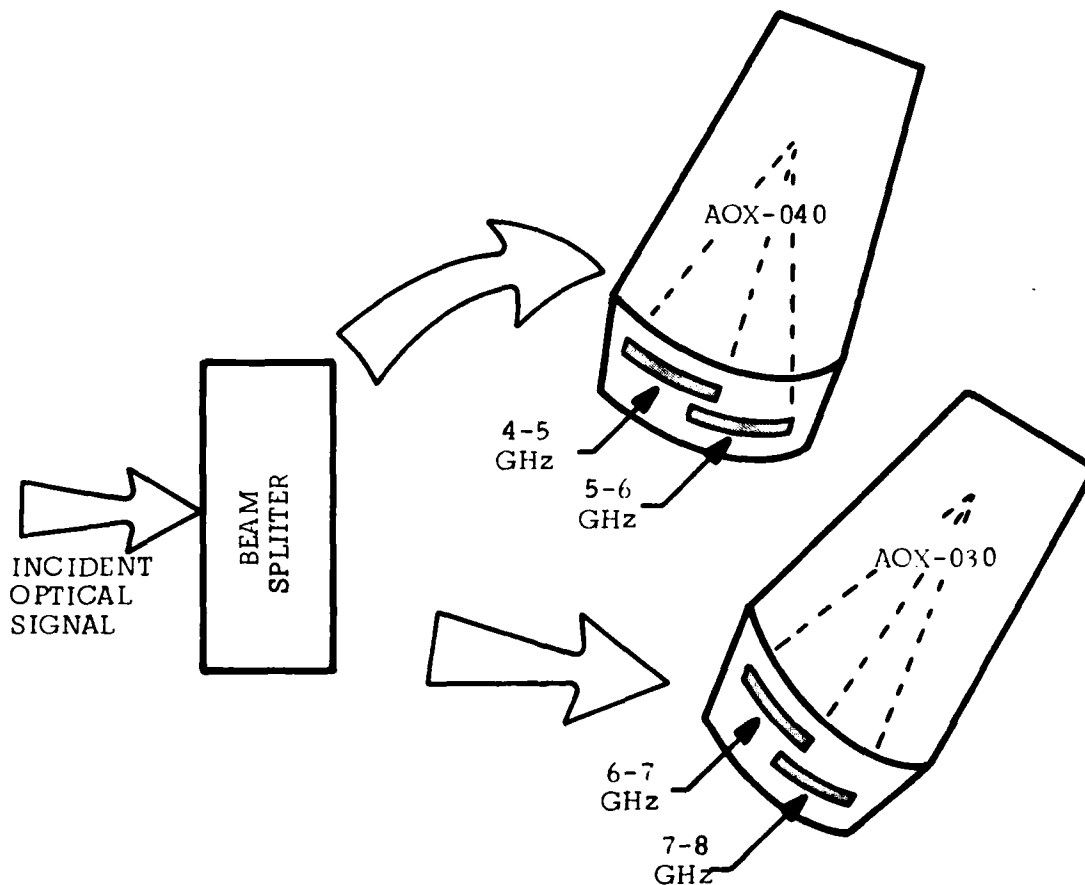
FIGURE 32. A DUAL CHANNEL, 4 GHz BANDWIDTH
SPECTRUM ANALYZER CONFIGURATION.

a. Lower Band Alignment; 4-6 GHz

Bragg cell AOX-040 was tested and Bragg aligned first. Figure 33 illustrates the initial Bragg matched data, where the Bragg angle was optimized at 5.2 GHz. The results indicate that the lowest channel (4-5 GHz) is shifted well into the 5-6 GHz channel region. Retuning the Bragg match for operation at 4.8 GHz (Figure 34), the performance is much improved and most of the desired bandwidth is accounted for.

b. Upper Band Alignment; 6-8 GHz

Both the AOX-030 and AOX-040 devices were tested for operation over the 6-8 GHz frequency range. Figure 35 shows the stronger performance achieved by AOX-030, in both bandwidth and efficiency. (The Bragg angle was optimized at 7.2 GHz in both cases.)

2. Bragg Cell Performance Improvements

Up to this point we have presented a variety of data on Bragg matched and Bragg channel-matched acousto-optic Bragg cell devices. In all cases the RF-to-acoustic piezoelectric transducer was unmatched. The reasoning for this approach is twofold. First, impedance transformations could possibly disguise many of the Bragg cell intricacies we are trying to study. Second, the design of such networks would be prohibitively expensive and time-consuming. However, it was felt that some preliminary experiments could be conducted which would provide insight into the ability to improve bandwidth and efficiency performance through microstrip matching techniques. The technique utilized was to simulate the thin film impedance transforming sections using small pieces of indium film, cut to size and inserted into the input RF section of each channel.
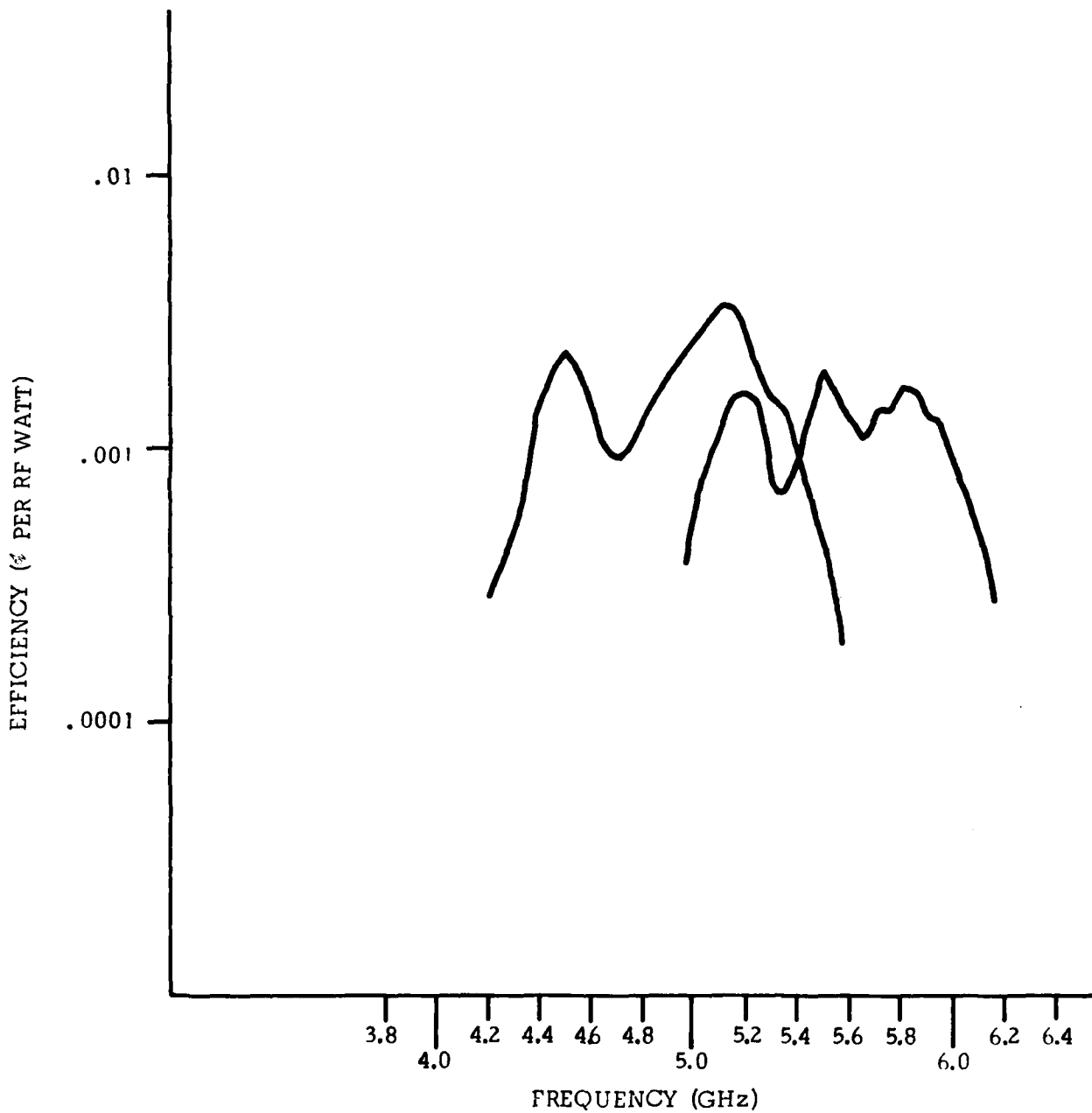
FIGURE 33. AOX-040 BRAGG RECEIVER EFFICIENCY DATA.
CHANNELS NO. 1 AND 2 (BRAGG ANGLE
FREQUENCY: 5.2 GHz).
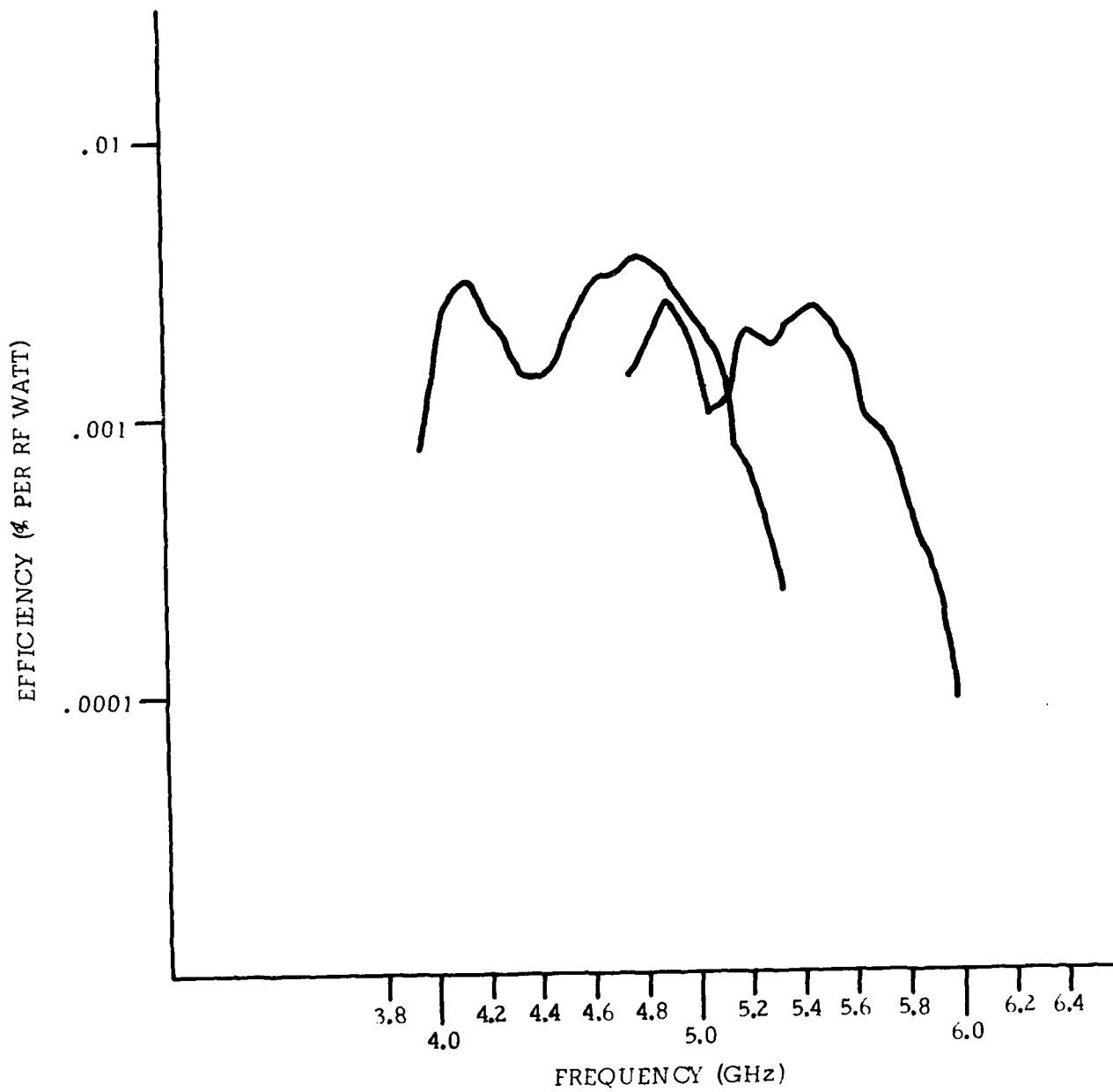
FIGURE 34. AOX-040 BRAGG RECEIVER EFFICIENCY DATA.
CHANNELS NO. 1 AND 2 (BRAGG ANGLE
FREQUENCY: 4.8 GHz).

EFFICIENCY (% PER RF WATT)
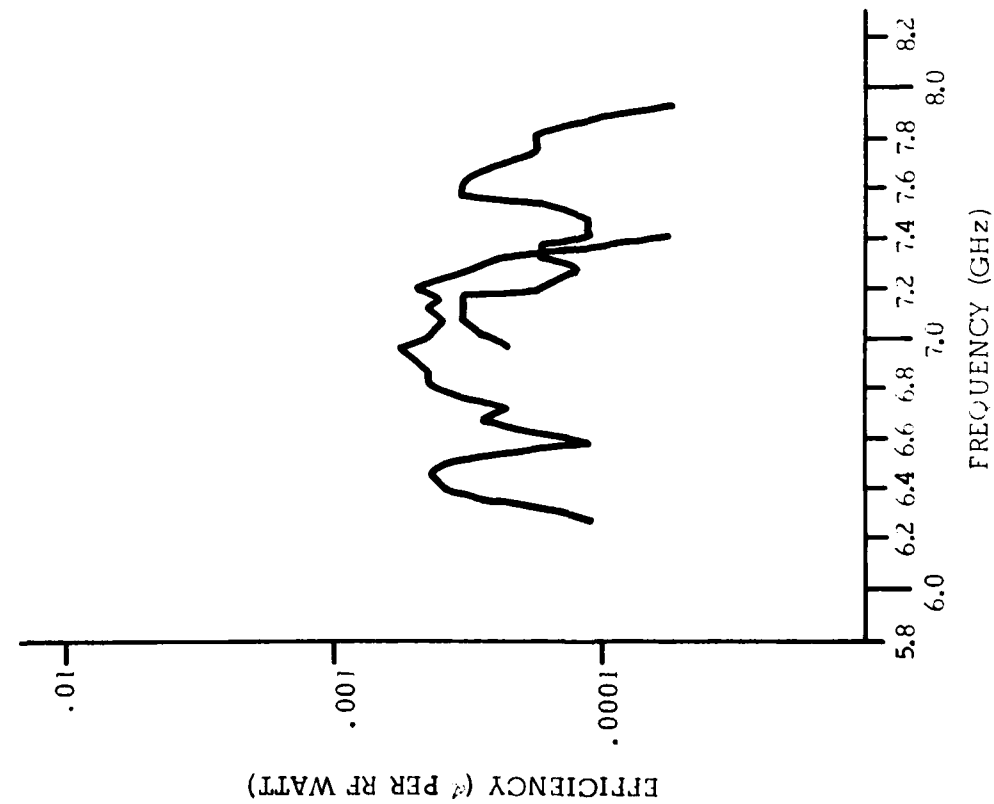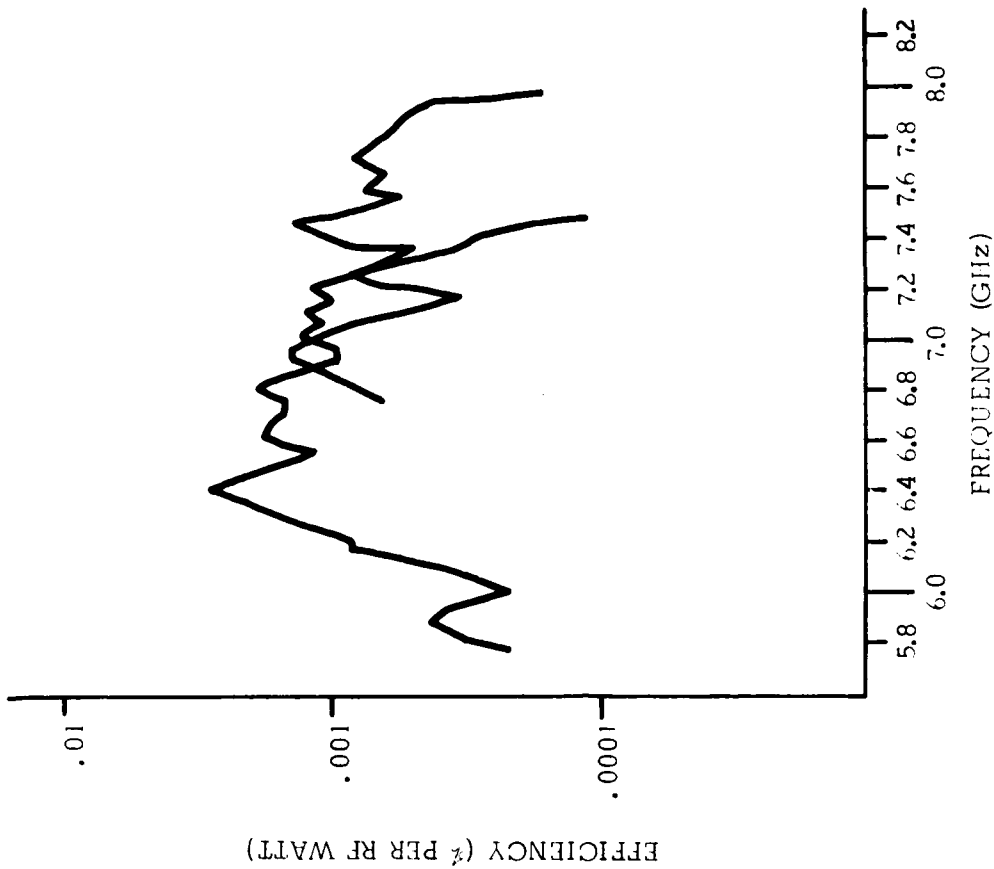
FREQUENCY (GHz)

A. AOX-040; BRAGG ANGLE FREQUENCY: 7.2 GHz.   B. AOX-030; BRAGG ANGLE FREQUENCY: 7.2 GHz.

FIGURE 35. BRAGG RECEIVER DATA. CHANNELS NO. 3 AND 4.

a. AOX-040, 4-5 GHz and 5-6 GHz

Figure 36 illustrates the improved performance achieved through the use of a 2-section, indium-film matching network on the two lower acoustic channels. The primary goal was to improve the low end (4-5 GHz) frequency response; and this was accomplished with no loss in bandwidth and with a gain in efficiency. In the 5-6 GHz channel, even though no broadening of the frequency response was achieved, we were able to shift its operation somewhat higher in frequency to cover the crossover between bands at 6 GHz. There was also a moderate improvement in the channel's acousto-optic efficiency. The micro-photograph accompanying the plotted data shows the simple indium "transformer" and its relationship to the acousto-optic crystal.

b. AOX-030; 6-7 GHz and 7-8 GHz

The goals for the two upper channels were essentially the same as those just described for the 4-6 GHz band. In short, it was desired to move the 6-7 GHz band toward 6 GHz to solidify the crossover region between spectrum analyzer bands while flattening its efficiency response. Figure 37 illustrates the level to which we were able to achieve these goals using the indium-synthesized technique. We were unable to improve the efficiency of either channel but did substantially improve both flatness and frequency coverage over the range of 6 to 7 GHz. The result of attempts to match the upper channel (7-8 GHz) was to narrow its bandwidth. Indications are that we were trying to force the transducer to operate in a frequency range where it could not work efficiently — due primarily to its overlap location (with respect to the 6-7 GHz channel) and the common Bragg angle needed to satisfy both channels simultaneously.

14-1173

AOX-040, #3, INDIUM MATCHED.
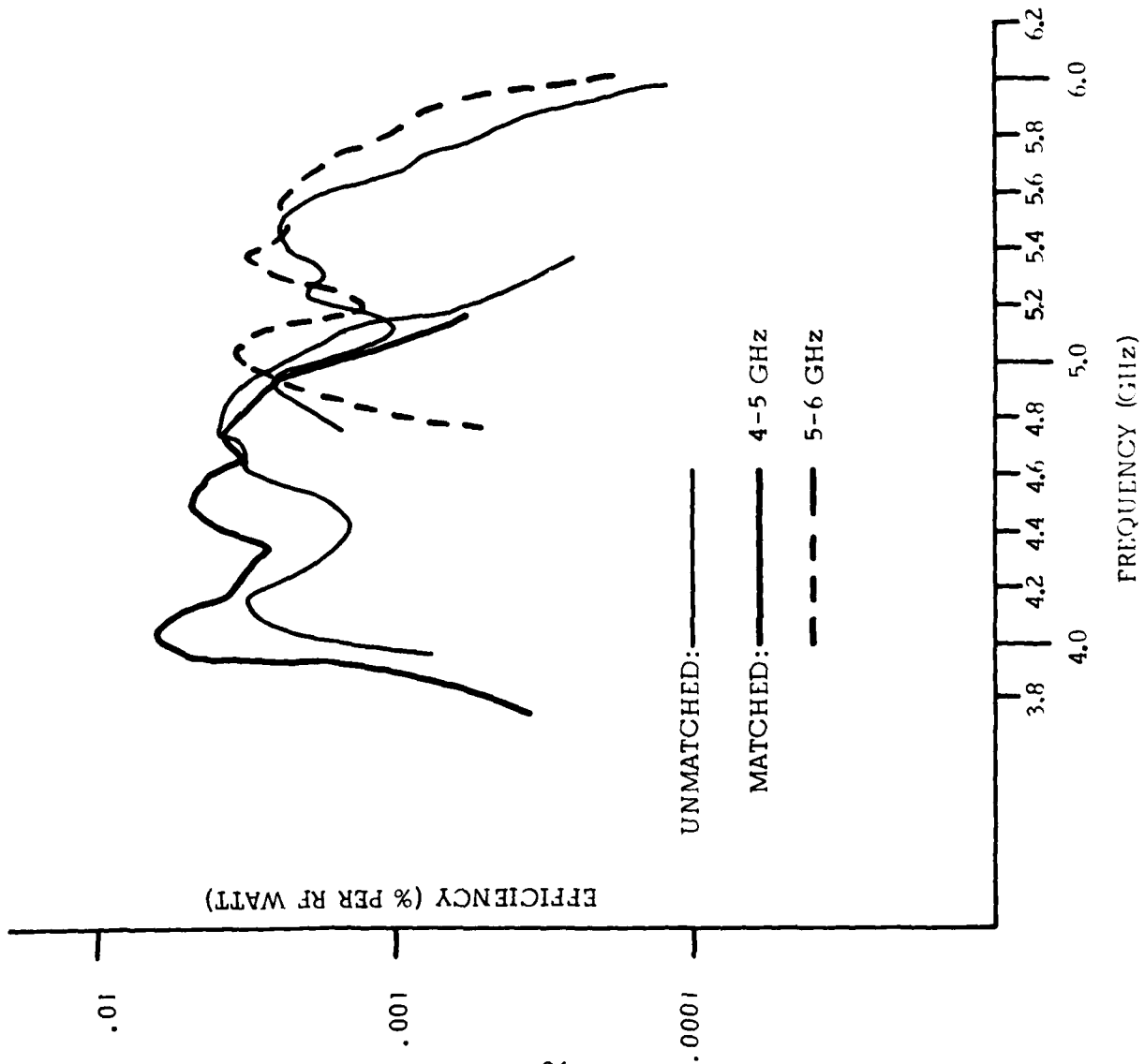
FIGURE 36. PERFORMANCE OF AOX-040, 4-5 GHz AND 5-6 GHz.

UNMATCHED: ————

MATCHED: ———— 4-5 GHz

———— 5-6 GHz

EFFICIENCY (% PER RF WATT)

FREQUENCY (GHz)
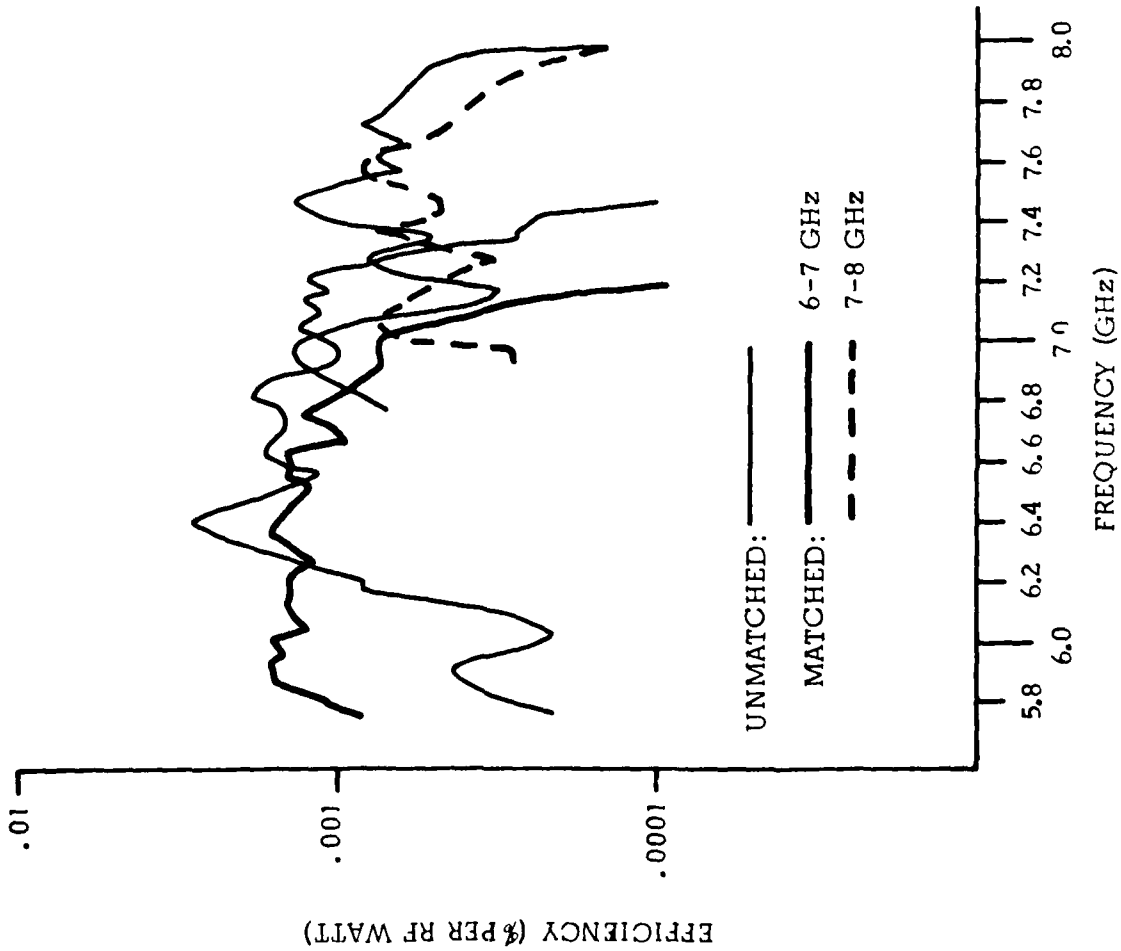
14-1172

AOX-030, #2, INDIUM MATCHED.

FIGURE 37. PERFORMANCE OF AOX-030, 6-7 GHz AND 7-8 GHz.

EFFICIENCY (% PER RF WATT)

FREQUENCY (GHz)

UNMATCHED:

MATCHED:

6-7 GHz

7-8 GHz

-46-

c. <u>Overall Spectrum Analyzer Efficiency</u>
<u>Response</u>

In general, TMEC's preliminary attempts to match the acoustic channels which make up the processor met with some success. We were able to substantiate that:

- The efficiency and bandwidth performance can be improved through the use of RF matching techniques.

- If combined with a coordinated transducer design, it would appear that a 7-10 dB efficiency improvement can be achieved in the lower (4-6 GHz) channels, with a 5-7 dB improvement attainable in the higher (6-8 GHz) channels.

- In addition, the overall response can be quite easily tailored using combined RF and Bragg matched techniques.

Figure 38 shows the final spectrum analyzer response covering the full 4 to 8 GHz frequency range. It is with in respect to this acousto-optic performance that the spectrum analyzer will be tested and evaluated.

3. <u>Spectrum Analyzer Test Configuration</u>

Figure 3 of this report presented a schematic of the A/O Spectrum Analyzer showing the various optics that would be required to exercise the acousto-optic Bragg cell as a spectrum analyzer. Throughout testing, this configuration has remained essentially unchanged. Figure 39, on the other hand, illustrates the microwave test equipment needed to perform the test demonstration. Even though all equipment is standard, off-the-shelf test components, a few words about how some of the key components were used in this particular test setup are probably pertinent.

-98-
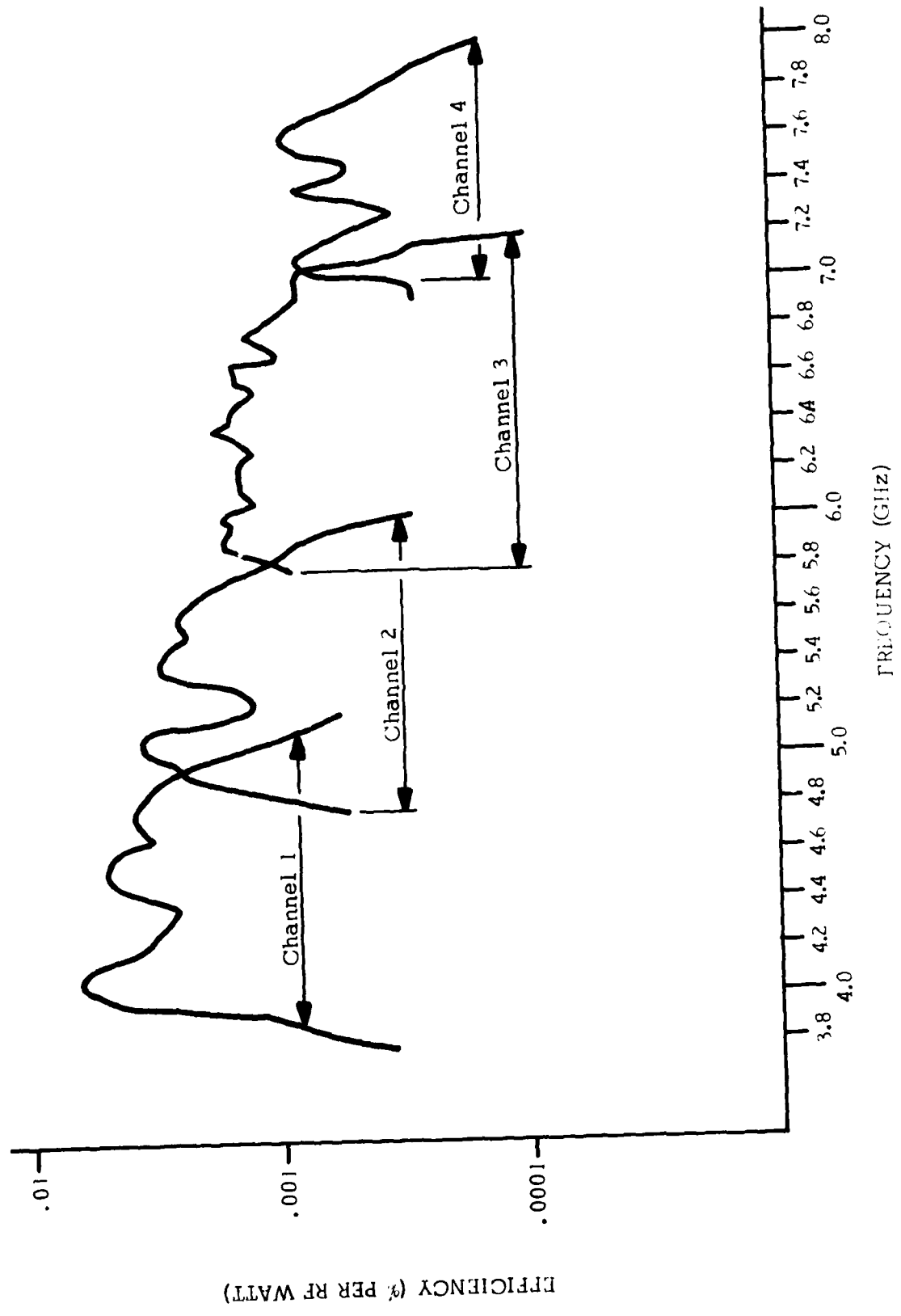
FIGURE 38. SPECTRUM ANALYZER BRAGG CELL EFFICIENCY DATA. (CHANNELS NO. 1 AND 2, AOX-040; CHANNELS NO. 3 AND 4, AOX-030).
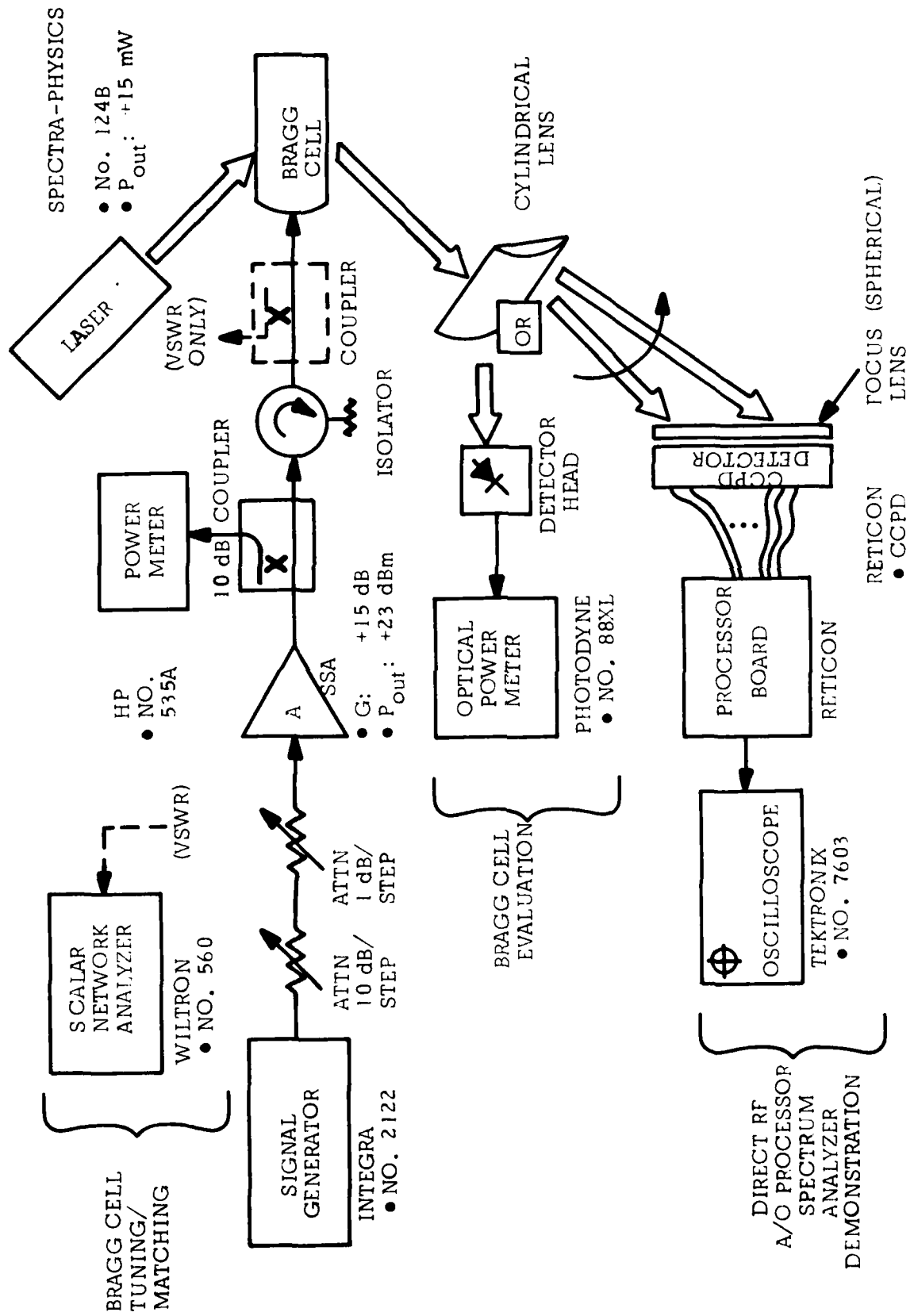
FIGURE 39. BLOCK DIAGRAM OF ACOUSTO-OPTIC SPECTRUM ANALYZER EVALUATION AND DEMONSTRATION TEST SETUP.

- Directional coupler-power meter:

  These test components are used to monitor the level of RF
  power being applied to the acoustic transducer of the Bragg
  cell. (All testing was performed at a 150 mW RF level, at
  the transducer.)

- Isolator:

  The isolator is used to "shield" the preceding test equipment
  from the generally poor VSWR (S11) provided by the Bragg cell.

- Directional Coupler:

  The second (dotted) directional coupler is used with the Scalar
  Network Analyzer during RF tuning of the acousto-optic devices.
  This approach provides for the near-simultaneous viewing during
  alignment of the Bragg cell's return loss and detected optical
  output (efficiency).

- Optical Detectors:

  There are two optical detector-types utilized — the single,
  detector-head and the linear detector array. The former is used
  for the day-to-day evaluation and alignment of the Bragg cells.
  The second detector (described in Appendix B) simulates the
  real-world processor that will be required to take the transformed
  optical signal and convert it into electrical signals that can be
  further processed by peripheral electronics. This is the detector
  that was used in the Spectrum Analyzer evaluation.

C.   Electrical Requirements and Test Results

The Direct RF A/O Processor Spectrum Analyzer is designed to provide the
capability to thoroughly evaluate a diverse electromagnetic signal environ-
ment using acousto-optical techniques. Previous sections of this report
presented in detail the design technology necessary for the realization of

this wideband signal processor, as well as the characterization of the Bragg cells themselves. This section addresses the ultimate goal of the program — the demonstration of the technical feasibility of a wideband acousto-optic processor spectrum analyzer. The data taken during the evaluation of the A/O processor was aimed directly at each paragraph of specification No. 57R16-34-002. Rev. A. At the conclusion of each performance subsection that does not meet the specification requirements, a statement is made concerning the possibility of improving the performance. The electrical tests and the conclusions drawn from them apply, of course, only to the laboratory environment conditions under which they were made.

1. RF Signal Input Characteristics

The Spectrum Analyzer is capable of accepting signal inputs in only one RF frequency channel at a time. It is important to remember that this is not a limitation of the technology or the approach, but rather on the peripheral electronics used to form the demonstration test setup; (e.g., the inability to simulate the "wide open" environment normally provided by the antenna system). However, to demonstrate the inherent ability of this type of equipment to detect and resolve more than one signal in a given band, "two simultaneous signal" tests were made. The results of these tests are summarized later in the subsection on "Spectral Resolution."

a. Input Signal Level

Specification: Sufficient RF signal gain will be provided in each channel to permit operation at the top of the dynamic range with a +10 dBm input signal to each channel.

Performance: Referring to the diagram of Figure 39, a solid state, laboratory-type amplifier was used to provide RF gain to the input signals. The amplifier has approximately 20 dB of gain and a +23 dBm compression point. The considerations with respect to dynamic range are discussed in a subsequent section.

b.   Signal Port Impedance

Specification: The input impedance of each IF (RF) port shall be 50 ohms nominal with a maximum VSWR of 1.5:1 over the processor band of operation.

Performance: Due to the poor VSWR characteristics of the Bragg cell's acoustic port, an isolator will be needed to meet this specification. Figure 40 illustrates the minimum performance achieved by the evaluation test setup: a VSWR of 1.39:1 over the 4-6 GHz band, and 1.33:1 over the 6-8 GHz band.

c.   Input Signal Temporal Characteristics

Specification: The input signals to the processor shall be pulsed signals exhibiting pulse widths in the 1.0 microsecond range. These signals are to be applied to the processor as single pulses and at rates between 500 PPS and 5000 PPS.

Performance: The relatively low level of Bragg cell efficiency prevented the observing of pulsed signals. However, experience gained by testing other, higher efficiency Bragg cell devices over similar parameters indicates that satisfactory pulsed operation can be achieved, with spectral analysis that is more than satisfactory.

2.   Center Frequency

Specification: The processor center frequency shall be as indicated in Table I of No. 57R16-34-002, Rev. A, for each of the four bands indicated.

Performance: The table below illustrates the basic compliance of performance with the specification.
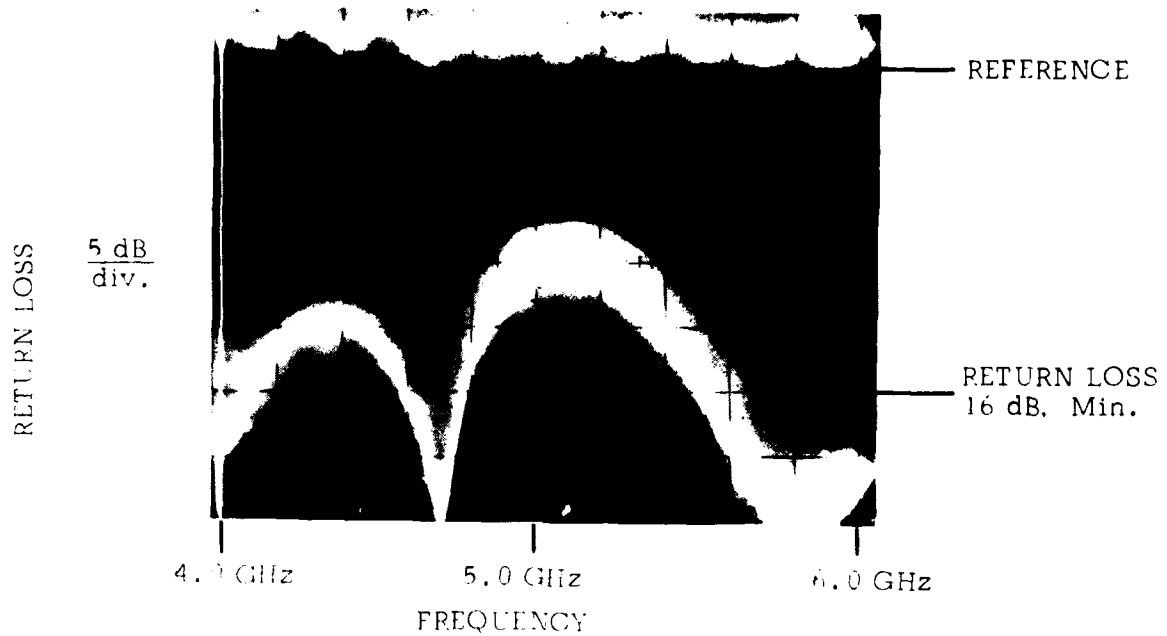
FIGURE 40A. AOX-030: 4-6 GHz.
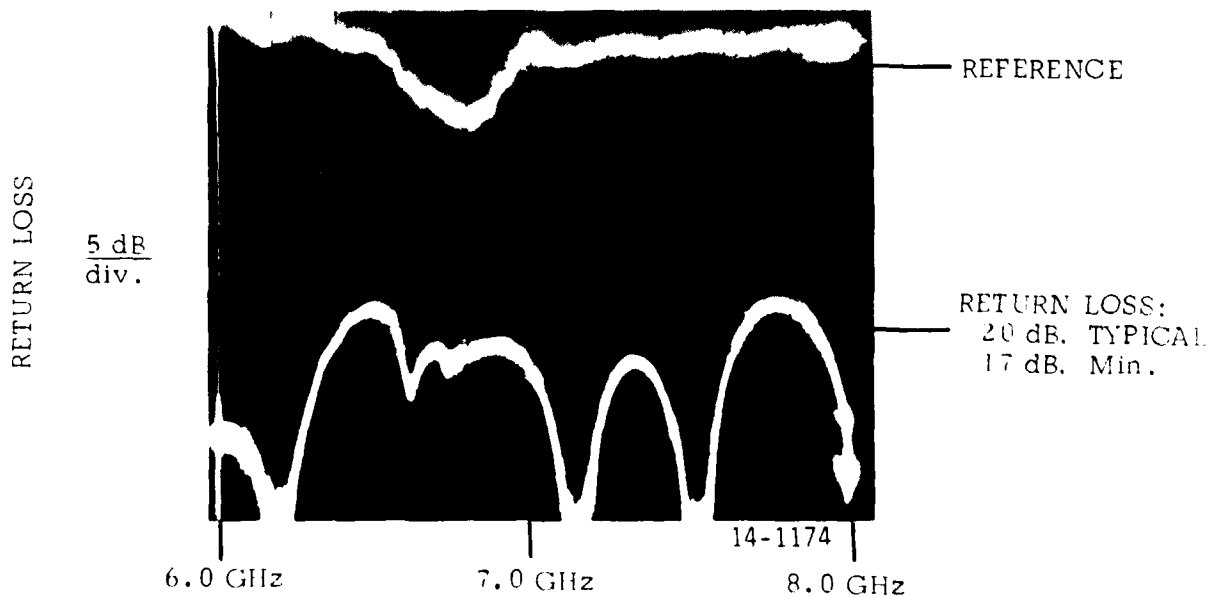
FIGURE 40B. AOX-040; 6-8 GHz.

FIGURE 40. VSWR CHARACTERISTIC OF THE
SPECTRUM ANALYZER RF INPUT PORT.

BAND NO.	CENTER FREQUENCY (GHz)	FREQUENCY RANGE (GHz)
1	4.5	4 to 5
2	5.5	5 to 6
3	6.5	6 to 7
4	7.5	7 to 8

3.   Bandwidth

Specification: The processor shall perform the required functions outlined in Paragraph 6.0 when subjected to pulsed signal(s) occurring within an instantaneous (approximately half-octave) bandwidth in Table 1 for each of four frequency bands.

Performance: The performance table presented in the previous paragraph illustrates the basic ability of the processor to cover the required frequencies. The tests were made with CW signals since the efficiencies achieved prohibited observing pulsed signal outputs.

4.   Efficiency

Specification: In accordance with Table 1 of Specification No. 57R16-34-002, Rev. A.

Performance: The following table illustrates the level of efficiency performance achieved.

BAND	FREQUENCY (GHz)	FREQUENCY RANGE (GHz)	(% PER RF UNIT) MIN.	MAX.
1	4.5	4 to 5	.0023	.0063
2	5.5	5 to 6	.0005	.0035
3	6.5	6 to 7	.00075	.0017
4	7.5	7 to 8	.00015	.0009
Reference: Figure 38.				

Comment: We have discussed at some length the efficiency response model necessary to accurately describe the level of performance to be expected from the processor. Reviewing this model along with the data accumulated, it is possible to make the following efficiency improvements:

- Impedance match the acoustic (RF) port. This should increase the minimum efficiency achieved by 7-10 dB in the 4-6 GHz frequency range, and by 5-7 dB in the 6-8 GHz range.

- Reduce the distance of the interaction region from the transducer face. This would buy about 2 dB in improved efficiency.

- Utilization of a shear mode acoustic signal also has the potential to improve the acousto-optic efficiency.

All in all, there is the potential of improving the 4-8 GHz efficiency by approximately 10 dB.

5.   Processing Functions

The feasibility model processor shall perform the following signal handling functions:

- Spectral Analysis

- Data Readout Interface

a. Spectral Resolution

Specification: The processor shall be capable of spectrally resolving the frequency of an input signal to the frequency indicated in Table 1 of 57R16-34-002, Rev. A.

Performance: Figure 41 illustrates the detected signal characteristic, and the performance of the video monitor (oscilloscope), both with and without a detected signal present.

Figure 42 is a four-part representation, one for each channel, showing the detected signal and detector-pixcel performance across the full 4 GHz bandwidth. Data was taken every 100 MHz and may be compared with the efficiency plot of Figure 38. The linear photodetector array has approximately 2000 resolution elements to cover the 4 GHz frequency range, providing about 2 MHz resolution.

Simultaneous Signals: Figure 43 demonstrates the ability of the spectrum analyzer to resolve two closely-spaced (in frequency and time) signals. In (a), an unknown signal is introduced in the vicinity of a known signal, at 6.68 GHz. In (b) and (c) the unknown signal is detected, coming closer to the known signal. In the last photo (d) it can be seen in the detector cell   adjacent to the known signal, 2 MHz away.

Comment: The specification requirement concerning "signal presence" being determined in the presence of a 50 dB larger signal, one resolution cell away, could not be tested. The 50 dB requirement is a system dynamic range specification that is being limited by the dynamic range of the linear detector array. The detector array is limited to about 20 dB dynamic range by the technology being used in currently available commercial detectors. The dynamic range of the acousto-optic Bragg cell is

(a)

200mV

DETECTOR ARRAY OUTPUT —
WITH NO RF INPUT.

(b)

200mV

DETECTOR ARRAY OUTPUT WITH AN
RF SIGNAL PRESENT AT 6.51 GHz.

OPTICAL
(DETECTOR)
NOISE
FLOOR
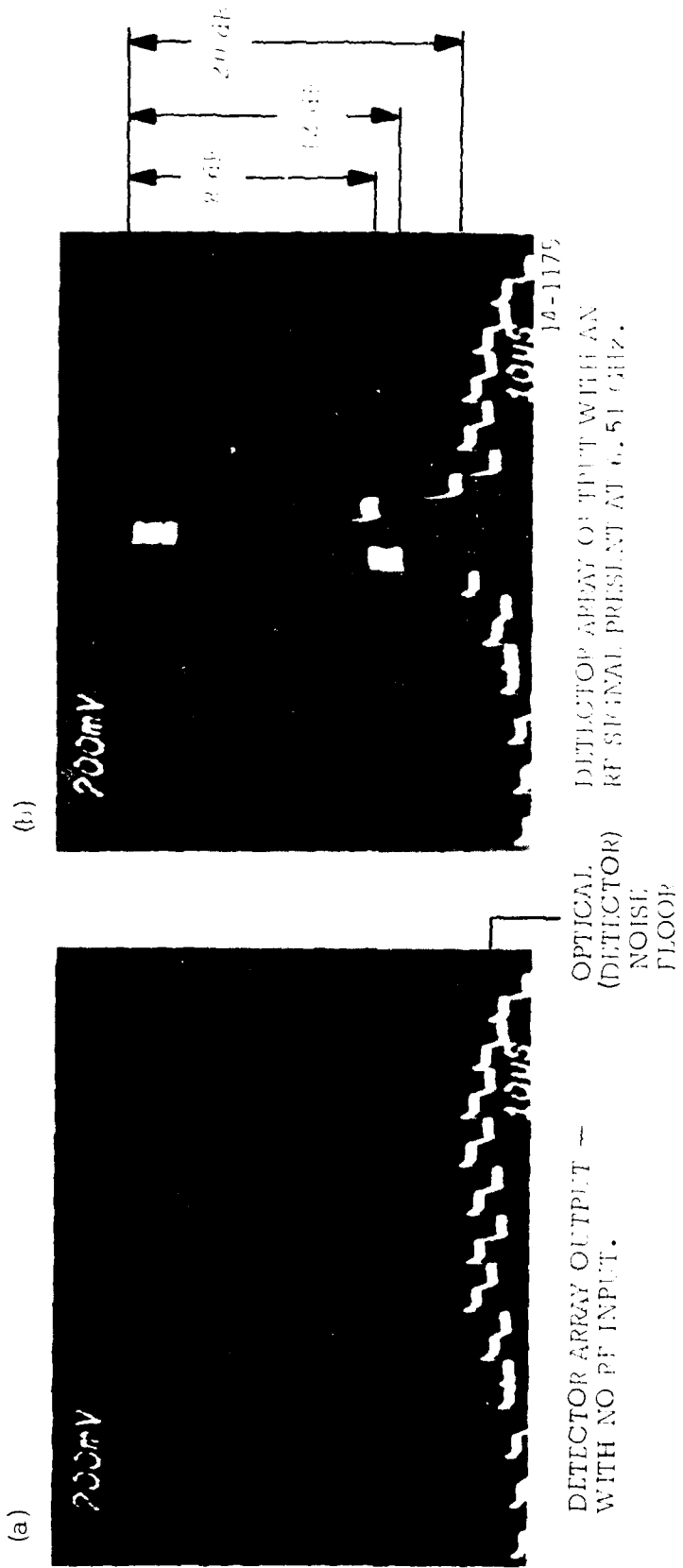
FIGURE 41. DETECTOR ARRAY OUTPUT WITH AND WITHOUT RF SIGNAL INPUT.

-108-
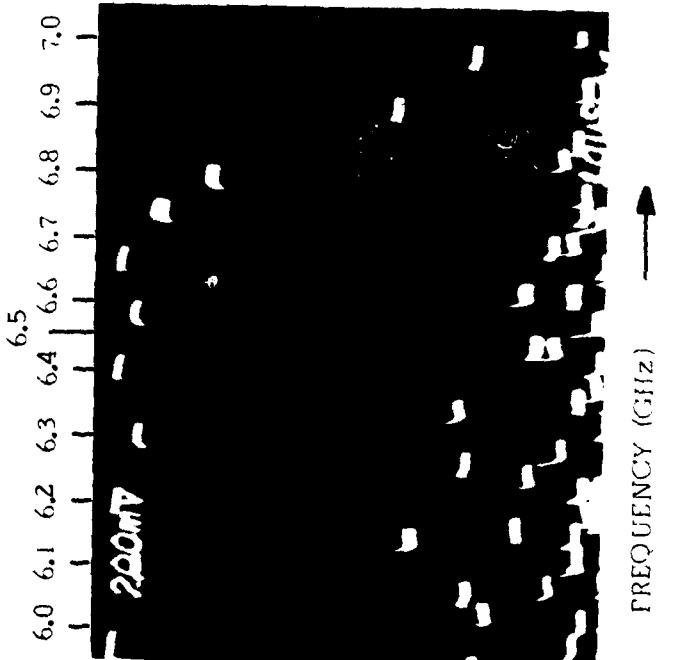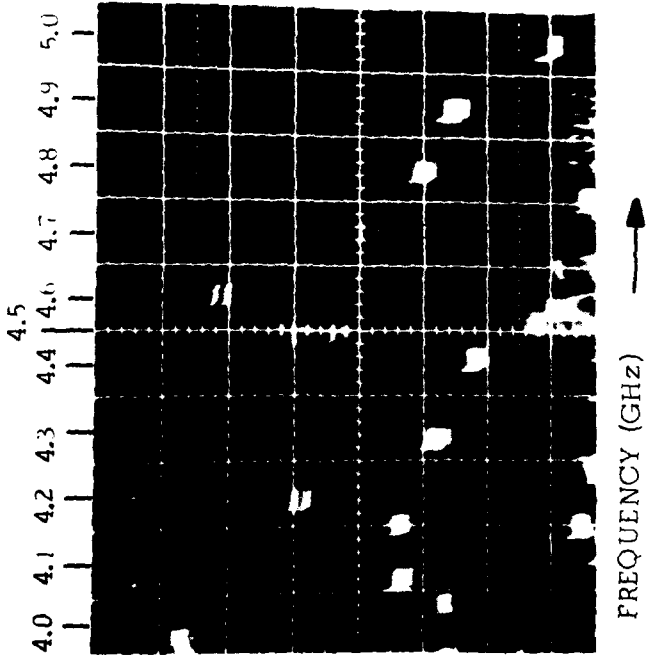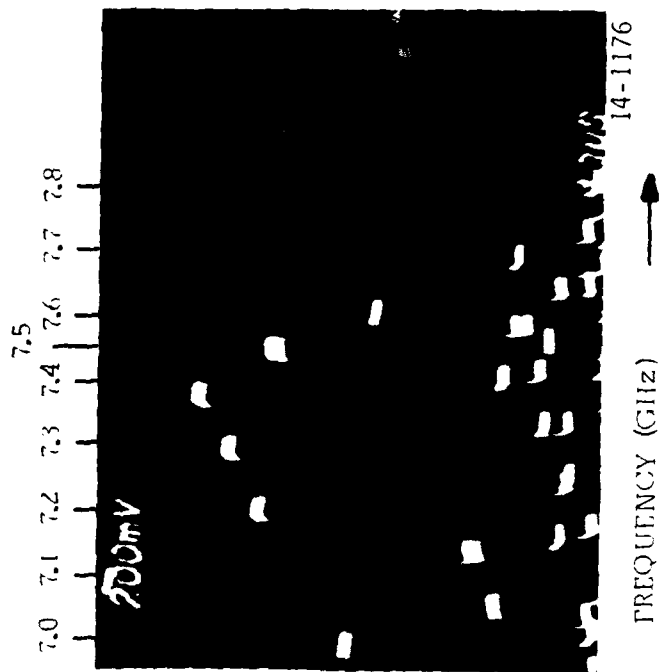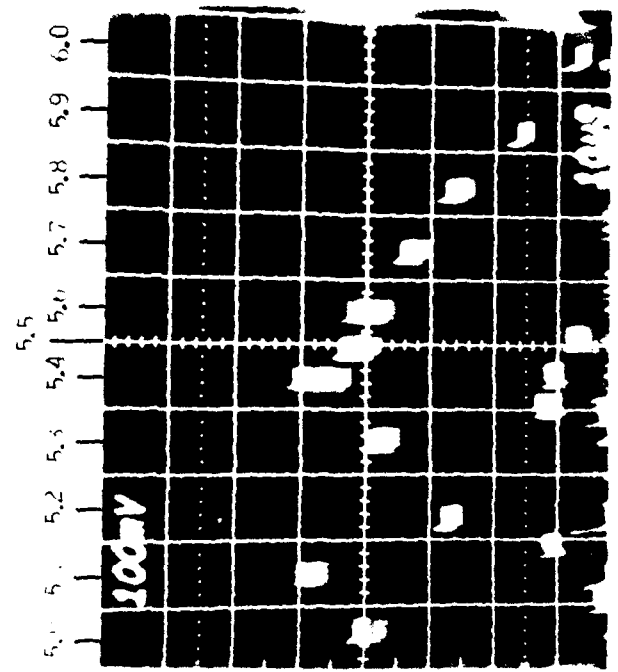
FIGURE 42. DETECTED OUTPUT FOR THE
4-8 GHz SPECTRUM ANALYZER.
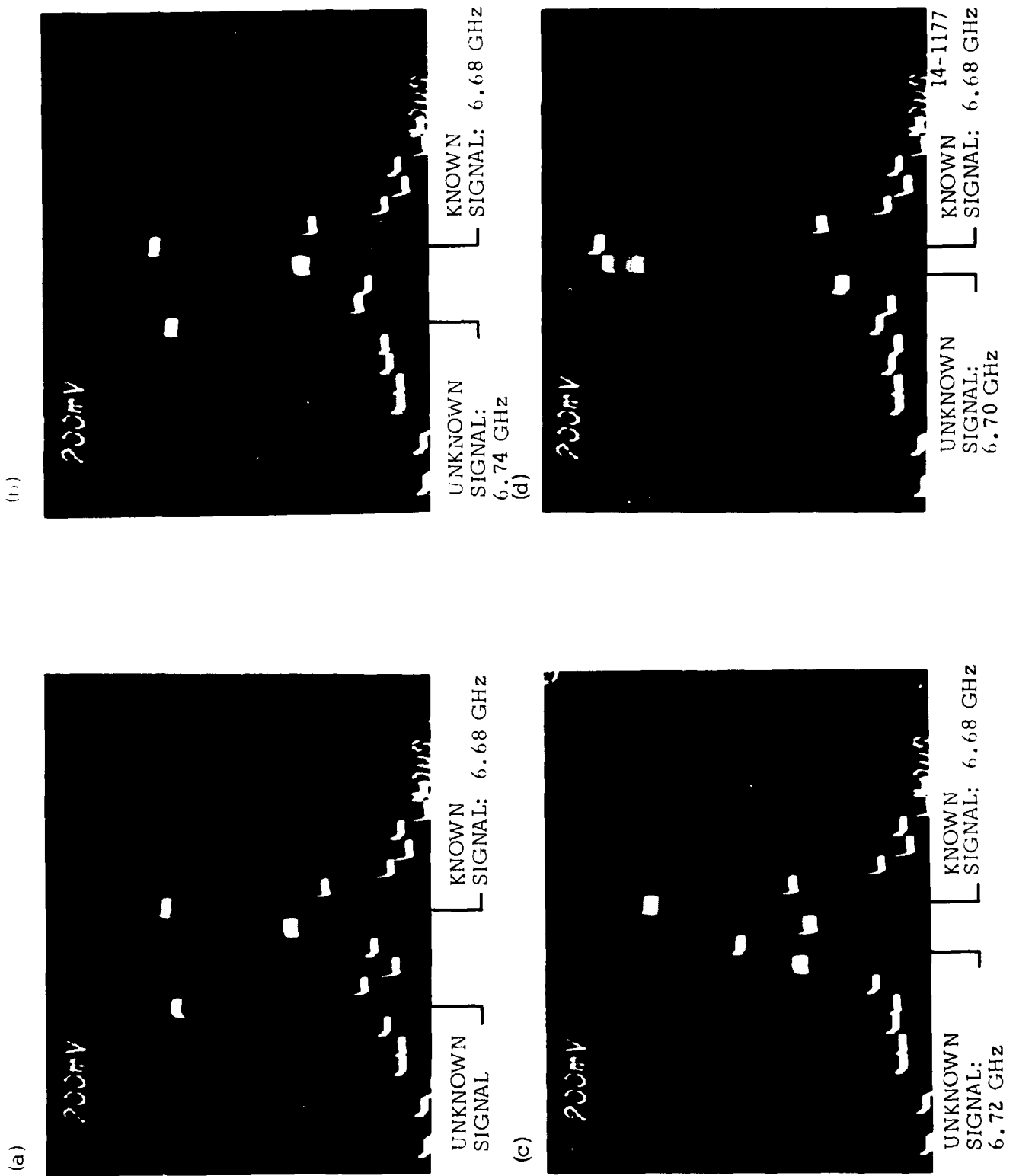
FIGURE 43. DETECTION OF SIMULTANEOUS SIGNALS
BY THE SPECTRUM ANALYZER.

estimated to be in excess of 45 dB over the full 4 GHz frequency range.

b.   Data Readout Interface

Specification: Provisions shall be made for interfacing the raw imager video output with a standard video monitor.

Performance: The requirement was met utilizing the Reticon CCPD linear detector array video interface board. Appendix B provides a more detailed description of the detector-type used during the demonstration, as well as the video processing circuitry used to interface with the monitor oscilloscope.

6.   Dynamic Range

Specification: The processor shall operate over an instantaneous dynamic range of 50 dB. The dynamic range is defined as the linear range over which the amplitude difference between one of two equal level coincident input signals driving the processor at the maximum signal input level, and an input signal providing an amplitude response equal to that of the in-band third order intermodulation product.

Performance: The 50 dB of dynamic range was not attainable because of the limited dynamic range of the detector array. The dynamic range performance varied with signal level and, hence, efficiency across the band. A value of 15 dB was typically observed.

The ratio of the maximum to minimum signals that can be unambiguously and simultaneously processed by the acousto-optic spectrum analyzer defines its dynamic range. However, intermodulation products (in the Bragg cell and the RF amplification) and the scattered light level (as seen at the detector) are also very important, and in some cases become the limiting parameters in achieving a large dynamic range.

Figure 44 illustrates the dynamic range considerations which surround the demonstrated Bragg cell processor. In addition, this figure presents an
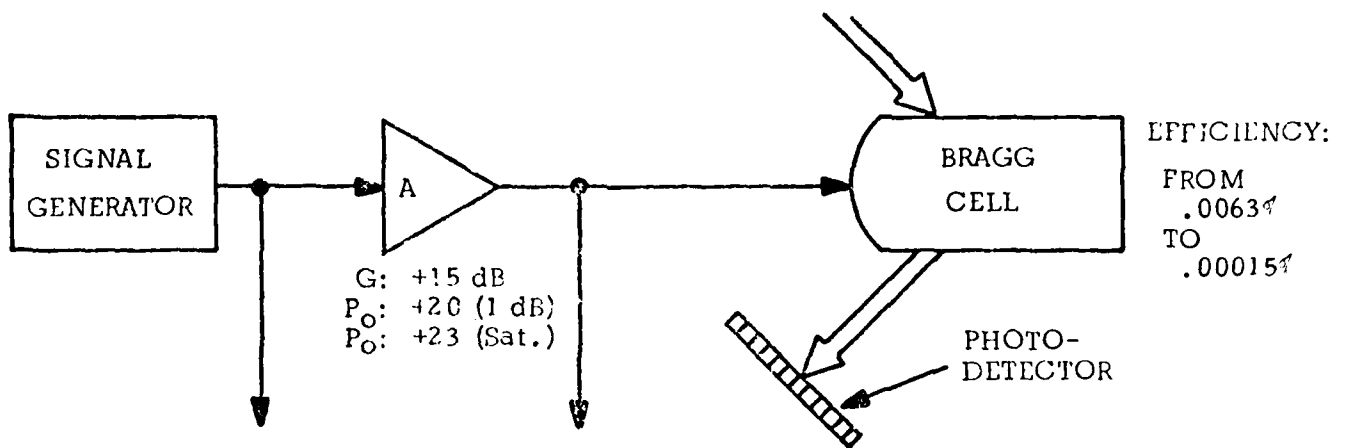
DYNAMIC RANGE: 16.5 dB

+6.8 dBm	(+21.8 dBm) 150 mW	133 nW: Maximum detected signal
-9.7 dBm	(+ 5.3 dBm) 3.4 mW	3 nW: Minimum detected signal

- 3rd order intercept dynamic range limit: ~30 dB
- Scattered light (detector) dynamic range limit: ~20 dB
- Detector dynamic range: 360 nW (sat)/3 nW $\cong$ 21 dB
- Bragg cell dynamic range: 50 dB

FIGURE 44A. SIGNAL LEVEL ANALYSIS: DEMONSTRATION TESTING.
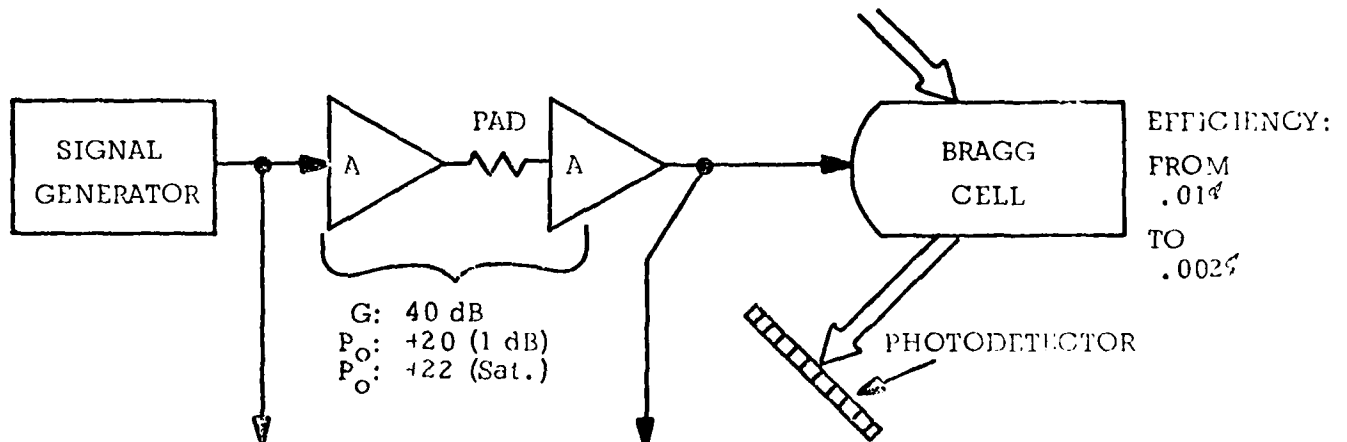
DYNAMIC RANGE: 50 dB

0 dBm	(+20 dBm) 100 mW	170 nW: Maximum detectable signal (in saturation)
-50 dBm	(-10 dBm) 0.1 mW	51 nW: Minimum detectable signal

- 3rd order intercept dynamic range limit: 45 dB
- Scattered light (detector) dynamic range limit: ~20 dB
- Detector dynamic range: 170 nW/2nW $\cong$ 21 dB
- Bragg cell dynamic range: 50 dB

FIGURE 44B. SIGNAL LEVEL ANALYSIS: AN IMPROVED SYSTEM.

FIGURE 44. SPECTRUM ANALYZER DYNAMIC RANGE.

"improved dynamic range" system, based on a more efficient Bragg cell. Figure 44a shows the typical signal levels experienced by the A/O spectrum analyzer processor during the demonstration tests. The factors which were observed to limit the dynamic range performance are the Bragg cell efficiency and the sensitivity (dynamic range characteristic) of the detector. Specifically, the minimum acousto-optic efficiency is sufficiently low to cause the detector to operate in its minimum detectable signal region. At the higher Bragg cell efficiencies there is insufficient deflected light to fully saturate the photodetector, thereby limiting its dynamic range. An examination of the notes included beneath the diagrams of Figure 44 indicates that the detector array dynamic range is also quite small (about 21 dB) even when extended to its full saturation level — at approximately 360 mW of incident light.

In Figure 44b an improved system is synthesized, primarily to help get a feel for those factors that will ultimately restrict the dynamic range performance. In the example, we have assumed an input sensitivity requirement of -50 dBm, and inserted the appropriate amount of RF amplification to ensure about +20 dBm at the acousto-optic transducers. This control over the level of RF amplification is necessary so as to prevent the system from operating in saturation where the intermodulation product level becomes a problem. The Bragg cell efficiency improvement is modest, but sufficient to support a system dynamic range of more than 45 dB at the detector.

It is now possible to identify what will probably be the ongoing limitation to achieving dynamic ranges of greater than 20 dB: the photodetector.

Even if operated over its full detectable signal range (from ~360 nW to ~3 nW) a dynamic range of about 20 dB is all that can be achieved. If an improvement of roughly half an order of magnitude can be obtained in the saturation level-dynamic range of the detector, coupled with improvements in the power output of small, solid-state, optical light sources, dynamic ranges on the order of 45 to 50 dB can be readily achieved for spectrum analyzer applications.

D. Mechanical Requirements

The Direct RF Acousto-Optic Processor Spectrum Analyzer was assembled for demonstration using standard microwave and optic test equipment. Figures 10 and 39 illustrate the basic components used, while Figure 1 is a photograph of the laboratory test setup.

1. Size, Weight and Configuration

While the "laboratory" approach is certainly acceptable for the purposes of demonstrating the technical feasibility of a technique or process, it is totally inadequate as an operational system. For that reason, some thought was given during the course of the program as to how a system such as the A/O Spectrum Analyzer could be packaged.

An analysis of the required optical focal lengths and lens sizes strongly indicates that the spectrum analyzer could be packaged quite efficiently. In fact, using a solid state laser, it is possible to package this system in a container of less than one foot in length.

Figure 45 illustrates an actual housing with its assembled components used to satisfy a need similar to that required of the equipment demonstrated on this program. All of the lens and lens mounts are standard, off-the-shelf components, while the lens bases were designed and manufactured especially for the particular application. The overall size of the processor shown in Figure 45 is 3 inches by 4 inches by 10 inches in length. TMEC is currently working on an improved lens system that shows promise of reducing the length by almost a factor of two. It would seem, therefore, that it is indeed possible to realize a broadband acousto-optic spectrum analyzer in a small and flyable hardware configuration.

E. Conclusions

Now that the data gathering and evaluation of the Direct RF A/O Processor

14-1161B

FIGURE 45. COMPONENTS AND HOUSING OF A TMEC PROCESSOR.

Spectrum Analyzer has been completed, it is possible to take account of those areas where it fell short of our expectations, as well as those areas of achievement.

1.   Performance Evaluation

There are two principal performance areas that were crucial to the success of this program: the realization of a full 4 GHz of operational bandwidth and a high level of acousto-optic efficiency (from 2 to 4 percent across the 4 GHz band). On the positive side, TMEC was able to develop processing technologies and manufacturing methods that produced an acousto-optic Bragg cell capable of covering the entire 4 to 8 GHz bandwidth. On the other hand, the efficiency performance fell far short of the specification requirements. The important thing to remember regarding the efficiency performance is that we are not only beginning to understand the "why" of the reduced performance, but through the developing efficiency model it is now possible to begin to predict a Bragg cell's efficiency performance.

Conclusion

The technology exists for achieving very broad acousto-optic processors through the use of thin-film piezoelectric transducers. This is not to say that the segmentation of the 4 GHz frequency range could not be improved — perhaps by using five channels instead of four — but the transducer technology itself is well in hand.

The major area of concern, therefore, is the level of efficiency achieved compared to that level required to make acousto-optic signal processing a viable alternative. There are technology and manufacturing improvements which can be incorporated relatively easily — techniques such as imped-ance matching, a better physical relationship between the external optics and the acoustic substrate, and an interaction region that is closer to the transducer surface. There are two areas which offer the potential of an even larger increase in the acousto-optic efficiency of broadband spectrum

analyzers and processors. These areas are the acousto-optic substrate material and the piezoelectric transducer used to launch the acoustic signal. A variety of techniques and materials exist (and have to some extent been investigated) for improved bulk acoustic wave delay line performance. Materials which have the potential for supporting higher efficiency acoustic shear waves currently exist. To support such new materials, a new transducer technology will be required — a technology perhaps like the bonded-piezoelectric transducers currently being manufactured from lithium niobate wafers. Although currently a narrowband process, the potential exists for achieving reproducible bandwidths approaching 2 GHz through the continued utilization of curved surfaces to focus the acoustic energy.

Overall Performance Assessment

Other than the reduced efficiency observed during the program, most specification requirements of 57R16-34-002 Rev. A will not be restricted by the acousto-optic device. Dynamic range and sensitivity, for example, are largely a function of the photodetector technology and the intermodulation products of the RF amplification process. This program, in conjunction with the data collected on similar investigations, has shown that the desired operation is achievable and in many cases, over narrower bandwidths, has been achieved.

One consideration of the overall performance of Bragg cells is the need to process pulsed signals. The investigation conducted during this program used CW signals due to the relatively low efficiency of the Bragg cell. Therefore, the efficiency improvements that have been discussed must be tempered by the fact that pulsed operation will negatively affect the gains in receiver sensitivity resulting from any such improvements. If it were possible to "synthesize" a longer signal by stretching or recirculating the incoming pulses prior to the Bragg cell, much of the lost "pulse" efficiency could be regained.

2. Technology Evaluation

Several technological hurdles were encountered during this program, the most severe being the polishing of the curved transducer surface. Through the diligence of a great many people, it is now possible to obtain high-quality, polished, transducer-grade, curved surfaces. Should this type of approach continue to be the one of choice, the basic processing procedures exist, and all that will be required is a Manufacturing Methods-type effort to transform them into production-proven techniques.

New Technologies

Material and transducer technology changes designed to produce performance improvements over and above existing technologies will require development and feasibility programs similar to the one just completed. Acousto-optic materials and configurations need to be investigated, and improved transducer techniques should be developed. The approach taken should be to develop a modular bandwidth Bragg cell with high efficiency. The bandwidth of the module would be a minimum of 2 GHz, using at most three transducers. The module would be designed with technologies that allow highly efficient operation over a basic frequency range of, for example, 2 to 4 GHz. The 2 GHz bandwidth efficiency, using improved RF matching techniques, should be in the 1 percent per RF watt range for this frequency band. The module would be usable as a fundamental processor operating directly at its RF frequency, or be capable of being frequency up-converted to cover broader bandwidth applications, all with the same high efficiency processor.

There is much work to be done and the potential payoff is quite large.

APPENDIX A

PATH OF THE DEFLECTED LASER BEAM AS IT TRAVERSES
THE ACOUSTO-OPTIC CRYSTAL

APPENDIX A

PATH OF THE DEFLECTED LASER BEAM AS IT TRAVERSES
THE ACOUSTO-OPTIC CRYSTAL

The angles of the deflected laser beam are calculated in this appendix.
These angles include the incident angle of the laser beam, the refracted
angle as the beam enters the acousto-optic crystal, the Bragg angle
internal to the crystal, and the laser beam's exit angles. Numerical
values of all these angles are determined for $LiNbO_3$, GaP and TeO_2.

Figure A-1 shows the path of the deflected laser beam as it passes through
the acousto-optic crystal. The incident angle is θ_1, the refracted angle
is θ_2, θ is the Bragg angle, and θ_3 and θ_4 are the two exit angles (as
shown in the illustration). For a crystal with an index of refraction equal
to n and an acoustic velocity equal to v, with a laser beam of wavelength
λ_o, the angles are related by the following expressions:

$$n \sin \theta_2 \; = \; \sin \theta_1 \qquad\qquad (1)$$

$$n \sin \theta_3 \; = \; \sin \theta_4 \qquad\qquad (2)$$

$$\theta_3 \; = \; 2\,\theta - \theta_2 \qquad\qquad (3)$$

$$\theta \; = \; \sin^{-1} (\lambda_o \, f/2nv) \qquad\qquad (4)$$

where f is the frequency of the acoustic wave.

Solving equations (1), (2), (3) and (4) for the exit angle θ_4, in terms of
the incident angle θ_1, gives the following:

$$\theta_4 = \sin^{-1} \left\{ n \sin [2 \sin^{-1} (\lambda_o \, f/2nv) - \sin^{-1} (n^{-1} \sin \theta_1] \right\} \qquad (5)$$

Component of
acoustic wave at
Bragg angle.

Path of Laser Beam

θ_1

air

θ_B θ_2

Acousto-optic crystal
with refractive index = n

θ_B θ_3

air

$2\theta_B$

θ_4
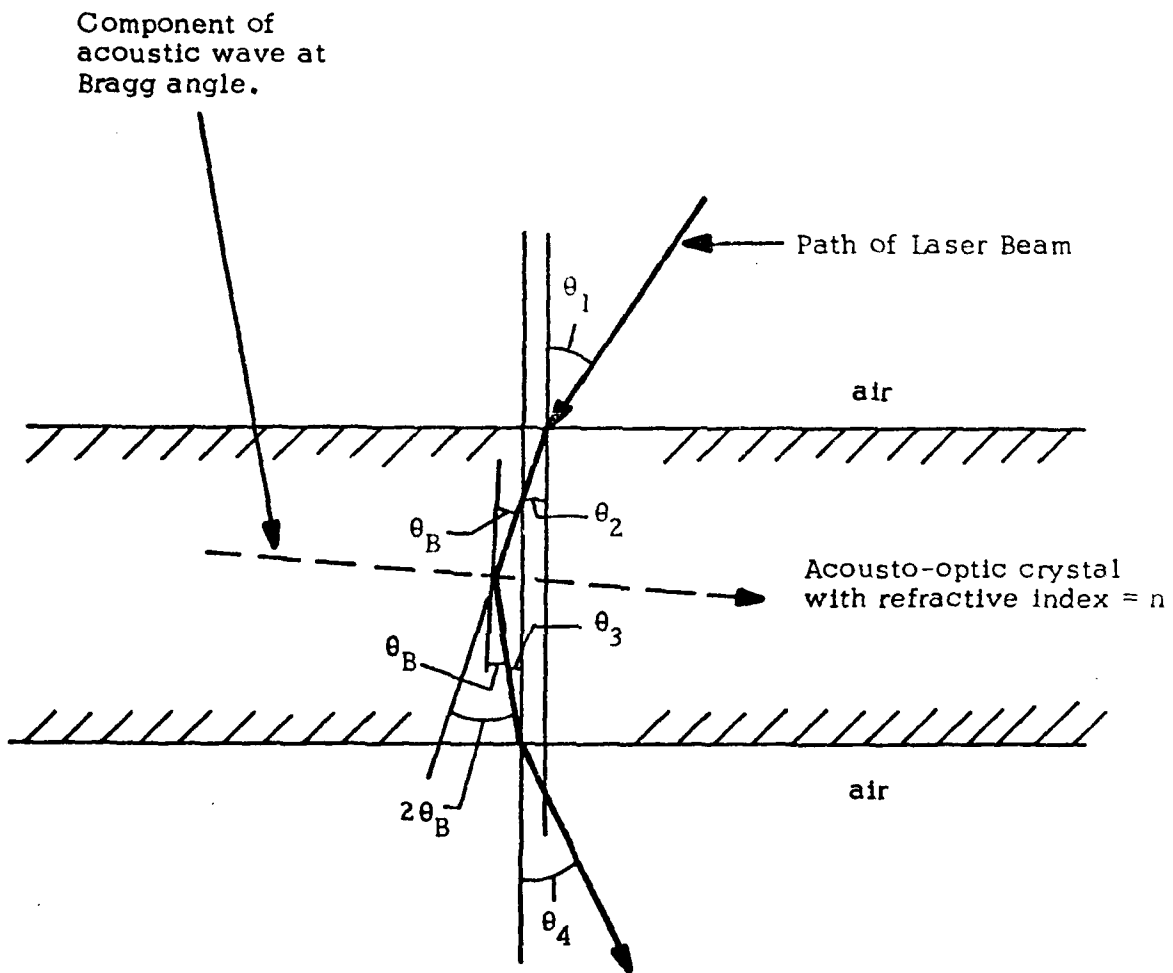
FIGURE A-1.   DIAGRAM SHOWING THE PATH OF THE
DEFLECTED LASER BEAM PASSING THROUGH
AN ACOUSTO-OPTIC CRYSTAL.

If θ_1 is set equal to the external Bragg angle at frequency f_o, then

$$\sin \theta_1 = \lambda_o f_o / 2v \qquad (6)$$

Substituting equation (6) into (5) gives the laser exit angle in terms of f_o:

$$\theta_4 = \sin^{-1} n \sin [2 \sin^{-1} (\lambda_o f/2 nv) - \sin^{-1} (\lambda_o f_o/2 nv)] \qquad (7)$$

Using equations (6) and (7), θ_1 and θ_4 can be determined. Then, using equations (1), (2) and (4), the angles θ_2, θ_3 and θ can be determined. Tables A-1, A-2 and A-3 show these angles for LiNbO$_3$, GaP and TeO$_2$ over the frequency range of 4 to 8 GHz, assuming that the incident laser beam angle is set equal to the Bragg angle at 6.0 GHz. The total deflection angle, which equals $\theta_1 + \theta_4$, is tabulated and plotted (Figure A-2) for LiNbO$_3$. The angle will be used to design the four-channel acousto-optic component for the 4 to 8 GHz spectrum analyzer.
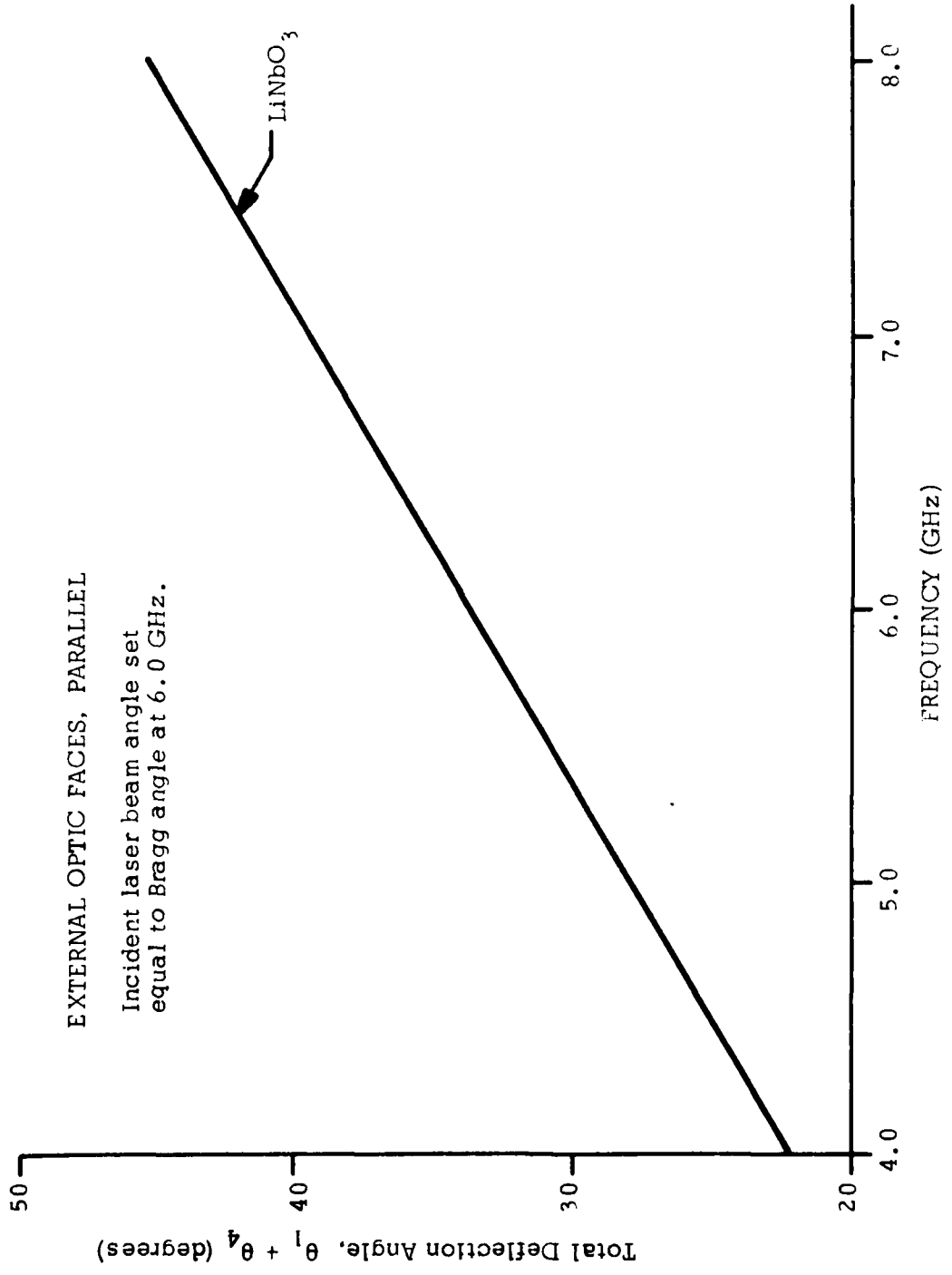
FIGURE A-2. TOTAL LASER BEAM DEFLECTION ANGLE THROUGH ACOUSTO-OPTIC CRYSTAL VERSUS FREQUENCY FOR LiNbO$_3$.

TABLE A-1

ANGLES OF DEFLECTED LASER BEAM AS IT PASSES THROUGH LiNbO$_3$ ACOUSTO-OPTIC CRYSTAL

Longitudinal acoustic wave propagating along X-axis.

Laser beam propagating 35° off Y-axis toward X-axis.

Laser beam polarized perpendicular to acoustic wave propagation direction.

f_o = 6.0 GHz

n = 2.2

v = 6.57 x 10^5 cm/sec.

λ_o = 6328 Å

Frequency f (GHz)	θ (deg.)	θ_1 (deg.)	θ_2 (deg.)	θ_3 (deg.)	θ_4 (deg.)	Total Deflection $\theta_1 + \theta_4$ (deg.)
4.0	5.023	16.795	7.547	2.500	5.506	13.053
4.5	5.653			3.759	8.293	15.840
5.0	6.284			5.020	11.100	18.647
5.5	6.915			6.283	13.931	21.478
6.0	7.547			7.547	16.795	24.342
6.5	8.180			8.813	19.698	27.245
7.0	8.814			10.081	22.650	30.197
7.5	9.449			11.352	25.660	33.207
8.0	10.086	16.795	7.547	12.624	28.739	36.286

TABLE A-2

ANGLES OF DEFLECTED LASER BEAM AS IT PASSES THROUGH
GaP ACOUSTO-OPTIC CRYSTAL

Longitudinal acoustic wave propagating along [110] axis

Laser beam polarized parallel to acoustic wave propagation direction.

f_o = 6.0 GHz

n = 3.31

v = 6.32 x 10^5 cm/sec.

λ_o = 6328 Å

Frequency f (GHz)	θ (deg.)	θ_1 (deg.)	θ_2 (deg.)	θ_3 (deg.)	θ_4 (deg.)	Total Deflection $\theta_1 + \theta_2$ (deg.)
4.0	3.468	17.480	5.207	1.730	5.736	23.216
4.5	3.903	↑	↑	2.599	8.631	26.111
5.0	4.337			3.467	11.548	29.028
5.5	4.772			4.337	14.495	31.975
6.0	5.207			5.207	17.480	34.960
6.5	5.642			6.077	20.513	37.993
7.0	6.078			6.948	23.605	41.085
7.5	6.513	↓	↓	7.820	26.768	44.248
8.0	6.950	17.480	5.207	8.693	30.017	47.497

TABLE A-3

ANGLES OF DEFLECTED LASER BEAM AS IT PASSES THROUGH
TeO_2 ACOUSTO-OPTIC CRYSTAL

Longitudinal acoustic wave propagating along [001] axis.

Laser beam polarized perpendicular to acoustic wave propagation direction

f_o = 6.0 GHz

n = 2.26

$v = 4.2 \times 10^5$ cm/sec.

λ_o = 6328 Å

Frequency f (GHz)	θ (deg.)	θ_1 (deg.)	θ_2 (deg.)	θ_3 (deg.)	θ_4 (deg.)	Total Deflection $\theta_1 + \theta_2$ (deg.)
4.0	7.662	26.872	11.537	3.788	8.586	35.458
4.5	8.627	↑	↑	5.717	13.010	39.882
5.0	9.594			7.651	17.512	44.384
5.5	10.564			9.591	22.120	48.992
6.0	11.537			11.537	26.872	53.744
6.5	12.513			13.490	31.816	58.688
7.0	13.493			15.450	37.017	63.889
7.5	14.478	↓	↓	17.418	42.572	69.444
8.0	15.466	26.872	11.537	19.395	48.634	75.506

APPENDIX C

EVALUATION TEST PLAN

EVALUATION TEST PLAN

DIRECT RF A-O PROCESSOR SPECTRUM ANALYZER

Prepared for

NAVAL RESEARCH LABORATORY
WASHINGTON, D.C.

CONTRACT NO. N00173-79-C-0239

9 MAY 1980

DIRECT RF A-O PROCESSOR SPECTRUM ANALYZER

The test plan is to provide detailed testing and support data for the feasibility demonstration of the optical processor (Bragg cell) in accordance with the "Specification for Direct RF A-O Processor Spectrum Analyzer, Number 57R16-34-002, Rev. A" and the subsequent clarifications and change.

Primary Test (PT)

The primary test for the optical processor is one in which the bandwidth, center frequency, efficiency and resolution will be measured. This test will be run on each one of the four (4) frequency bands individually and the 3 dB bandwidths noted. The RF signal will be amplified to permit operations at the top of the dynamic range with a +10 dBm input signal to each channel.

The primary test thus measures the optical processor for the specifications noted in Paragraph 6.1 through Paragraph 6.5, with the exception of Paragraph 6.4.2 (VSWR).

VSWR Test

This test will be run specifically to verify that the optical processor meets the feasibility demonstration as noted in Paragraph 6.4.2.

The test is a standard VSWR measurement to be performed on each of the four (4) inputs to verify the specification of 50 nominal impedance with a maximum VSWR of 1.5:1 over each RF frequency band.

Dynamic Range Test

The dynamic range, as defined in Paragraph 6.6, references the difference in signal level between the two-tone third order intermodulation product and that of the two equi-level input signals that generate the intermodulation product. This range will be tested by increasing the input signals in 10 dB increments until the third order intermodulation is detected.

APPENDIX D

ACCEPTANCE TEST PROCEDURE
FOR
DIRECT RF A-O PROCESSOR SPECTRUM ANALYZER

ACCEPTANCE TEST PROCEDURE

FOR

DIRECT RF A-O PROCESSOR SPECTRUM ANALYZER

NRL SPECIFICATION 57R16-34-002, REV. A

JUNE 1980

REV																									
SHEET	26	27	28	29	30	31	32	33	34	35	36	37	38	39	40	41	42	43	44	45	46	47	48	49	50
REV																									
SHEET	1	2	3	4	5	6	7	8	9	10	11	12	13	14	15	16	17	18	19	20	21	22	23	24	25

TITLE:

ACCEPTANCE TEST PROCEDURE
FOR
DIRECT RF A-O PROCESSOR SPECTRUM ANALYZER

TELEDYNE MEC

ONE POTTER DRIVE PALO ALTO CALIFORNIA 415 493-1770

SIZE	CODE IDENT NO		REV
A	11312	107028	

SCALE		SHEET 1 OF 10

F-0638

1.0 INTRODUCTION

1.1 Purpose

This document establishes the detailed tests and procedures to be used in testing the Direct RF A-O Processor Spectrum Analyzer as described in NRL's Specification No. 57R16-34-002, Rev. A, and amendment to Solicitation No. N00173-79-R-PL30. The Processor is to meet the test limits detailed in Paragraph 3.0 of this procedure and the results are to be entered on the test data sheets of Paragraph 4.0.

1.2 Component Familiarization

The Direct RF A-O Processor Spectrum Analyzer (Figure 1) is composed of an optically transparent crystal, a transducer and a matching network. The RF signal is matched into the transducer via the input (matching) circuit. The transducer then launches acoustic waves in the crystal at the same frequency as the input RF signal.

1.2.2

The acoustic plane wave is made up of areas of dense and less dense regions in the crystal that propagate through the crystal. Under certain conditions, the acoustic wave acts as a diffraction grating when illuminated by a laser beam. This interaction of the laser beam (optic) with the acoustic wave steers a portion of the beam away from the primary laser beam.

1.2.3

The angle formed by the diffraction beam relative to the primary beam is known as the Bragg angle (actually twice the Bragg angle since the Bragg angle is referenced to the crystal surface). The diffraction angle is a function of the acoustic frequency; i.e., the frequency of the RF signal applied to the transducer, and thereby forms the basis of the spectrum analyzer. The position (frequency dependent) of the diffracted beam is detected by a linear array of detector pixels that determine the corresponding frequency.

| SIZE	CODE IDENT NO.		REV
A	11312	107028	
SCALE		SHEET 2 OF 10	
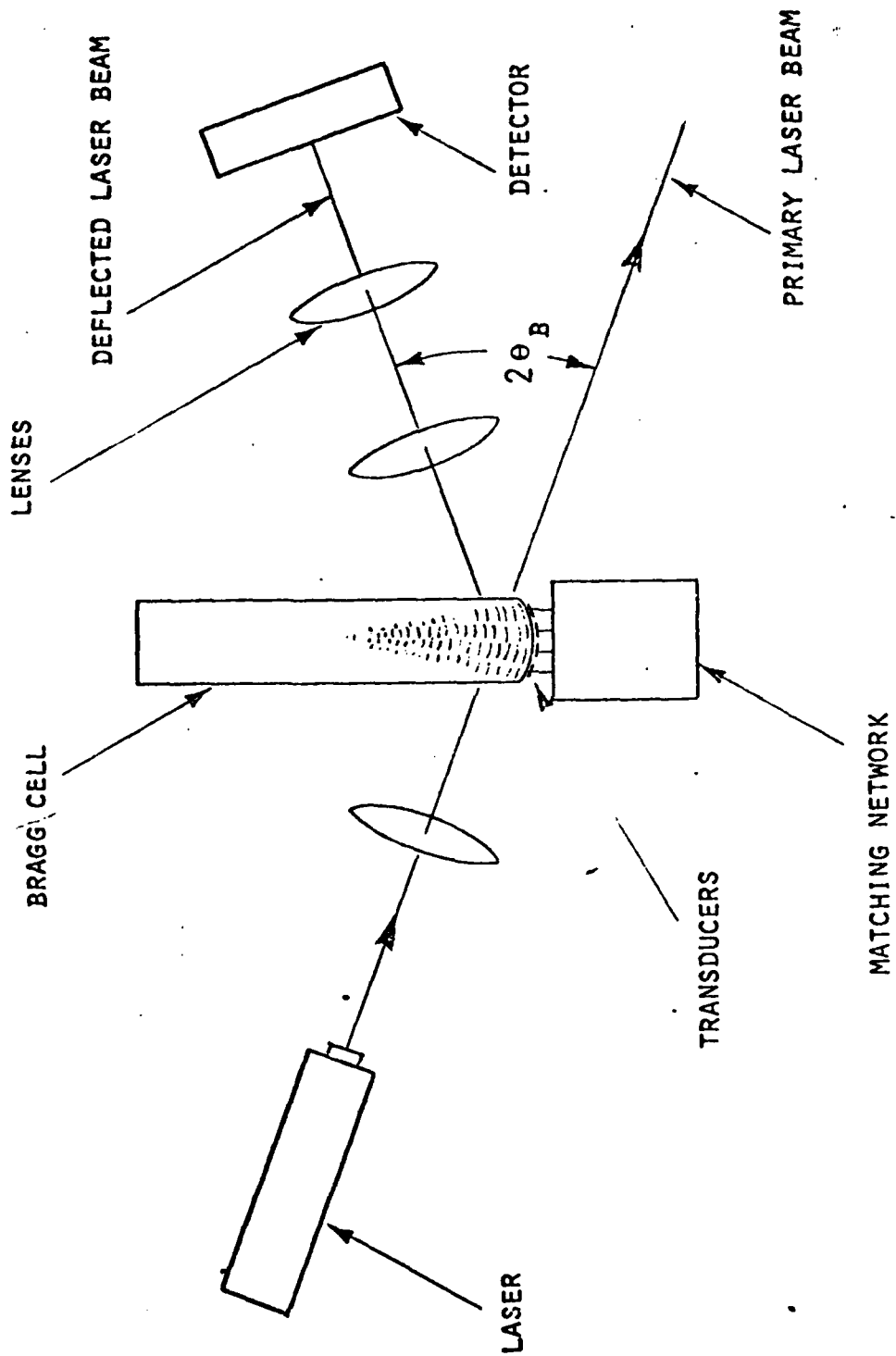
DIRECT RF A-O PROCESSOR SPECTRUM ANALYZER

FIGURE 1

DEFLECTED LASER BEAM

DETECTOR

PRIMARY LASER BEAM

$2\theta_B$

LENSES

BRAGG CELL

MATCHING NETWORK

TRANSDUCERS

LASER

1.3   General Test Approach

1.3.1   There are three major areas of the testing to be considered. These consist of the RF test circuitry, the optical system (laser and lenses) and the detector circuit. The areas are indicated in Figure 2 by the dotted lines. Note, the A-O Processor (or Bragg Cell) is common to both the RF circuit and optical system.

1.3.2   The RF circuitry is used to form input signals as required by the specifications so as to demonstrate the technical feasibility of the program. Specifically, the frequency, power and pulse characteristic of the input signals will be realized.

1.3.3   The laser and associated lens form the optical portion of the system. The laser beam is formed into the proper "interaction aperture" to allow the required frequency resolution and acousto-optic interaction efficiency. The beam is then recollimated and focused to a diffraction limited spot for proper frequency detection.

1.3.4   The frequency dependent position of the diffracted beam is detected by a linear array of photo diodes (pixels). The evaluation circuit associated with the detector has a video output that may be displayed on an oscilloscope. The display indicates the pixel array of the detector with the amplitude of the pixel signal (above the noise floor) representing the amount of light (and, therefore, the amplitude) striking the pixel.

1.3.5   The summation of this outline represents the fundamentals of the acceptance test procedure.

SIZE	CODE IDENT NO.			REV
A	**11312**		107028	
SCALE			SHEET 4 OF 10	
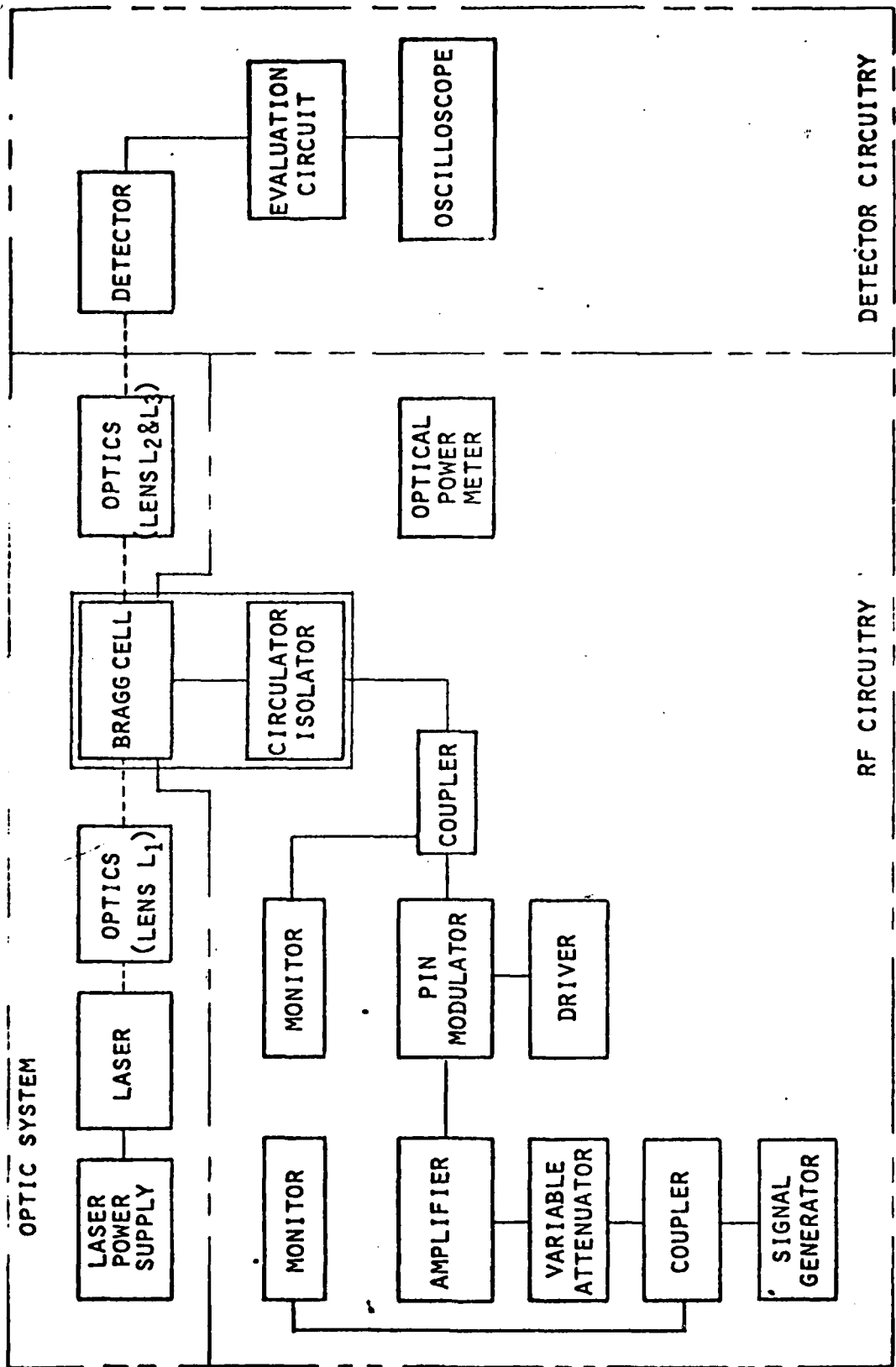
TEST EQUIPMENT BLOCK DIAGRAM
FIGURE 2A

SIZE	CODE IDENT NO.		REV
A	**11312**	107028	
SCALE		SHEET 5 OF 10	

ITEM	QTY	MANUFACTURER	MODEL
Laser Power Supply	1	Spectra Physics	255
Laser (HeNe)	1	Spectra Physics	Stabilite
Lens L_1	1	Klinger Scientific Corp.	063422
Lens L_2	1	Klinger Scientific Corp.	063422
Lens L_{3a}	1	Klinger Scientific Corp.	TBD
Lens L_{3b}	1	Klinger Scientific Corp.	TBD
Signal Generator	1	Kruse Electronics Sweeper	540
Amplifier (TWT)	1	Teledyne MEC (or equivalent transistor amp 1W)	M5901C
PIN Modulator	1	Hewlett-Packard	8731B
Driver (PIN Mod)	1	Hewlett-Packard	8403A
Coupler	2	Narda	3044-10 (or 20)
Power Meter (Monitor)	2	Hewlett-Packard	435A
Detector	1	EG&G Reticon	CCPP256
Evaluation Circuit	1	EG&G Reticon	RC700A
Detector	1	EG&G Reticon	S-1024
Evaluation Circuit	1	EG&G Reticon	RC-1024SA
Oscilloscope	1	Tektronix	475
Variable Attenuator (0-9)	1	General Microwave	M180
Variable Attenuator (0-60)	1	General Microwave	M181

FIGURE 2B

2.0 GENERAL TEST CONDITIONS

2.1 Input Signal

The variable attenuator and amplifier should result in sufficient
signal gain in each channel to permit operation at the top of
the dynamic range with +10 dBm input signal to each channel.

2.2 Pulse Characteristics

The input signals shall be pulsed signals exhibiting pulse
widths in the 1.0 µsec range. The signals shall be single
pulses and at rates between 500 pps and 5000 pps.

2.3 Environmental Test Procedures

The electrical specifications shall apply to laboratory environ-
ment conditions.

SIZE	CODE IDENT NO.		REV
A	11312	J07028	
SCALE		SHEET 7 OF 10	

3.0   TEST PROCEDURES

3.1   VSWR

3.1.1   The VSWR will be measured on the Hewlett-Packard automatic network analyzer.

3.1.2   The data may be printed as a graph and/or a table with data points every 100 MHz maximum interval.

3.2   Bandwidth and Center Frequency

3.2.1   Set up the test equipment as indicated in Figure 2.

3.2.2   Set the frequency generator to sweep the band.

3.2.3   Adjust the Bragg angle for maximal flat response across the band.

3.2.4   Set the frequency generator to single frequency.

3.2.5   Adjust the variable attenuator so that a +10 dBm signal of approximately 1 μsec pulse width will just saturate the detector. This adjustment is to be made in the most efficient portion of the response. Record data.

3.2.6   Measure and record the response from f_1 to f_2 at 100 MHz intervals.

3.3   Resolution

3.3.1   Set the signal generator f_1 + 500 MHz (center frequency).

3.3.2   Adjust the variable attenuator so the signal is just saturating the associated detector pixel (pixels for pixel size corresponding to less than 5 MHz).

SIZE	CODE IDENT NO.			REV
A	11312		107028	
SCALE			SHEET 8 OF 10	

3.3.3 Increase the input signal by 30 dB.

3.3.4 Note and record the noise floor for a center frequency 10 MHz away (i.e., 5 MHz between two signals centered in 5 MHz pixels).

3.4 Dynamic Range

3.4.1 Modify the setup of Figure 2 so that two input signals are fed into the variable attenuators.

3.4.2 Pick the two input signals f_a and f_b ($f_a < f_b$) so that $2f_a - f_b$ and $2f_b - f_a$ fall within the band of interest.

3.4.3 Adjust the signal generators so that the detected signals for f_a and f_b just saturate the associated detector pixels for a maximum pulse length of 1 µsec.

3.4.4 Increase the pulse length to 1 msec (i.e., factor of 30 dB).

3.4.5 Observe the detector output and record any intermodulation product signals.

3.4.6 Verify that the input signals to the processor do not contain intermodulation products of level of concern.

3.5 Efficiency

3.5.1 With the optical power meter, measure and record the primary laser beam power, no RF applied, after it passes through the crystal.

3.5.2 Apply 1 watt RF drive power CW.

3.5.3 Measure and record the power of the deflected beam.

BAND 1 2 3 4

Frequency Range
_____ to _____

VSWR

f_1 _____ f_{1+500} _____ f_{1+1000} _____

f_{1+100} _____ f_{1+600} _____ (f_2)

f_{1+200} _____ f_{1+700} _____

f_{1+300} _____ f_{1+800} _____

f_{1+400} _____ f_{1+900} _____

BANDWIDTH

f_1 _____ V f_{1+300} _____ f_{1+600} _____ f_{1+900} _____

f_{1+100} _____ f_{1+400} _____ f_{1+700} _____ f_{1+1000} _____

f_{1+200} _____ f_{1+500} _____ f_{1+800} _____ (f_2)

RESOLUTION

TEST FREQUENCY

NOISE FLOOR f_{r+10} MHz _____ volts

NOISE FLOOR f_{r-10} MHz _____ volts

DYNAMIC RANGE

f_a _____

f_b _____

INTERMOD PRODUCTS: FREQ.   LEVEL

EFFICIENCY

LASER; PRIMARY BEAM POWER _____ mW

DEFLECTED LASER BEAM POWER _____ mW

SIZE	CODE IDENT NO.		107028	REV
A	11312			
SCALE			SHEET 10 of 10	

ATE
L MED